

THE POTASH DEPOSITS AND THEIR ASSOCIATES IN THE AREA
OF THE BOULBY MINE, CLEVELAND

VOLUME 2. FIGURES

by

John K. Milne B. Sc.



This thesis is presented for the degree
of Doctor of Philosophy of the University
of Edinburgh in the Faculty of Science

1978

Table of Contents

	<u>page</u>
<u>FIGURES FOR CHAPTER 1</u>	1
Figure 1.1. The location of the Boulby Mine and important boreholes around Whitby.	2
" 1.2. The configuration of the Zechstein basin.	3
" 1.3 Generalized cross-sections into the southern North Sea basin.	4
" 1.4 The process for manufacturing KCl products of the Boulby Mine.	5
 <u>FIGURES FOR CHAPTER 2</u>	 6
Figure 2.1. The localities of the boreholes in the Cleveland Potash Ltd. Concession area.	7
" 2.2. Plan of the underground workings of the Boulby Mine.	8
" 2.3. North-south cross-section through the rocks of the Teesside Group (Z3) in the Boulby Mine.	9
" 2.4. Map showing the area of outcrop of the principal stratigraphic units in the Mine.	10

		<u>page</u>
Figure 2.5.	Photograph of recrystallized sylvinite veins in the Boulby Shale.	11
"	2.6. Fibrous sylvinite veins emanating from the top of the Boulby Potash.	12
"	2.7. Fibrous sylvinite veins cross- cutting slickensides.	13
"	2.8. Fibrous sylvinite veins which have accumulated beneath slickensides.	13
"	2.9. Curved fibres of sylvite in a sylvinite vein.	14
"	2.10. Evidence for overfolds in the East Spearhead.	15
"	2.11. Important tectonic features and their probable interpretation in roadway G of the East Spearhead.	16
"	2.12. Typical anhydritic shale/siltstone breccia in Panel No. 1.	17
"	2.13. Diagram of the nose of an overfold in the south of the East Spearhead.	18
"	2.14. A small swell in the top of the Boulby Potash in the South Spearhead.	19
"	2.15. The contact between the upper part of the Boulby Halite and the Boulby Potash in the South Spearhead.	19

	<u>page</u>
Figure 2.16. The thrust plane of the overthrust in the Upper Magnesian Limestone and Billingham Main Anhydrite in the Shaft Bottom Drive.	20
<u>FIGURES FOR CHAPTER 3</u>	21
Figure 3.1. Coarse grey-brown halite rock of bed B.H.1.	22
" 3.2. Colour banding in bed B.H.1.	23
" 3.3. Evidence for mud cracks in bed B.H.1.	23
" 3.4. Pink-white halite band in bed B.H.1.	24
" 3.5. Photomicrograph of crenulated shale laminae in bed B.H.1.	24
" 3.6. Area of bed B.H.1 enriched in shale containing carnallite.	25
" 3.7. An irregular white patch of sylvinite in bed B.H.1.	25
" 3.8. Texture of granular halite rock of bed B.H.1.	26
" 3.9. Typical texture of bed B.H.2.	27
" 3.10. Photomicrograph of sylvite porphyroblast enclosing halite crystals.	27

	<u>page</u>
<u>FIGURES FOR CHAPTER 4</u>	28
Figure 4.1. Horizontal colour banding in the Boulby Potash.	29
" 4.2. Typical texture of gneissoze sylvinite.	29
" 4.3. Photomicrograph of shaly sylvinite.	30
" 4.4. Aggregates of pyrite associated with "mucous-like" carbonaceous matter in a shale laminae.	30
 <u>FIGURES FOR CHAPTER 5</u>	 31
Figure 5.1. Photomicrograph of anhydrite which has replaced or displaced sylvite in bed B.S.4.	32
" 5.2. Photomicrograph of the various textures of anhydrite in the upper part of bed B.S.4.	32
" 5.3. Photomicrograph of hexagonal halite crystals, after carnallite, in the clay matrix of bed B.S.1.	33
" 5.4. Photomicrograph of large sylvite and halite porphyroblasts in the lower rocks of bed B.S.4.	33

		<u>page</u>
Figure 5.5.	Photomicrograph of part of a sylvite porphyroblast enclosing clays, hematite, quartz and halite in bed B.S.4.	34
" 5.6.	Small magnesite nodules in bed B.S.6.	34
" 5.7.	Photomicrograph of bed B.S.2 - type (i).	35
" 5.8.	Photomicrograph of bed B.S.2 - type (ii).	35
" 5.9.	Map showing the outcrop of the Borate Nodule Bed (B.S.3) in the Mine.	36
" 5.10.	A fragment of bed B.S.3 containing parahilgardite nodules in the East Spearhead.	37
" 5.11.	Photomicrograph of ericaite cubes in an iron-boracite nodule.	37
" 5.12.	Photomicrograph of large twinned ericaite crystals and small turbid iron-boracite crystals in an iron-boracite nodule.	38
" 5.13.	Aggregates of iron-boracite set in a matrix of sylvite and magnesite in an iron-boracite nodule.	38

		<u>page</u>
Figure 5.14.	Parts of triangular diagrams showing the variations in apparent concentrations of FeO, MgO and MnO in iron-boracite and ericaite crystals in iron-boracite nodule 1.	39
" 5.15.	As above but for iron-boracite nodules 2 and 4.	40
" 5.16.	Parts of triangular diagrams showing the variations in apparent concentration of MgO, MnO and FeO of points in 6 ericaite and iron-boracite crystals scattered in a parahilgardite nodule.	41
" 5.17.	Part of an FeO-MgO-MnO triangular diagram showing the variation in apparent concentrations of these cation oxides in remnant crystals of iron-boracite from the S-20 borehole.	42
" 5.18.	Plot of all the apparent concentrations of MgO, MnO and FeO in the iron-boracite and ericaite crystals analysed using the electron microprobe analyser.	43

	<u>page</u>
Figure 5.19. Photomicrograph of the junction between a parahilgardite nodule and its host rock.	44
" 5.20. 'V' shaped extinction bands in a parahilgardite crystal from a nodule.	44
" 5.21. Extinction bands resembling ostrich plumes in a parahilgardite crystal from a nodule.	45
" 5.22. Deformation lamellae in nodular parahilgardite.	45
" 5.23. Photomicrograph of a parahilgardite crystal in which many of the deformation lamellae have coalesced.	46
" 5.24. Three typical nodules from the area of iron-boracite nodules in bed B.S.3.	47
" 5.25. Photomicrograph of an almost pure iron-boracite nodule composed of granular crystals.	48
" 5.26. Thin section evidence for sylvite being replaced by halite in iron-boracite nodules.	48

	<u>page</u>
Figure 5.27. Photomicrograph of evidence for recrystallization of sylvite in an iron-boracite-sylvite-magnesite nodule (see also Table 5.15).	49
" 5.28. Thin section evidence for two generations of magnesite intergrown with sylvite in an iron-boracite-sylvite-magnesite nodule (see also Table 5.15).	49
" 5.29. Photomicrograph of magnesite which has been replaced by sylvite in an iron-boracite-sylvite-magnesite nodule.	50
" 5.30. Photomicrograph of iron-boracite which has been replaced by sylvite in an iron-boracite-sylvite-magnesite nodule.	50
" 5.31. Evidence for the replacement of magnesite by secondary halite in a sylvite-magnesite-halite nodule.	51
" 5.32. Photomicrograph of small parahilgardite rosettes in the parahilgardite nodule host rock.	51
" 5.33. Photomicrograph of aggregated rosettes of parahilgardite in a parahilgardite nodule.	52

	<u>page</u>
Figure 5.34. Photomicrograph of parahilgardite crystals in a nodule which have been partially replaced by halite.	52
" 5.35. Chemical, modal and mineralogical data for the sequence examined in the S-20 borehole.	53
" 5.36. Photomicrograph of two typical remnant crystals of iron-boracite which are all that remain of the iron-boracite nodules in bed B.S.3 in the S-20 borehole.	54
" 5.37. Photomicrograph of a halite-clay rock from bed B.S.5 which has been partially pervaded by secondary colourless halite.	54
" 5.38. Part of a sylvinite vein in which much of the sylvite appears to have been replaced by halite.	55
<u>FIGURES FOR CHAPTER 6</u>	56
Figure 6.1. The localities of the sections of the Boulby Halite and Boulby Potash from which samples were taken for boron analysis.	57

	<u>page</u>
Figure 6.2. Profiles of the boron content of 6 sections through the Boulby Halite and Boulby Potash.	58-59
<u>FIGURES FOR CHAPTER 7</u>	60
Figure 7.1. Jänecke ternary diagram for the system MgCl_2 -KCl-NaCl- Na_2SO_4 - H_2O at 25°C .	61
" 7.2. Ternary diagram for the system MgCl_2 - CaCl_2 -KCl-NaCl- H_2O at 93°C .	62
" 7.3. Ternary diagram for the system MgCl_2 - CaCl_2 -KCl-NaCl- H_2O at 35°C .	62
<u>FIGURES FOR CHAPTER 8</u>	63
Figure 8.1. Diagrammatic representation of the possible configuration of the basin/lagoon in which the beds of the third Zechstein evaporite cycle may have been deposited.	64
<u>FIGURES FOR CHAPTER 11</u>	65
Figure 11.1. Map of the marine borate mineral localities of the world.	66
" 11.2. Stassfurtite nodules in a sylvite-halite rock in the Salzdettfurth Mine, north Germany.	67

	<u>page</u>
" 11.3. Photomicrograph of a stassfurtite nodule.	67
<u>FIGURES FOR CHAPTER 12</u>	68
Figure 12.1. Equilibrium diagram for the system NaCl-H ₂ O at 25°C, and up to 16 kilobars (after Adams (1931)).	69
" 12.2. Piezometer used by Adams (1931) to study the system NaCl-H ₂ O.	70
" 12.3. Pressure vessel of the type used by Sourirajan and Kennedy (1962) to study the system NaCl-H ₂ O.	70
" 12.4. Hydrothermal equipment of the type used by Dickson et al. (1963) to study the system CaSO ₄ -H ₂ O.	71
" 12.5. Pressure vessel used in this study of the system NaCl-H ₂ O.	72
" 12.6. Plan of the pressure circuit employed in these experiments to study the system NaCl-H ₂ O.	73
" 12.7. Graph of Wt.% NaCl v. time to determine the equilibrium time of the experiment at 25°C.	74

	<u>page</u>
Figure 12.8. The equilibrium solubility curve in the system NaCl-H ₂ O, at 25°C, and pressures up to 2.5 kilobars (this study).	75
<u>FIGURES FOR APPENDIX 2</u>	76
Figures A2.1 Structural interpretation of the - A2.3. boreholes in the C.P.L. concession area.	77
<u>FIGURES FOR APPENDIX 5</u>	78
Figure A5.1. Geometric interpretation of the polymorphic relations in the hilgardite group of minerals (after Braitsch (1959)).	79
 <u>IN BACK ENVELOPE</u>	
Plate I	The lithologies of the upper part of the Boulby Halite, the Boulby Potash and the Boulby Shale in the boreholes in the C.P.L. concession area.
Plate II	Structural map of the Boulby Mine up until 10th January, 1977.
Plate III	Type section of the Borate Nodule Bed.

FIGURES FOR CHAPTER 1

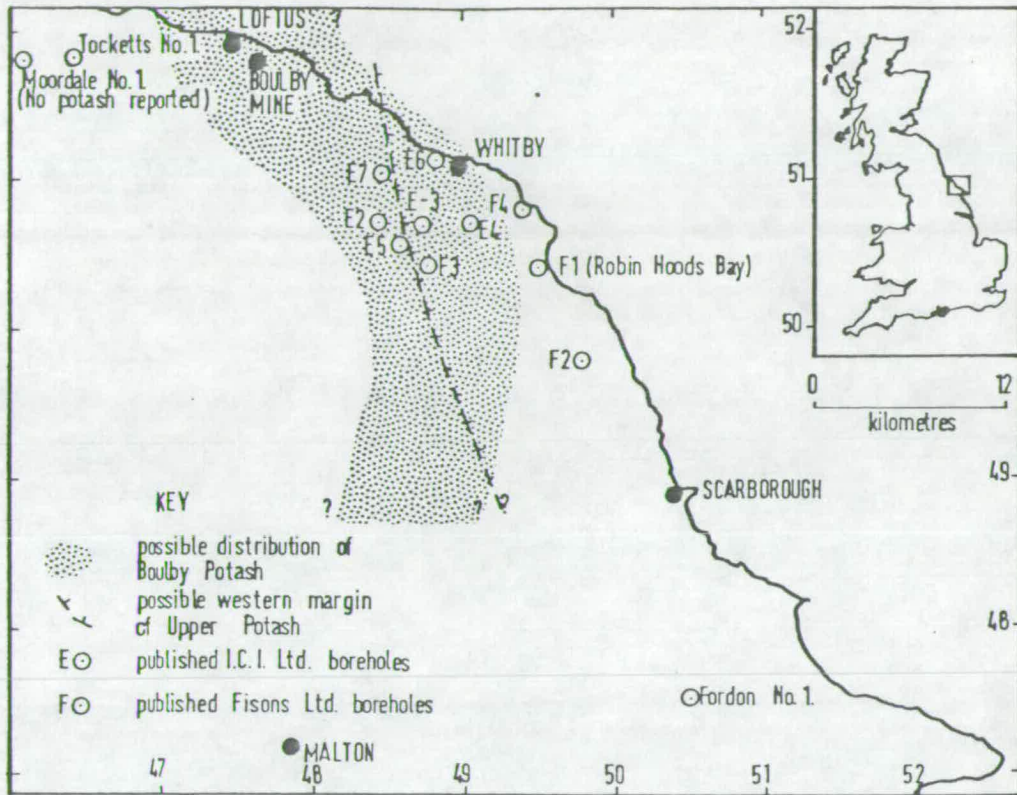


Figure 1.1

The location of the Boulby Mine and important boreholes around Whitby and the approximate distribution of the Middle and Upper Potash beds in north-east England. (Modified after Smith, 1973).

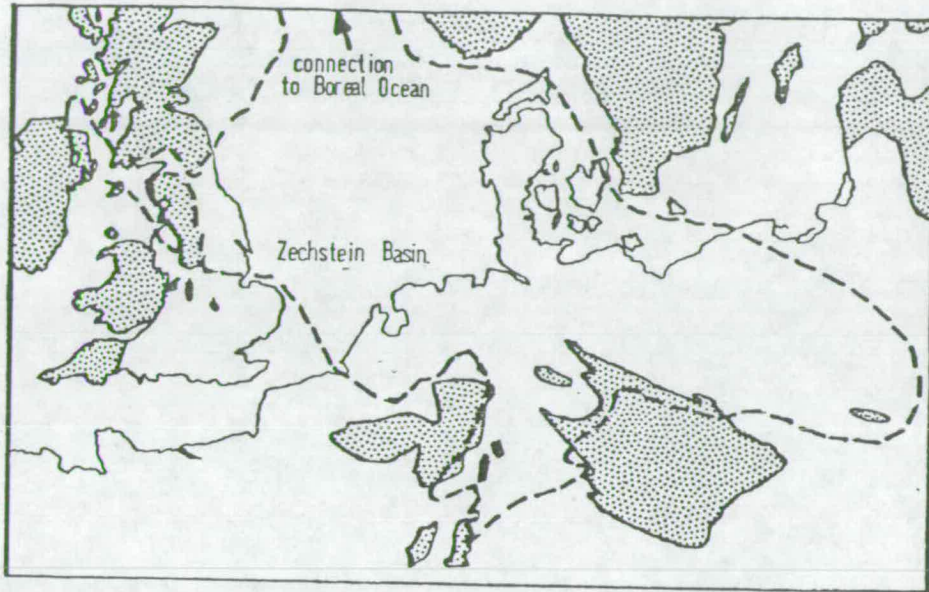


Figure 1.2

The configuration of the Zechstein Basin in northwest Europe. The dashed lines mark the edge of the basin and the stippled areas indicate folded pre-Permian rocks.

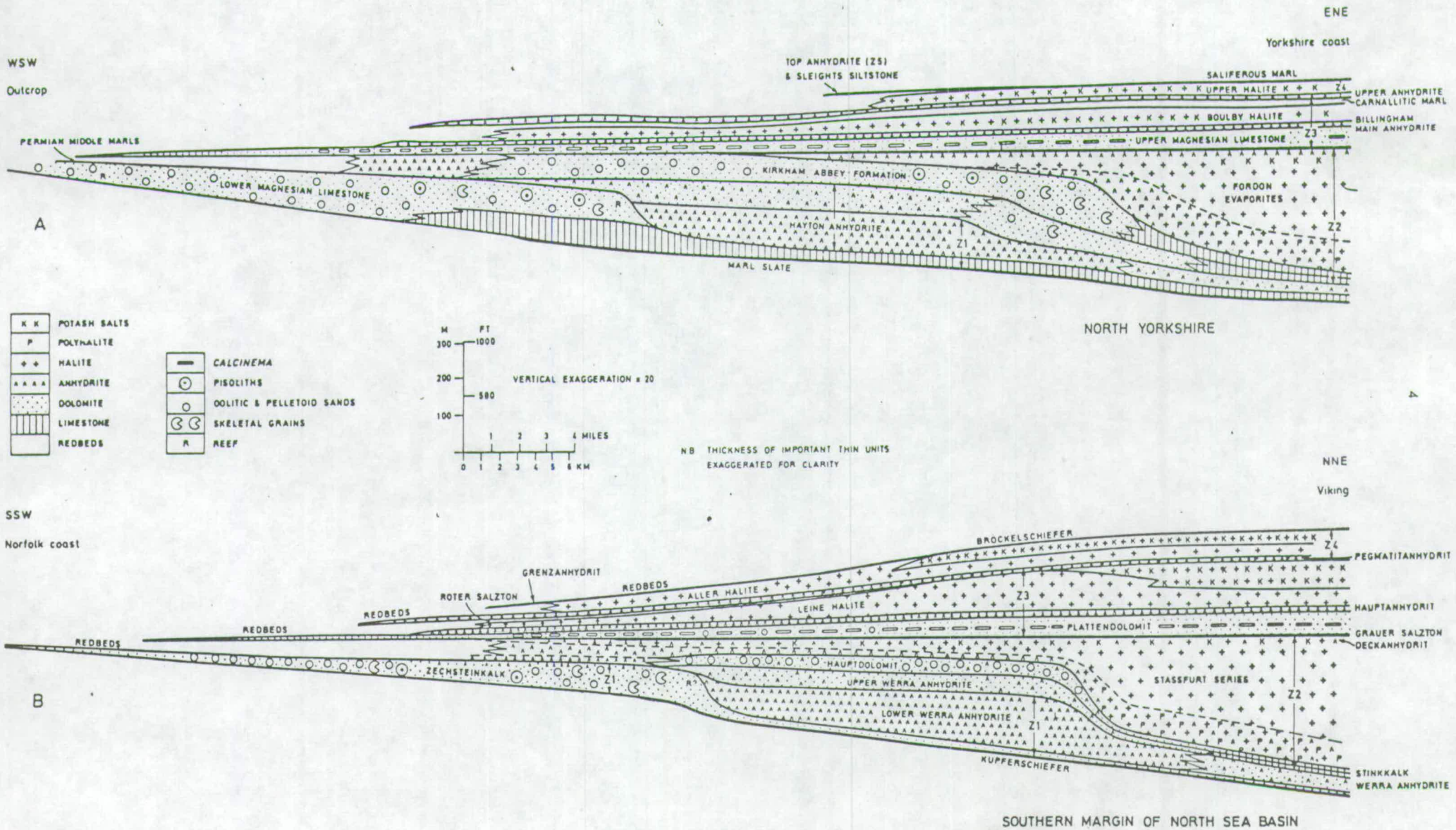


Figure 1.3

Generalized cross-sections into the southern North Sea Basin. A across north-east England and B Norfolk coast towards the Viking Graben. (After Taylor and Colter, 1974)

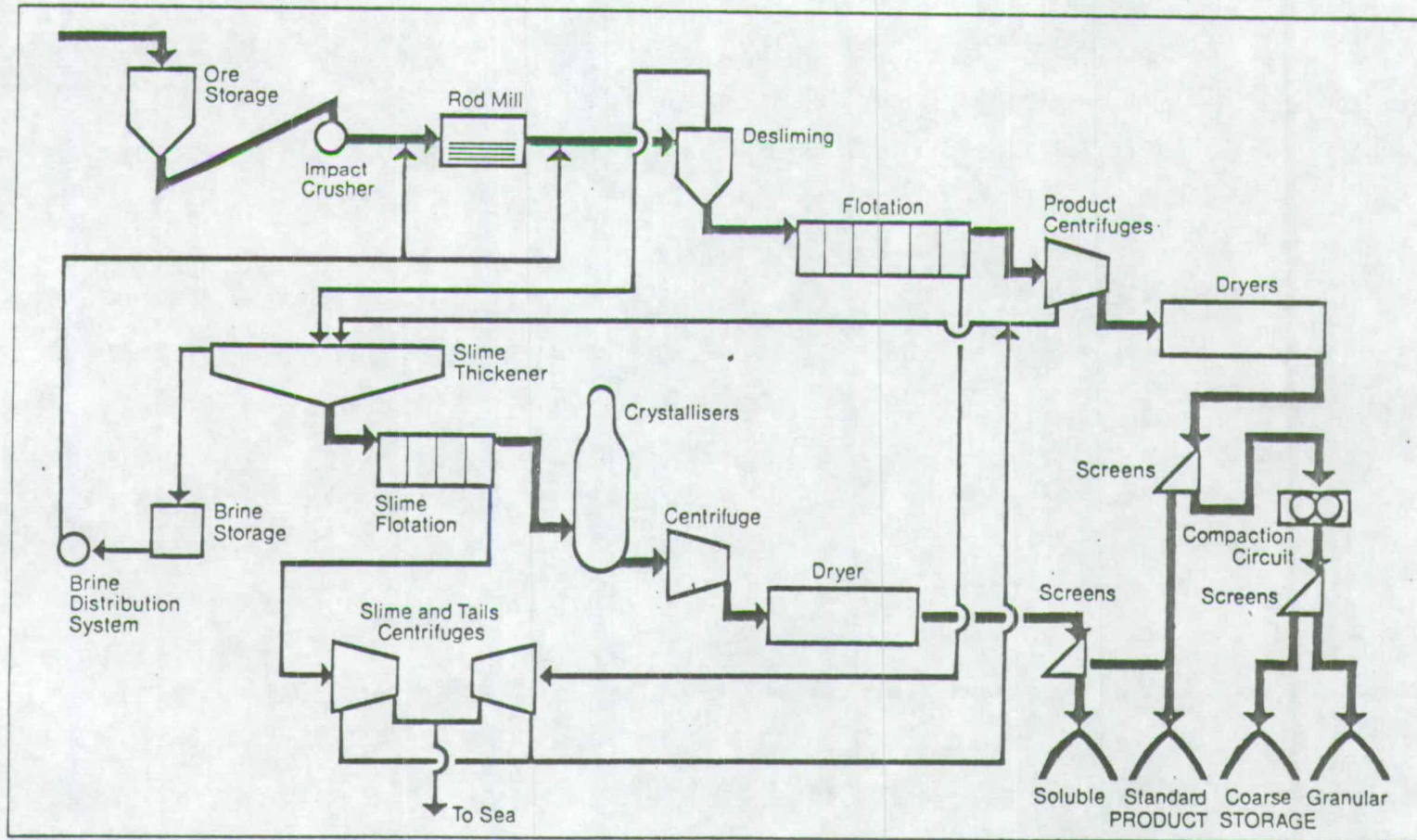
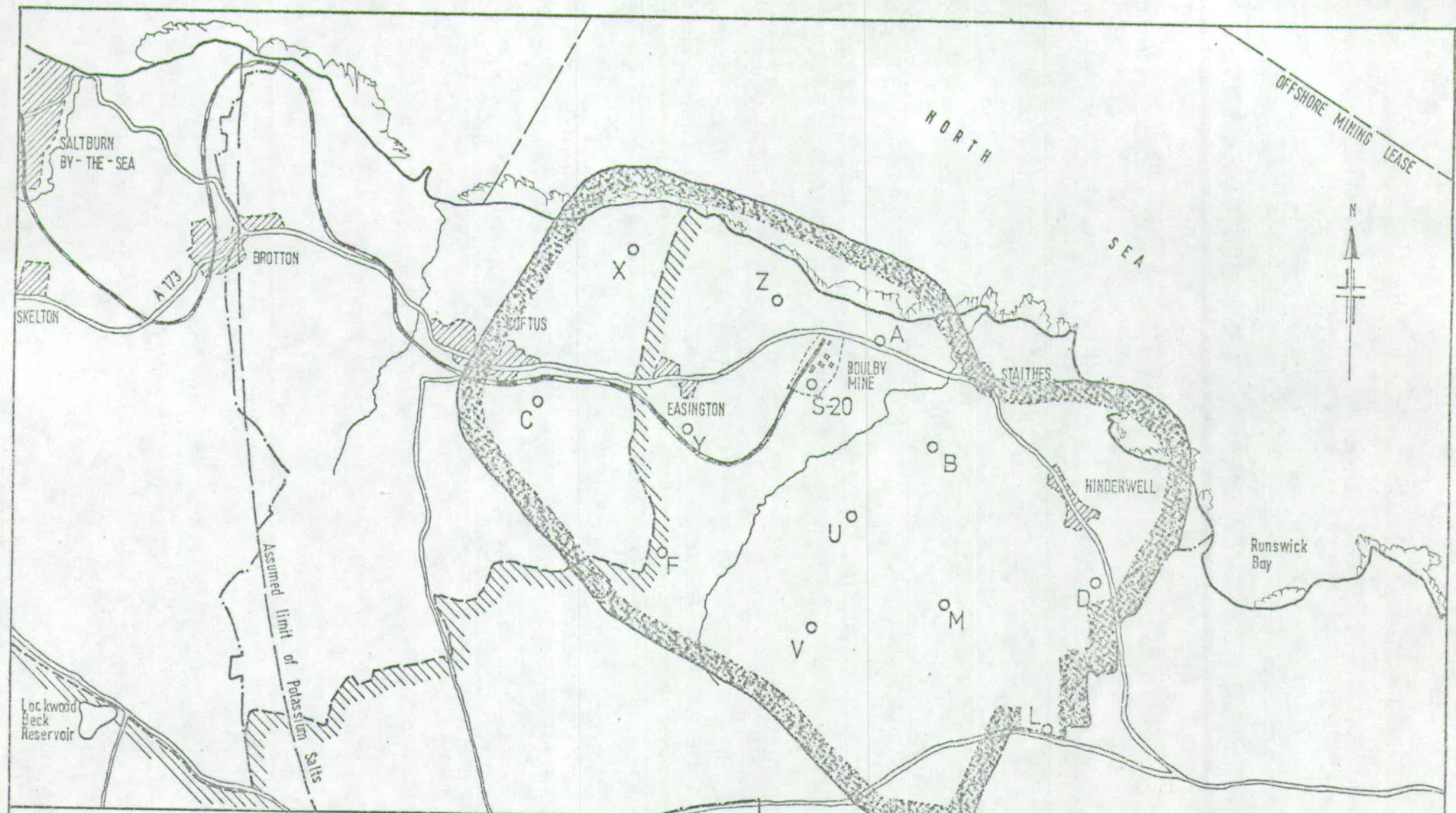


Figure 1.4

The process for manufacturing KCl products at the Boulby Mine.

FIGURES FOR CHAPTER 2



LEGEND


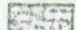


-  Cleveland Potash Limited Planning Permission Boundary
-  Area of indicated reserves
-  National Park Boundary
-  Borehole location



FIGURE 2.1
 THE LOCALITIES OF THE BOREHOLES
 IN THE CLEVELAND POTASH LTD.
 CONCESSION AREA.

Figure 2.2

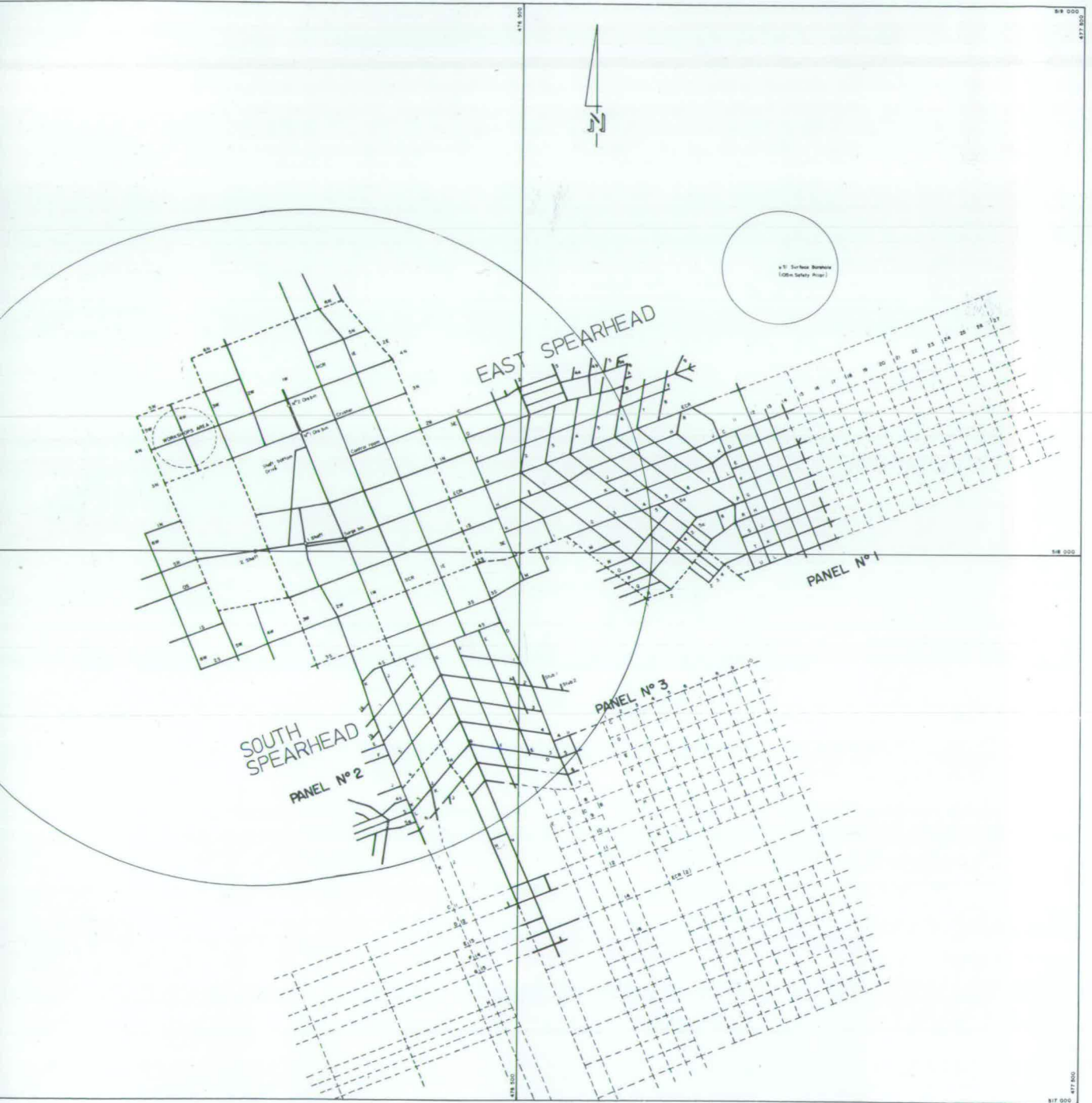
Plan of the underground workings of the Boulby Mine.

Method of location

The method of naming localities in the underground workings is similar to that employed in Ordnance Survey maps. Shaft No. 2, for example is located on roadway S.R., 15 metres west of roadway 3W.

Key to plan

- workings up to 10th January, 1977.
- - - - - main travelling roads.
- - - - - proposed development.



0 100 200 300
metres

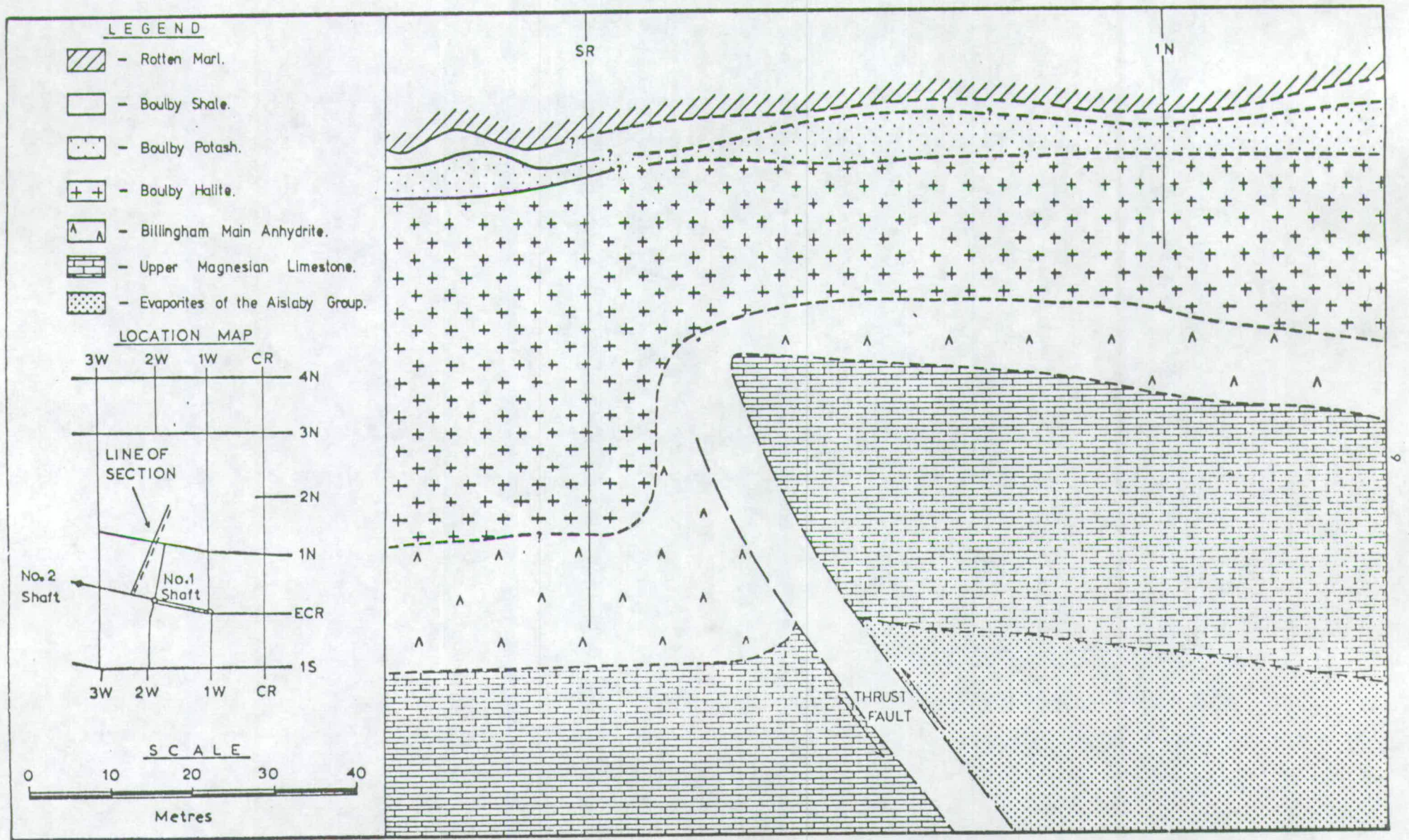
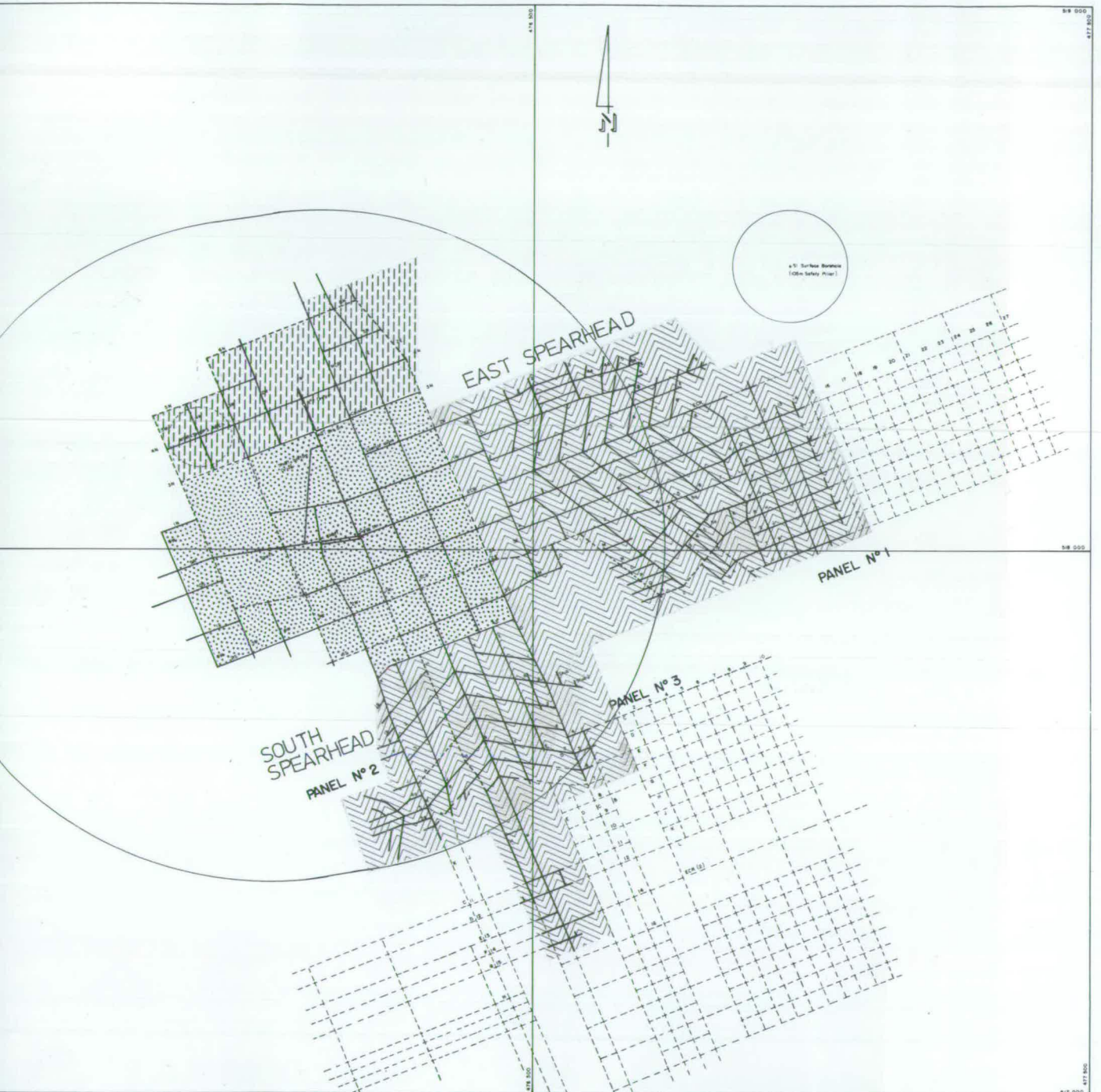


Figure 2.3

North-South cross-section through the rocks of the Teesside Group (Z3) in the Boulby Mine.

Figure 2.4

Map showing the area of outcrop of principal stratigraphic units in the Mine. Roadways as for Figure 2.2.



KEY



BOULBY SHALE

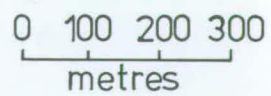


BOULBY POTASH



BOULBY HALITE

SCALE



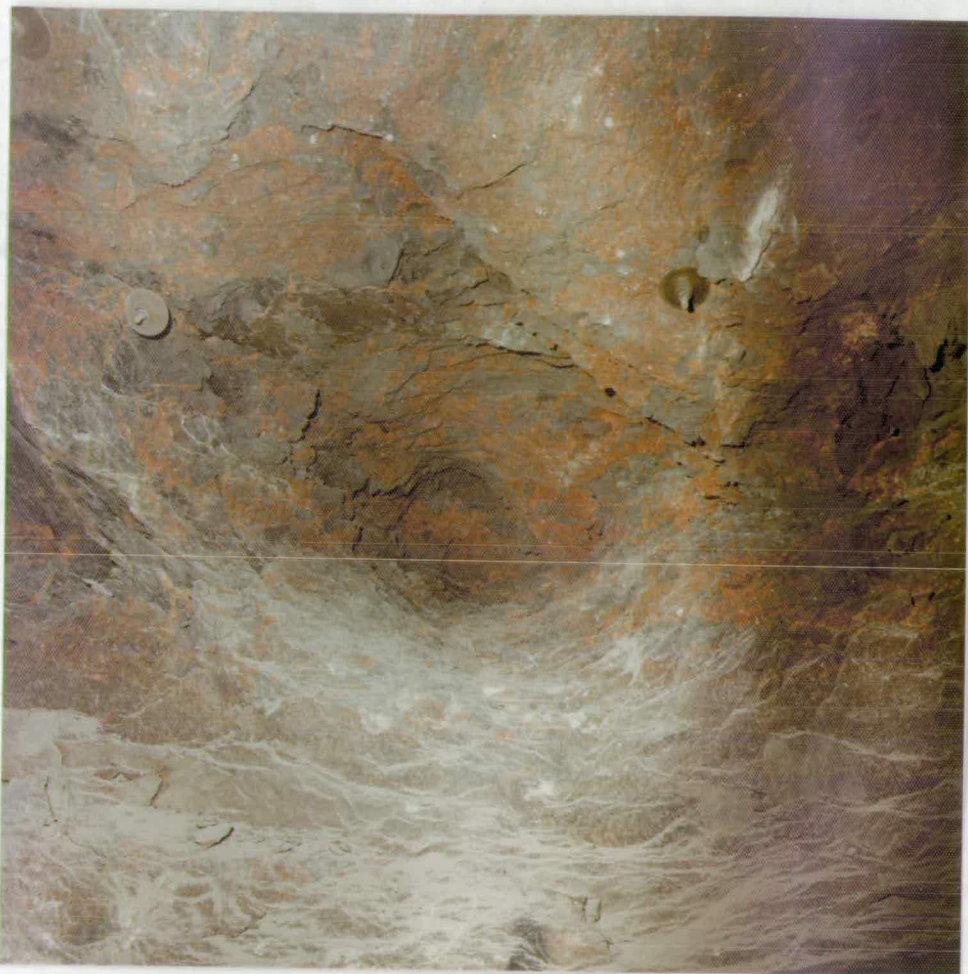


Figure 2.5

Photograph of recrystallized sylvinite veins cross-cutting the rocks of the Boulby Shale in a blowhole in Panel No. 1. The metal rings are 15 cm. in diameter.

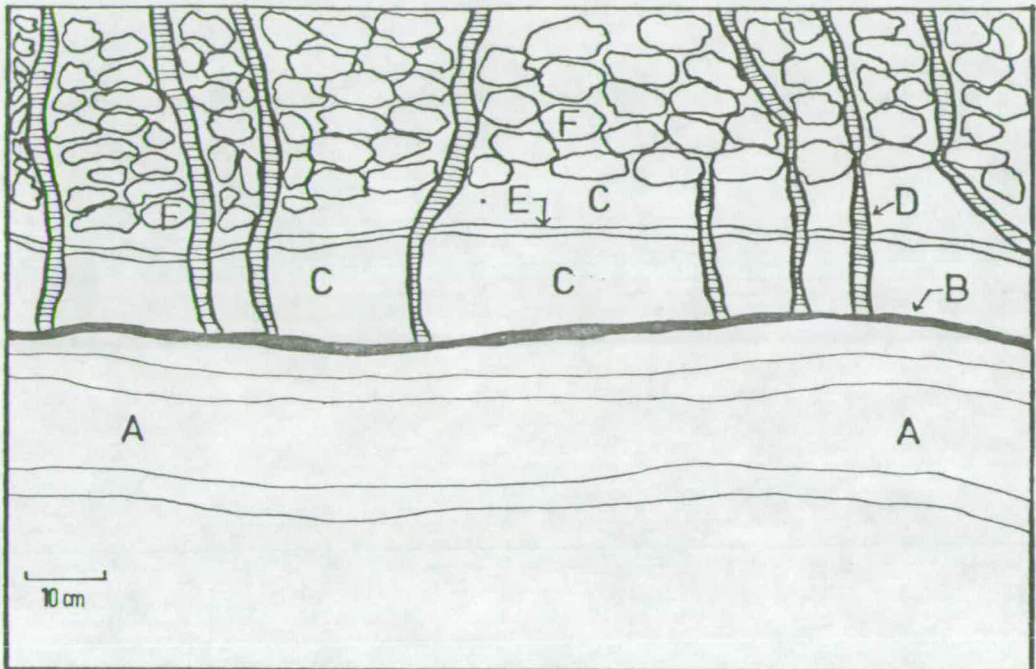


Figure 2.6

Diagram of fibrous sylvinite veins emanating from the top of the Boulby Potash in the South Spearhead. A = banded sylvinite; B = deep red colour band at the top of the sylvinite; C = black sylvite-halite-clay shale; D = fibrous sylvinite veins; E = anhydrite-halite band; F = iron-boracite nodules.

Figure 2.7

Photograph of fibrous sylvinite veins cross-cutting small slickensides (pencil lying in the plane of slickensiding) of minor lateral extent indicating movement had occurred before these veins were formed. The pencil is 10 cm. long. Locality:- South Spearhead at the junction of roadways K and F.

Figure 2.8

Photograph of red sylvinite veins cross-cutting the anhydritic shale/siltstone and which have accumulated under slickensides of minor lateral extent. The metal rod is 0.75 m. in length. Locality:- Roadway K of the South Spearhead.



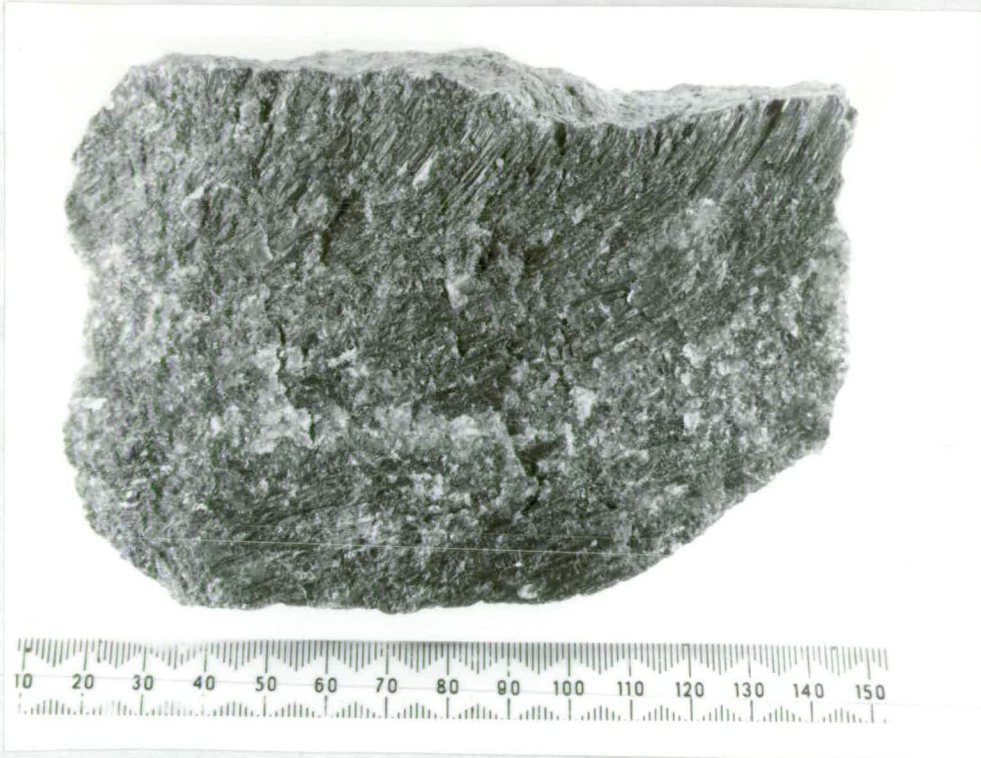


Figure 2.9

Curved fibres of sylvite in a vein from the Boulby Shale. The centre of the vein has recrystallized. The upper and lower surfaces of the specimen are the vein walls.

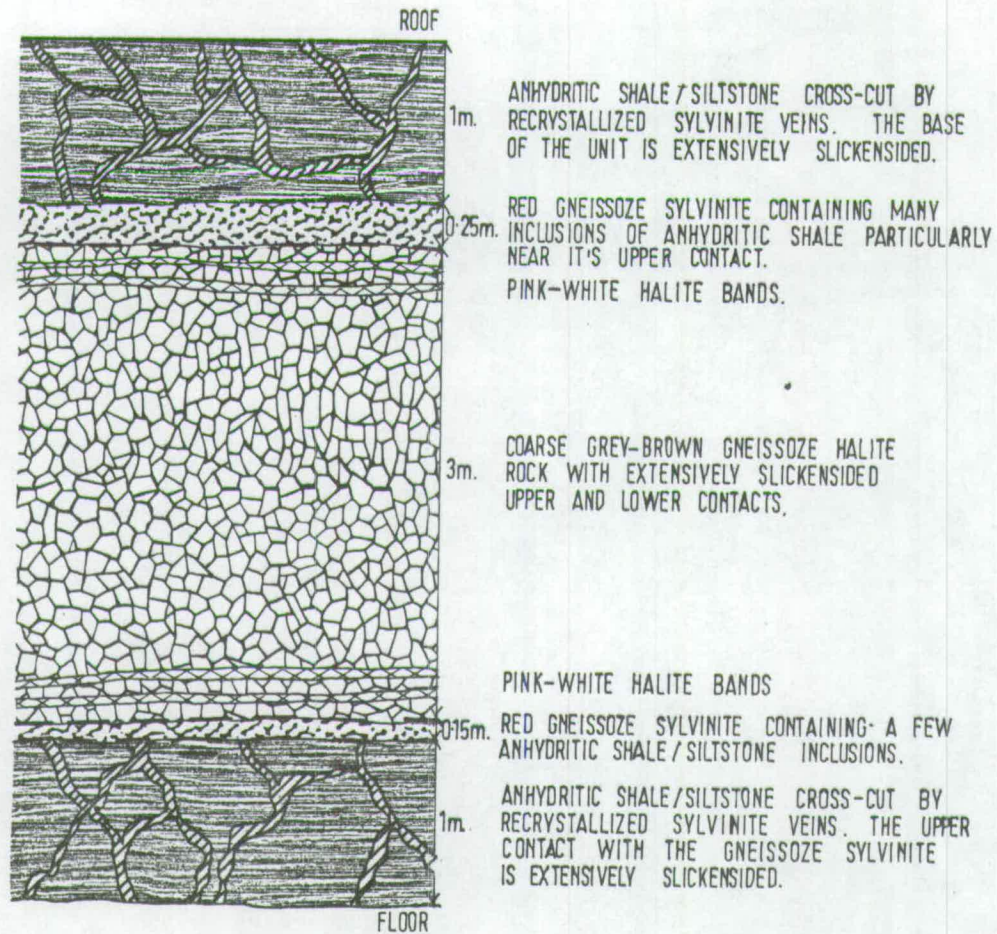
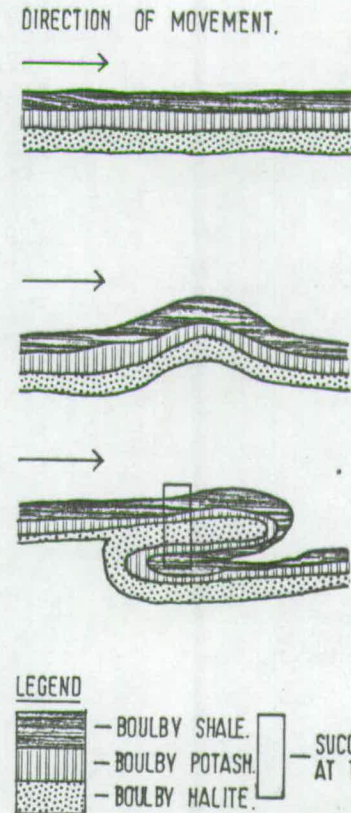


FIGURE 2.10

(A) CROSS SECTION OF THE END FACE OF ROADWAY B. IN THE EASTERN SPEARHEAD SHOWING BED REPETITION ABOUT THE BOULBY HALITE.



(B) DIAGRAMMATIC REPRESENTATION OF THE STAGES OF DEVELOPMENT OF AN OVERFOLD WHICH HAS LED TO THE SUCCESSION OBSERVED IN ROADWAY B. IN THE EASTERN SPEARHEAD.

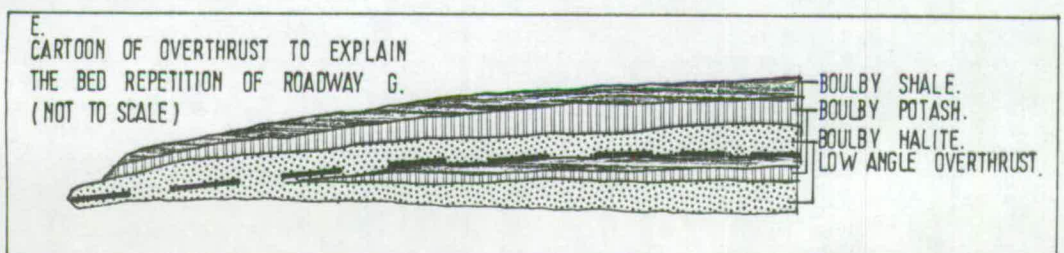
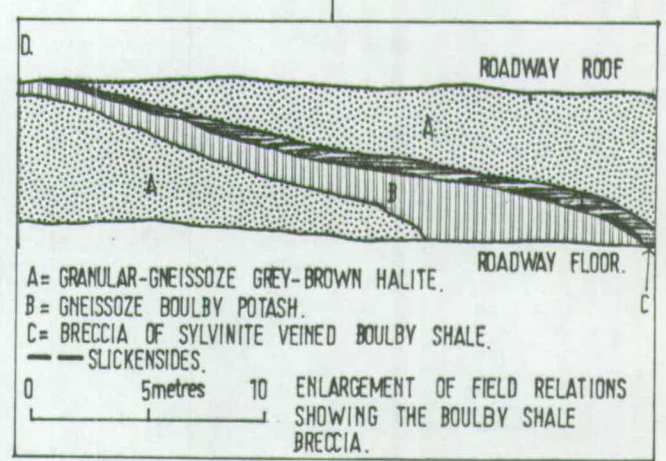
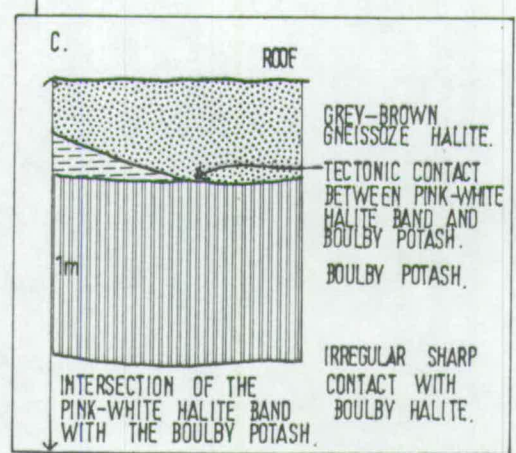
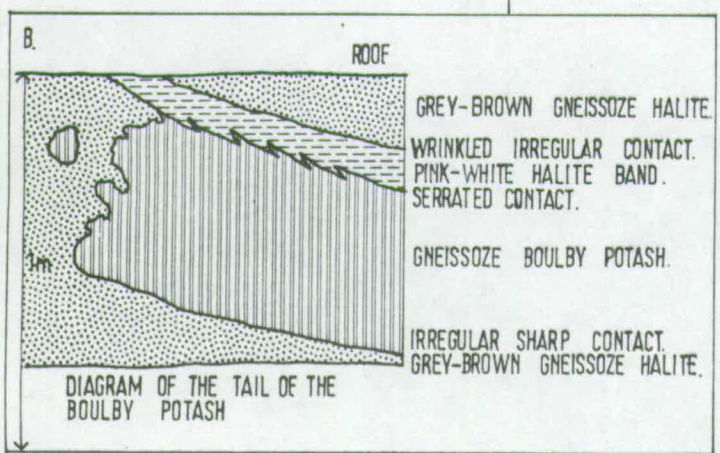
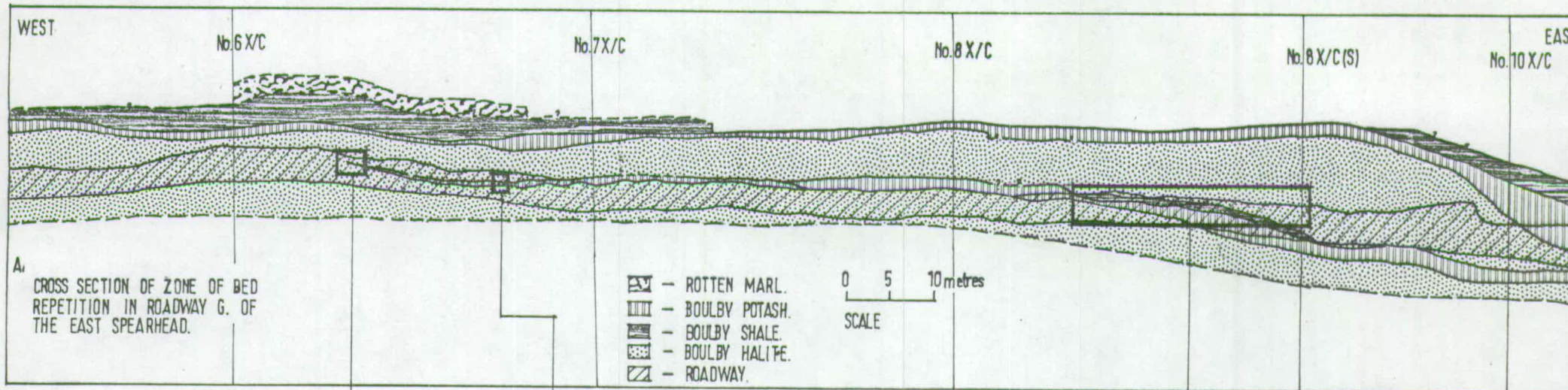


FIGURE 2.11
 IMPORTANT TECTONIC FEATURES
 AND THEIR PROBABLE INTERPRETATION
 IN ROADWAY G. OF THE EAST
 SPEARHEAD



Figure 2.12

Photograph of a typical breccia of anhydritic shale/siltstone set in a matrix of rolled recrystallized sylvinite veins. The laminations of the different blocks are differently orientated. The metal rod is 1 metre long. Locality:- No. 11 cross-cut in Panel No. 1.

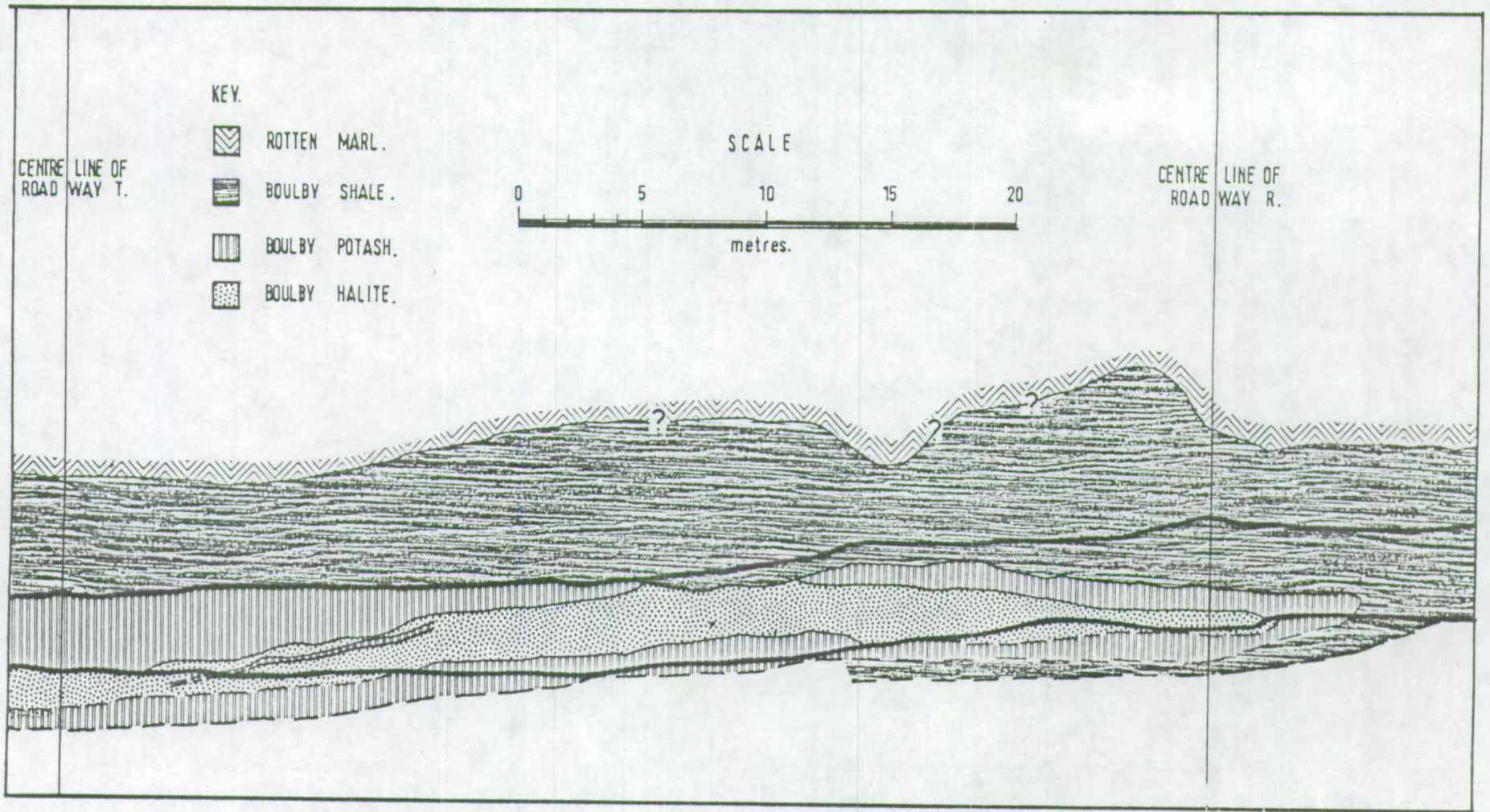


Figure 2.13

Diagram of the nose of an overfold observed in No. 5 cross-cut between R and T in the south of the East Spearhead.

Figure 2.14

Photograph of a small swell in the top of the Boulby Potash in the South Spearhead - the ink line marks the upper contact.

Figure 2.15

Photograph of the contact between the upper part of the Boulby Halite and the Boulby Potash (marked with an arrow). A continuous slightly crenulated shale parting marks the contact. The hammer shaft is 0.3 m. in length. Locality:- No. 3 cross-cut between roadways H and J in the South Spearhead.





Figure 2.16

Photograph of the thrust plane of the overthrust in the Upper Magnesian Limestone and Billingham Main Anhydrite in the Shaft Bottom Drive. Bedded Upper Magnesian Limestone on the right of the photograph abuts vertical mylonitized Billingham Main Anhydrite. The hammer handle is 0.5 metres in length.

FIGURES FOR CHAPTER 3



Figure 3.1

Photograph of the coarse grey-brown halite rock of bed B.H.1. Note the fragmented and interstitial shale laminae.

Figure 3.2

Grey and white colour bands in bed B.H.1. The bands vary in thickness up to 20 cm. and usually have boundaries which are diffuse over a few centimetres. They are further accentuated by layers which are slightly enriched in red sylvite crystals or which contain halite crystals of an even grain size. In no areas of the Mine were the colour bands seen to merge into the massive variety of the rock. Locality:- Roadway H of the East Spearhead. The metal rod is 1 metre in length.

Figure 3.3

Grey-black and white colour banding formed by alternating layers of halite and clay laminae in bed B.H.1. The inclined grey laminae are also composed of clays. These features have been interpreted as cross-sections through mud cracks (see text). Locality:- Roadway H in the East Spearhead, 30 metres south of No. 4 cross-cut. The metal rod is 0.75 metres in length.



Figure 3.4

A thick pink-white halite band in bed B.H.1. The upper and lower contacts are irregular and just below the end of the metal pointer this band merges into the coarse grey-brown halite rock. The red horizontal laminae in this band are composed of sylvite crystals containing hematite inclusions. Locality:- Roadway H of the South Spearhead at its junction with No. 3 cross-cut. The metal pointer is 1 metre long.

Figure 3.5

Photomicrograph of a crenulated and partially disrupted shale lamina (L) in bed B.H.1. Halite (H) forms the majority of the rock. Sylvite (S) occurs as rounded grains in the interstices among the halite crystals. Scale x 10; plane polarized light.

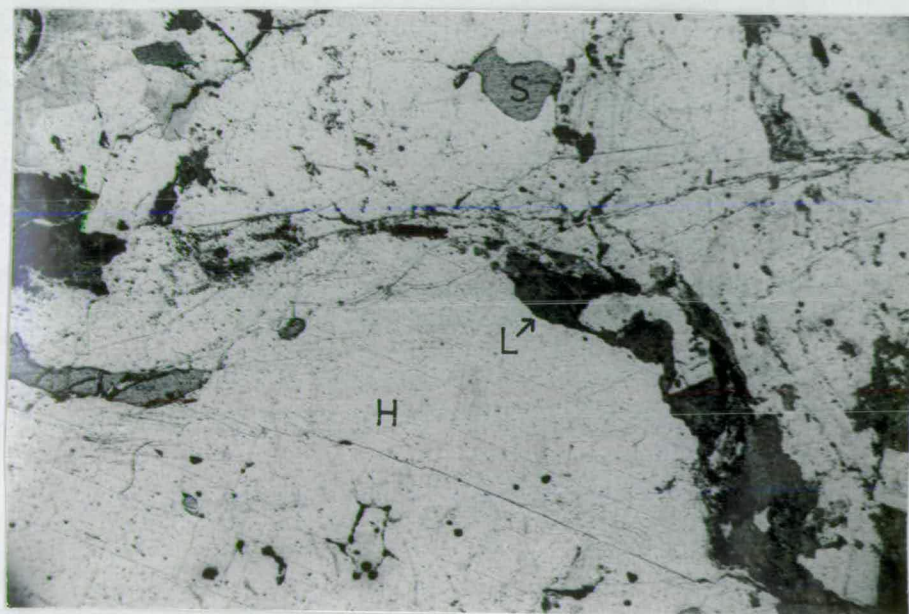


Figure 3.6

Coarse grey-brown halite rock of bed B.H.1. containing about 10% shale in laminae and irregular pockets. The deep red specks in the shale are carnallite. The red colouration along the boundaries between the shale and the host rock is caused by sylvite crystals containing abundant inclusions of tiny hematite platelets. Locality:- In the South Spearhead in No. 5 cross-cut between K and J. The metal rod is 0.5 metres long.

Figure 3.7

An irregular white sylvinite patch in bed B.H.1. The red specks in the bed are carnallite. Locality:- Roadway H of the South Spearhead. The metal rod is 0.75 metres in length.





Figure 3.8

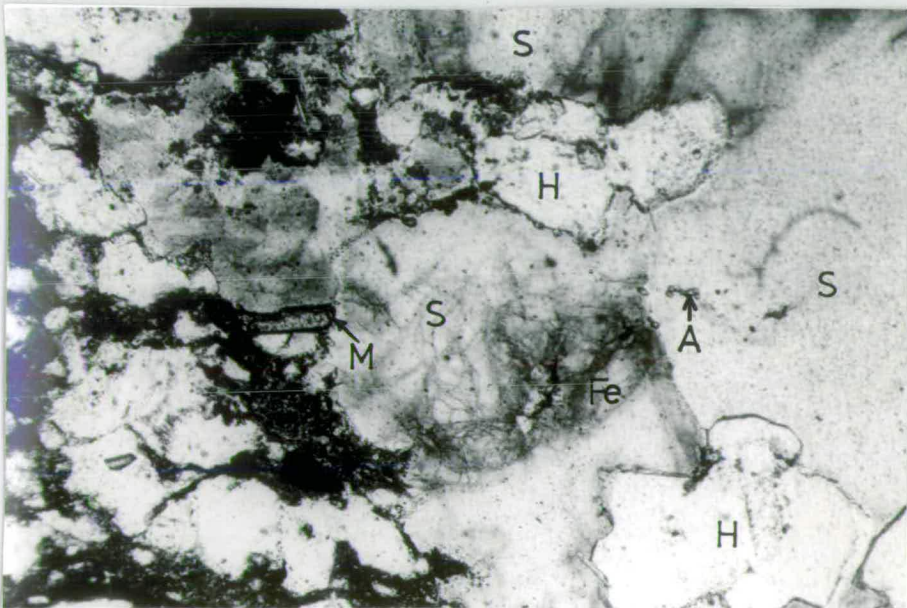
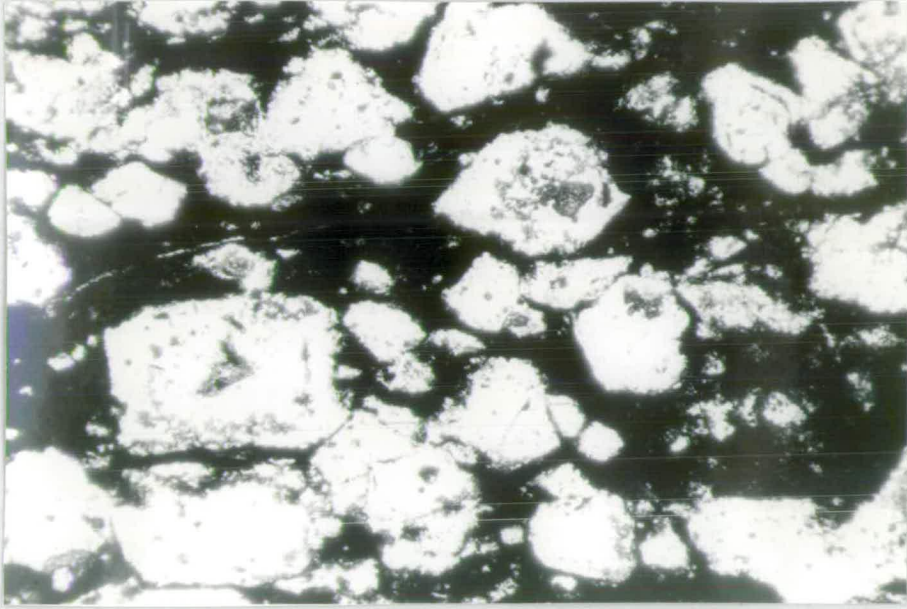
Granular halite rock of bed B.H.1. with rounded interstitial sylvite and small euhedral equant anhydrite crystals lining the grain boundaries. The anhydrite is sometimes associated with clays. Halite = clear; sylvite = light stippling; anhydrite = heavy stippling; clays = black. Scale x 40.

Figure 3.9

Photomicrograph of a typical texture of bed B.H.2. Euhedral to anhedral halite porphyroblasts (white) are set in a carbonaceous clay matrix. Some of the halite porphyroblasts contain inclusions of the matrix suggesting they grew within a host sediment. Scale x30; plane polarized light.

Figure 3.10

Photomicrograph of a sylvite porphyroblast (S) enclosing clays and halite crystals (H) in the uppermost 0.3 metres of bed B.H.2. The sylvite porphyroblast contains numerous inclusions of minute hematite platelets (Fe) around clay inclusions suggesting the hematite has been derived from the clays by leaching. Authigenic magnesite (M) projects from the clays into the sylvite. Occasional euhedral equant anhydrite crystals (A) are associated with clays enclosed in sylvite. Scale x30; plane polarized light.



FIGURES FOR CHAPTER 4

Figure 4.1

Horizontal colour banding in the Boulby Potash at the junction of roadways H and 3E at the west end of the East Spearhead. The "H" is 0.3 metres high.

Figure 4.2

Typical texture of gneissoze sylvinite. The sylvite and halite crystals have curved to ragged boundaries. Notice the small inclusions of euhedral anhydrite crystals. Black = clays; clear = halite; light stipple = sylvite; heavy stipple = anhydrite; hatched edge = magnesite. Scale x 30.

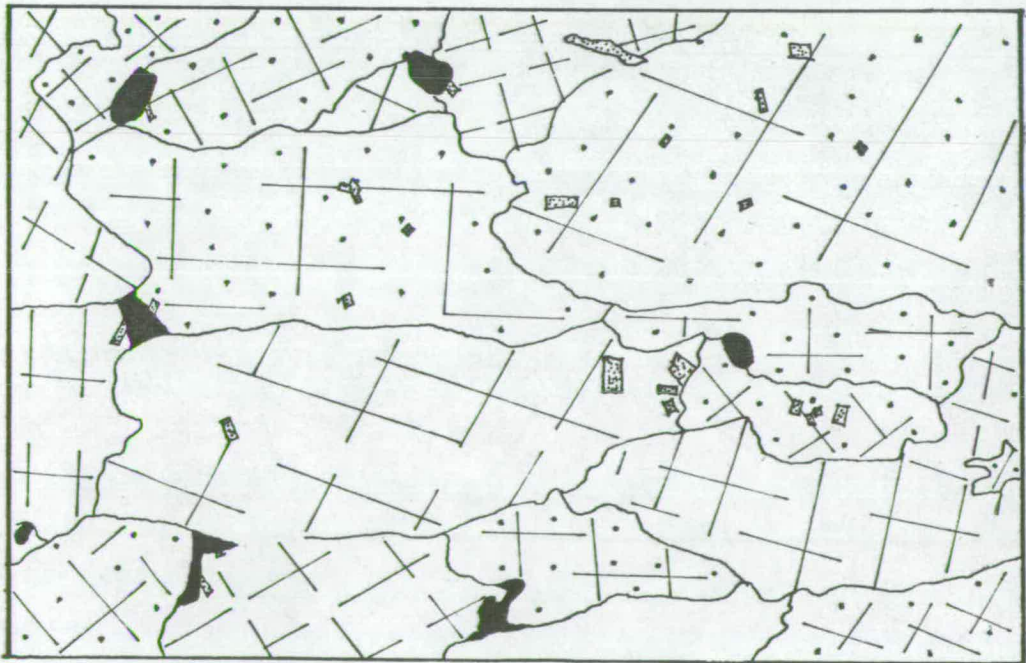
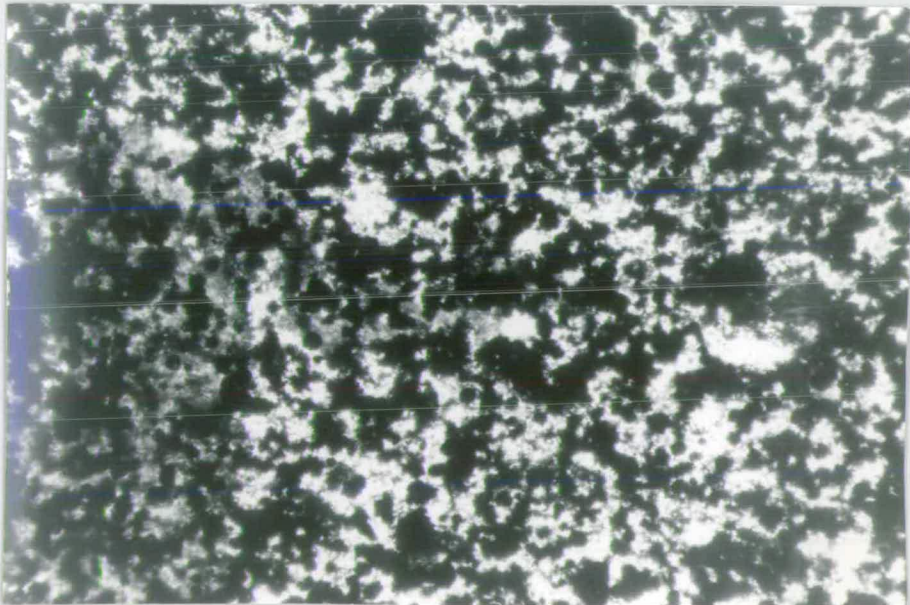
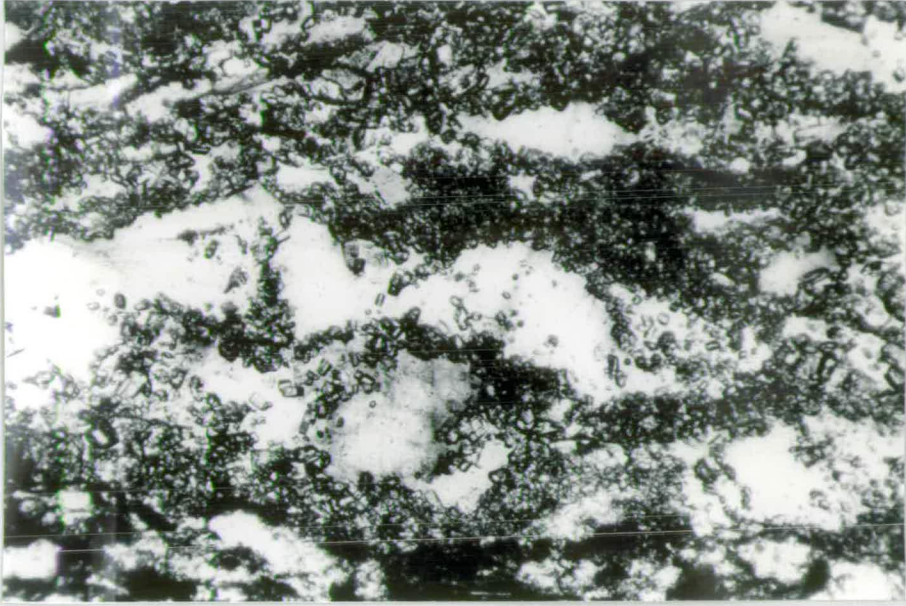


Figure 4.3

Photomicrograph of sylvinite containing an abnormally high proportion of shale between sylvite crystals (colourless). The small euhedral equant anhydrite crystals which line the contacts between the sylvite and shale have probably grown by recrystallization. Note the numerous inclusions of anhydrite within the sylvite. Scale x 30; plane polarized light.

Figure 4.4

Photomicrograph of aggregates of euhedral to subhedral pyrite octohedra (black) associated with "mucous-like" carbonaceous matter (grey) set in a matrix of anhydrite (white) in a shale inclusion of the Boulby Potash. Scale x 120; plane polarized light.



FIGURES FOR CHAPTER 5

Figure 5.1

Photomicrograph of fine grained granular - equant anhydrite crystals (yellow-white-blue) which have partially replaced or displaced small sylvite porphyroblasts (black) near the top of B.S.4. Authigenic magnesite laths cross-cut the anhydrite. Scale x 30; crossed-polars.

Figure 5.2

Photomicrograph of an anhydrite-sylvite-clay rock from the upper part of B.S.4. The anhydrite (high relief) adopts lath-like, granular and equant crystal habits and enclose remnant areas a clay laths (grey) which have been almost completely replaced or displaced by anhydrite. The large black crystal at the base of the picture is sylvite. Scale x 50; crossed polars.

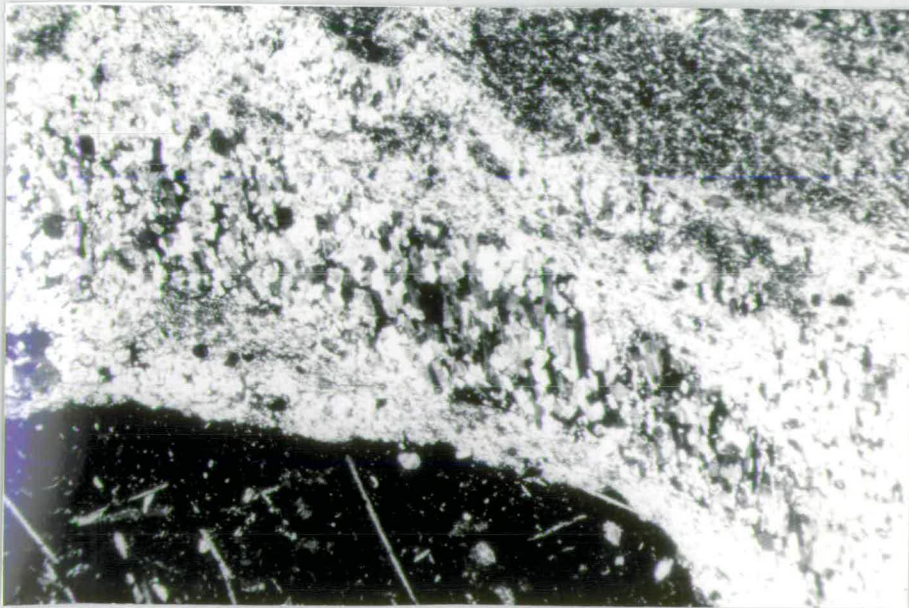
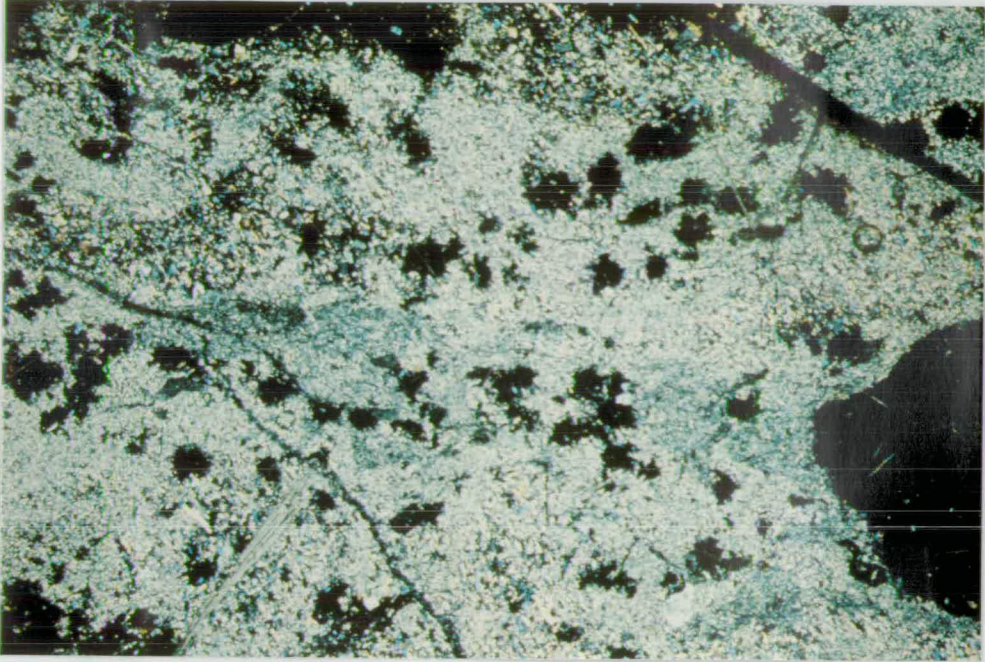


Figure 5.3

Photomicrograph of B.S.1. showing small pseudo-hexagonal halite crystals (black) and a large halite porphyroblast (black at the bottom of the picture) set in a matrix of fine grained parallel aligned and randomly oriented clays. Magnesite plates (yellow-white) project from the clays into the halite crystals, particularly the large porphyroblasts. Small subhedral quartz crystals (white with high relief) are evenly distributed in the clays. Scale x 20; crossed polars.

Figure 5.4

Photomicrograph of large sylvite and halite porphyroblasts (black) set in a matrix of clays with minor anhydrite in the lower rocks of B.S.4. The sylvite crystals are the two squares towards the top of the picture whilst the halite porphyroblasts are the large ellipsoidal crystals near the base of the picture. Note the large number of magnesite plates which have grown in the cleavage of halite. Scale x 10; crossed polars.

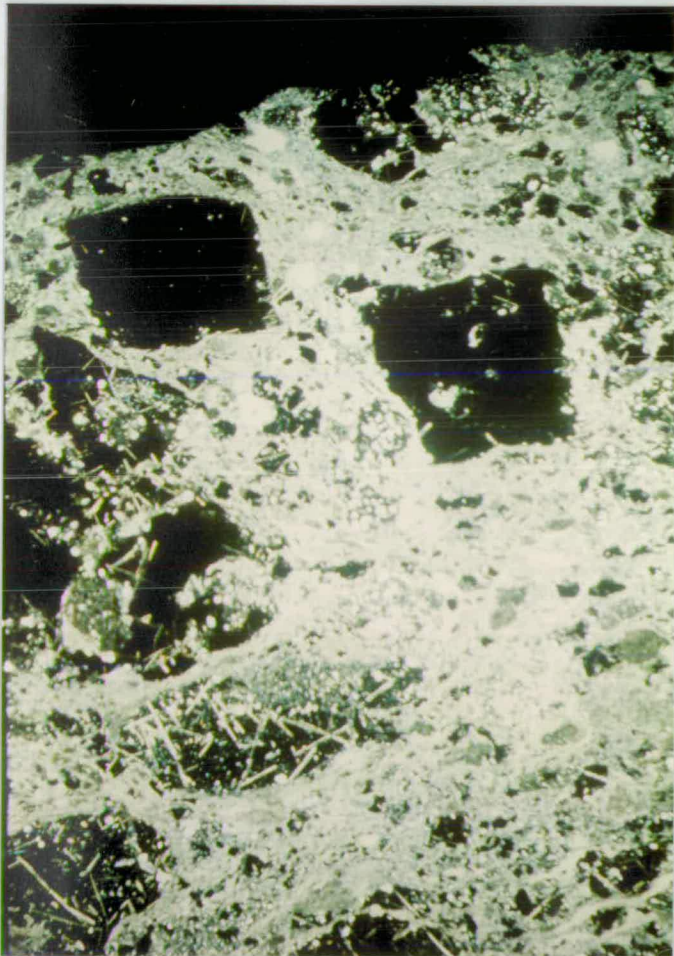
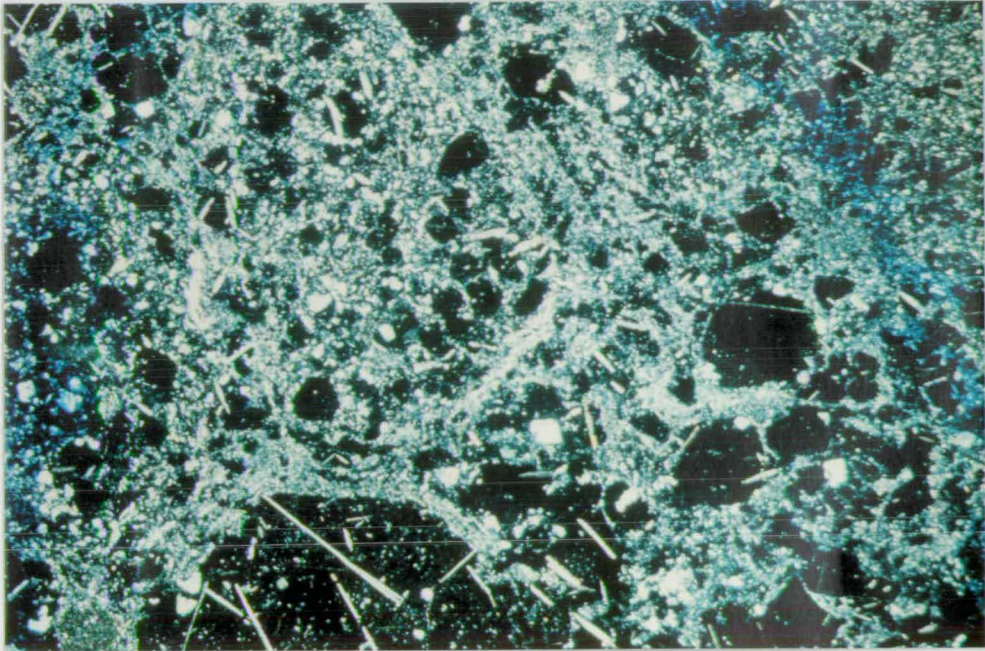


Figure 5.5

Photomicrograph of part of a large sylvite porphyroblast which encloses clays (black), hematite (red-brown), quartz (white with brown centres and partially developed outlines) and halite (white) from the lower rocks of B.S.4. The close association of hematite and quartz with the clays suggests they have formed by the breakdown of clays (see text). The black colouration of the clays is caused by small quantities of carbonaceous matter. Scale x 20; plane polarized light.

Figure 5.6

Diagram of small magnesite nodules along the contact between the anhydritic-clay matrix and halite porphyroblasts in B.S.6. Scale x 30. Black = quartz; stippled areas = magnesite; clear, with cubic cleavage = halite; felted areas = areas of parallel aligned clay platelets with subordinate anhydrite.

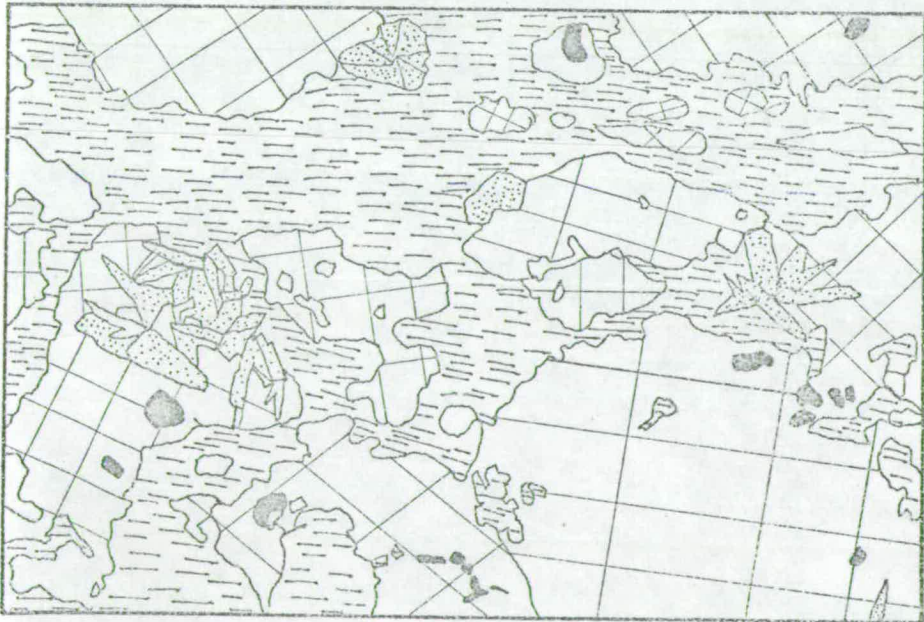
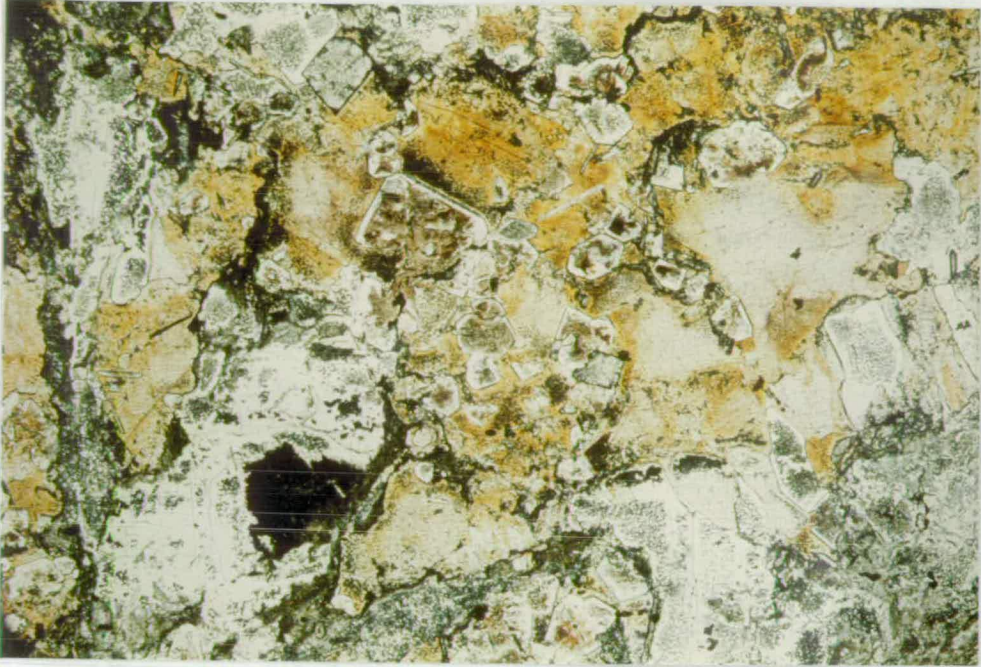
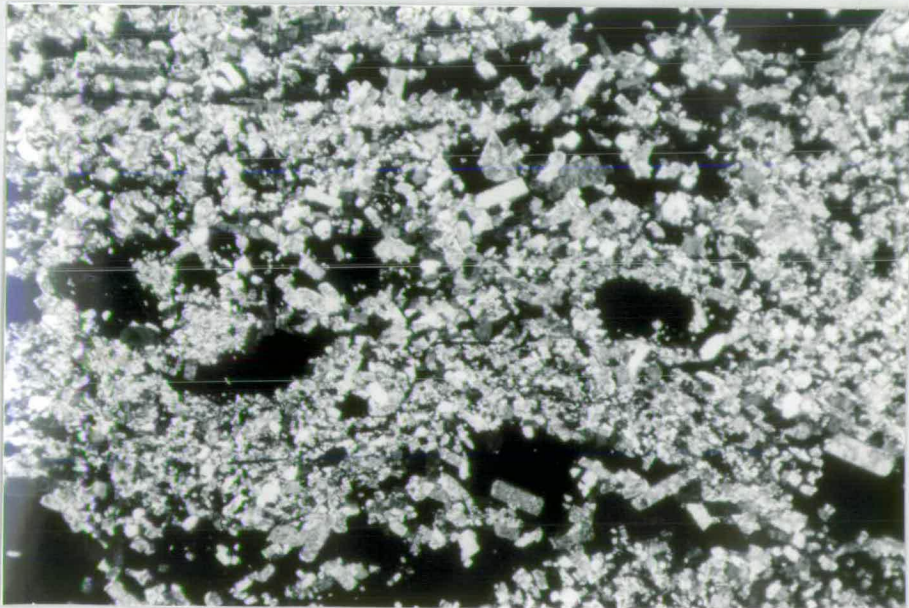
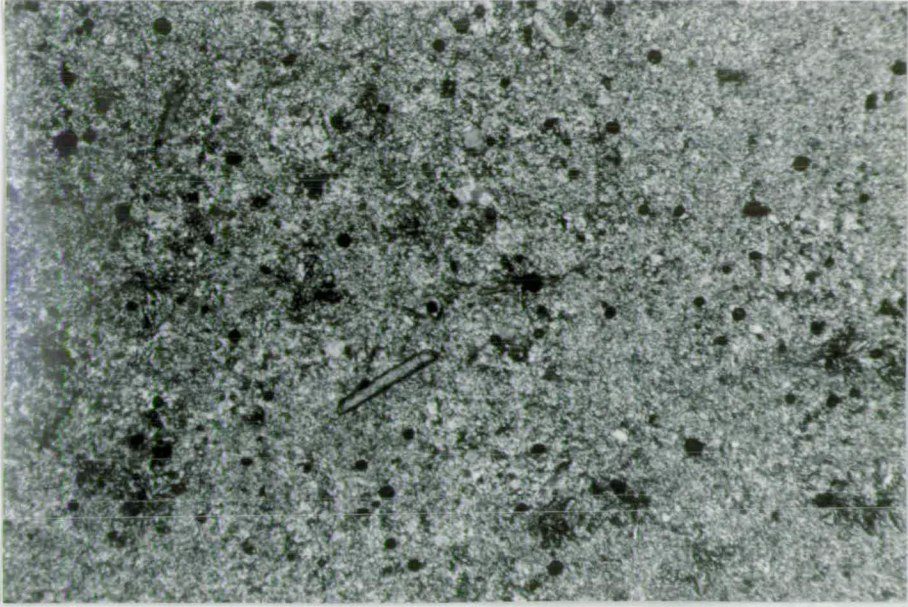


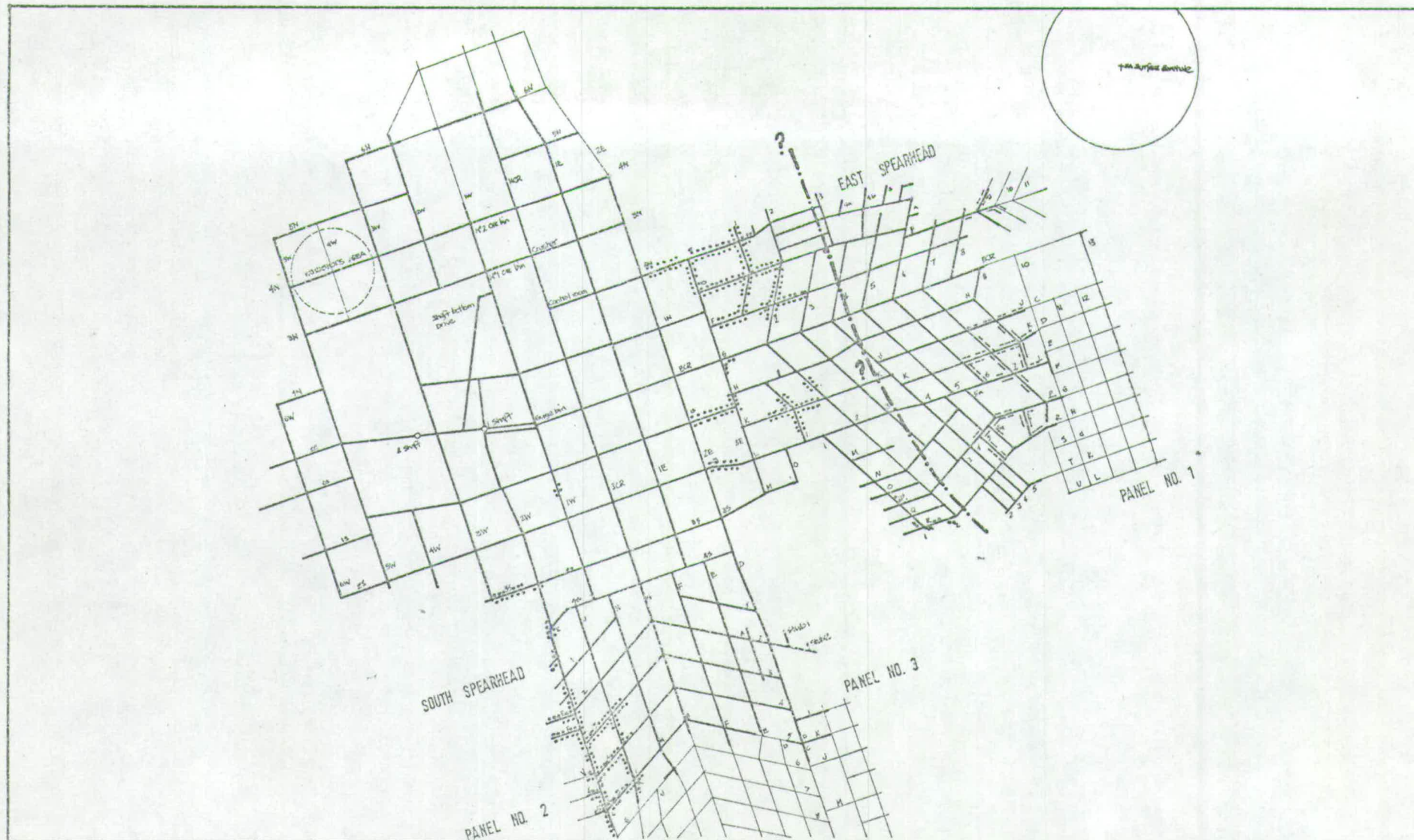
Figure 5.7

Photomicrograph of B.S.2. type (i), which is composed of parallel aligned to randomly orientated anhydrite laths. An authigenic magnesite plate cross-cuts the anhydrite laths. The black spots are carborundum in the thin section. Scale x 40; plane polarized light.

Figure 5.8

Photomicrograph of B.S.2. type (ii). Anhedral halite crystals (black) are set in a matrix of granular and euhedral equant anhydrite crystals. Notice that many of the anhydrite crystals exhibit undulose extinction. Scale x 40; crossed polars.





LEGEND

- outcrops of iron-boracite nodules
- — — — — outcrops of parahilgardite nodules
- — — — — approximate line of transition between iron-boracite and parahilgardite nodules in Borate Nodule Bed

SCALE

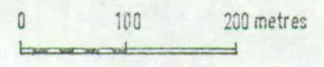


FIGURE 5.9

MAP SHOWING THE OUTCROP OF THE BORATE NODULE BED IN THE MINE

Figure 5.10

A fragment of bed B.S.3. containing parahilgardite nodules in a breccia in the area of overfolding (Plate II) in the East Spearhead. The rock also contains recrystallized sylvinite veins. The metal rod of the gas detector is 1 metre long. Locality:- East Spearhead, roadway J, 10 metres east of No. 8 cross-cut.

Figure 5.11

Photomicrograph of ericaite cubes showing complicated sector twinning. These cubes are enclosed in sylvite (black) which has partially replaced them around the edges. Scale x 5; crossed polars.

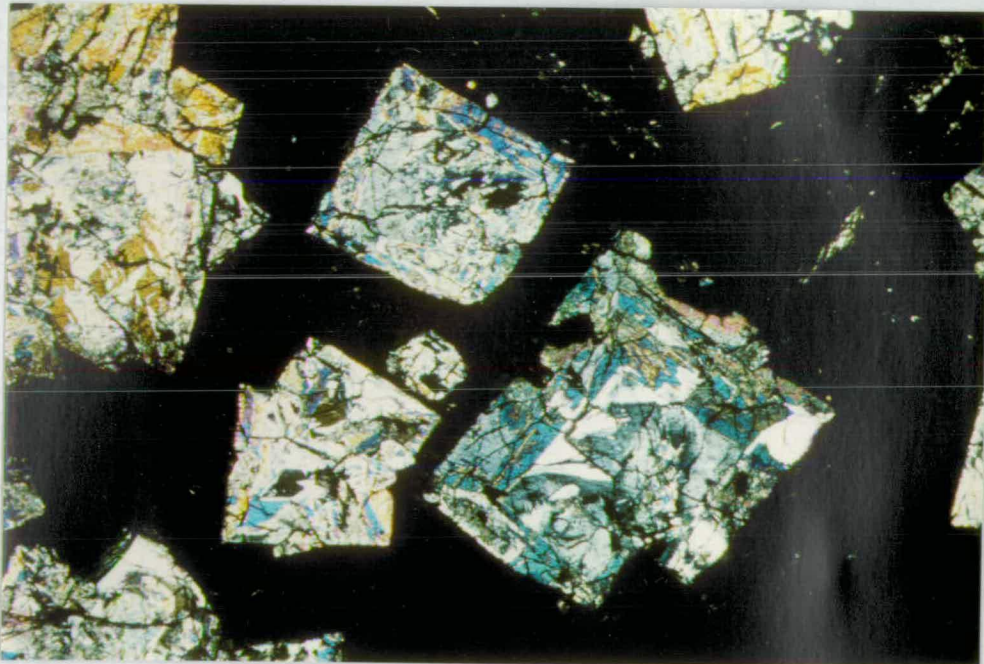
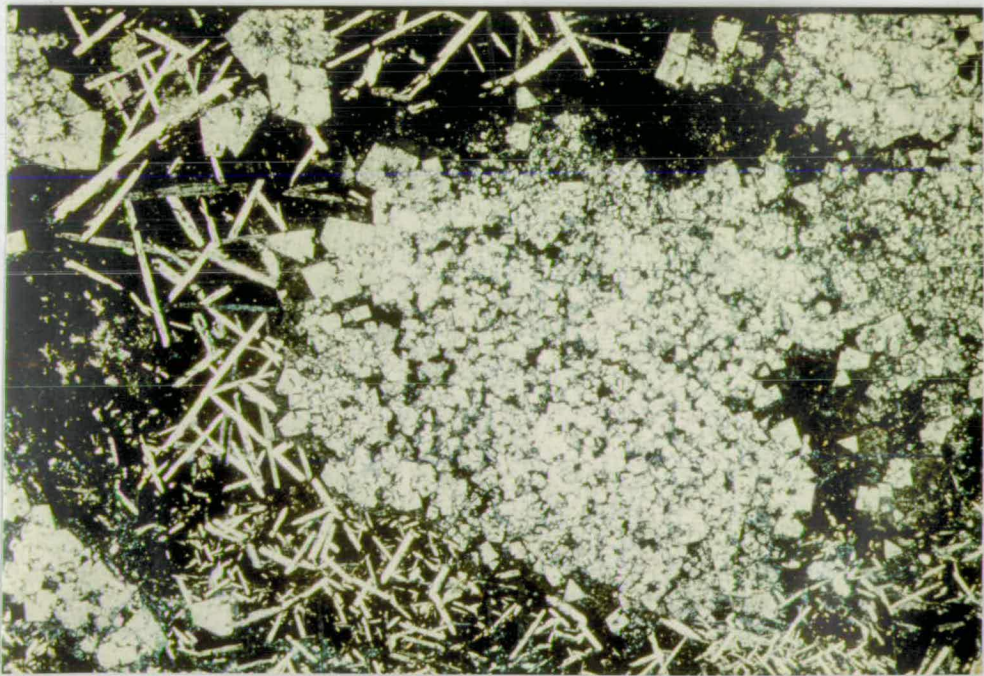
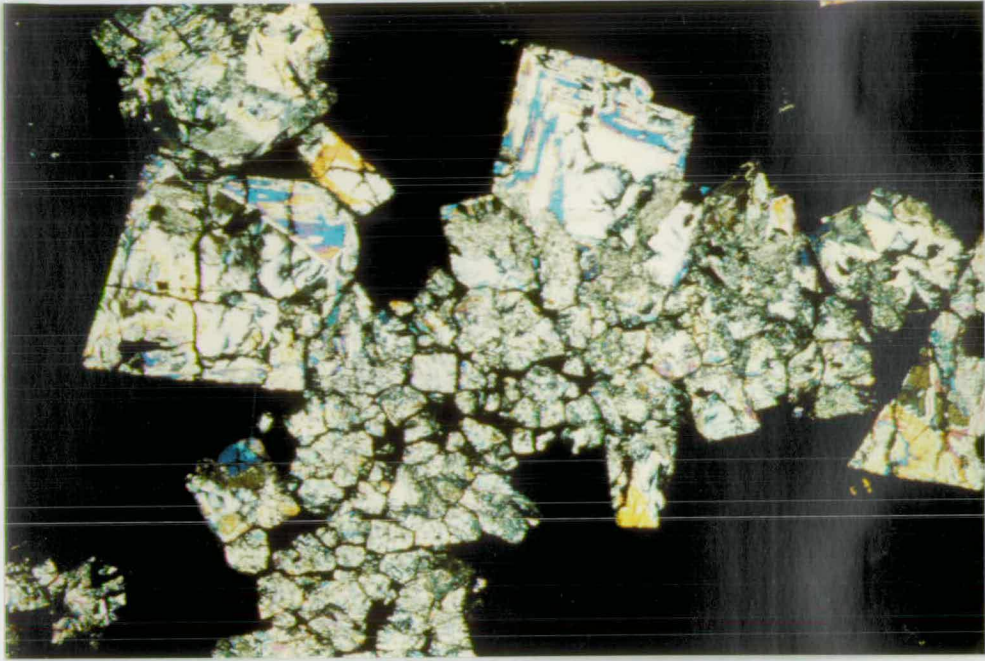


Figure 5.12

Photomicrograph of large twinned ericaite crystals and small turbid iron-boracite crystals set in sylvite (black) in an iron-boracite-ericaite-sylvite nodule. The ericaite crystals have broken down to form iron-boracite. Scale x 10; crossed polars.

Figure 5.13

Photomicrograph of aggregates of iron-boracite (the cubic mineral with high birefringence) set in a matrix of magnesite plates (lath-like with high birefringence) and sylvite (black) in an iron-boracite-sylvite-magnesite nodule. Notice how the iron-boracite crystals at the outside of the aggregates are larger than those in the interiors. The magnesite crystals stop abruptly at the outer edge of the iron-boracite aggregates. Scale x 10; crossed polars.



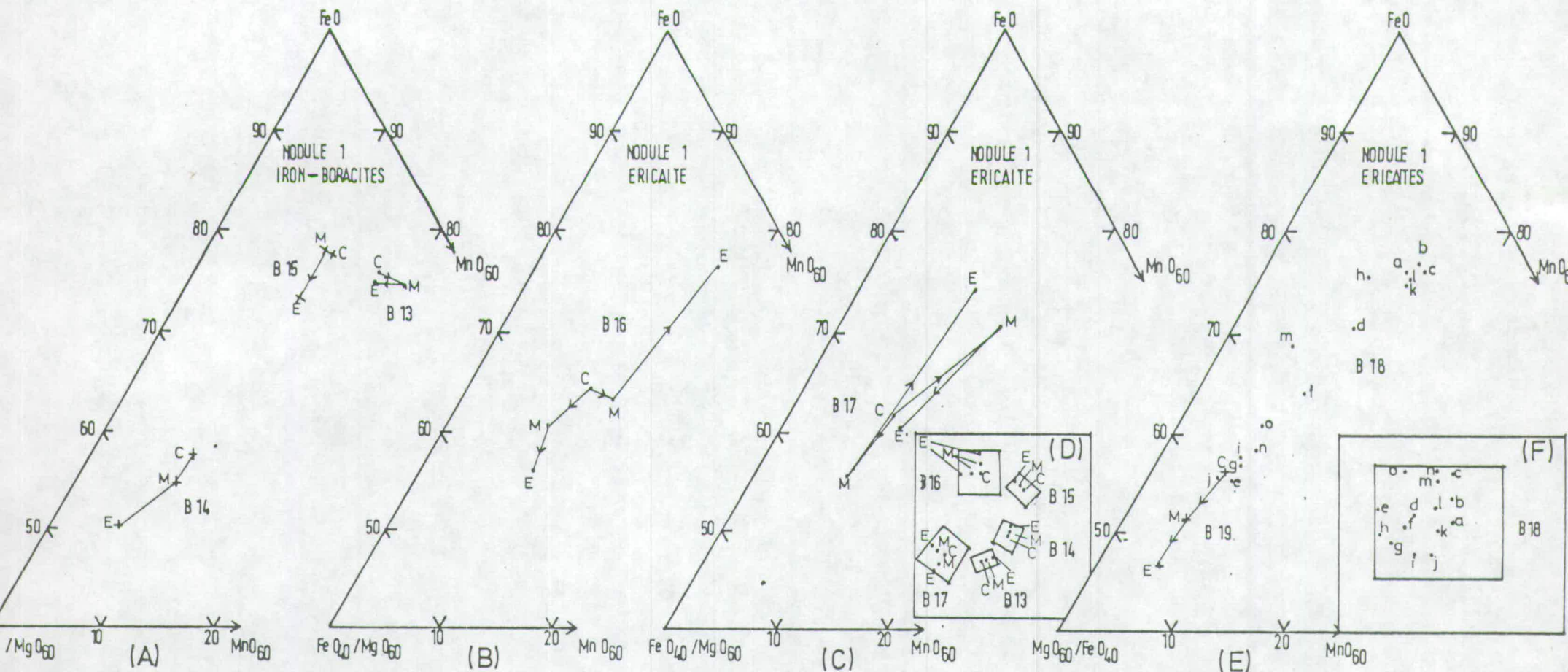
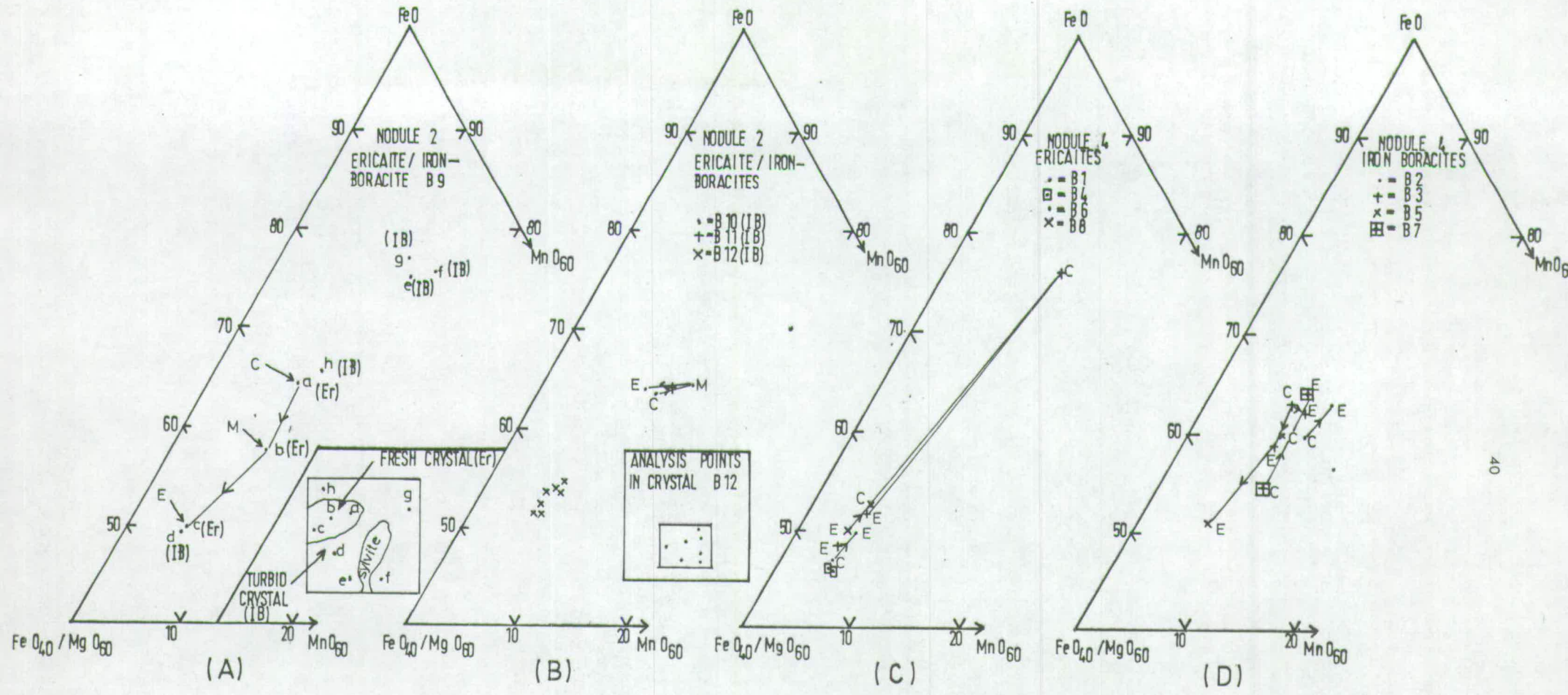


Figure 5.14

Parts of triangular diagrams showing the variation in apparent concentrations of FeO, MgO and MnO (determined on the electron microprobe and recalculated to 100%) in iron-boracite and ericaite crystals in iron-boracite nodule 1. (A) gives the variations in apparent concentrations in iron-boracite crystals co-existing with ericaite crystals in (B) and (C). (D) shows the disposition of the iron-boracite and ericaite crystals in (A) to (C) and indicates the analysis points in these crystals. (E) gives the variation in apparent concentrations of two single ericaite crystals (B18 and B19) in the nodule. The letters next the points of B18 in (E) refer to the analysis points shown in (F). (F) shows diagrammatically the points analysed in ericaite B18. Note that the ranges in composition exhibited by the iron-boracite and ericaite crystals are very similar. B16 = crystal identification; C = analysis in the centre of the crystal; M = analysis between the centre and edge of the crystal; E = analysis at the edge of the crystal.

Figure 5.15

Parts of an FeO-MgO-MnO triangular diagram showing the variation in apparent concentrations (analyses determined by the electron microprobe) of these cation oxides in iron-boracite and ericaite crystals in crystal aggregates from iron-boracite nodules 2 and 4. (A) and (B) give the compositions of co-existing ericaite and iron-boracite crystals in nodule 2. (C) and (D) give the composition of co-existing ericaite and iron-boracite crystals in nodule 4. (A) shows the variation in these cation oxides within a single crystal which includes both iron-boracite (I.B.) and ericaite (Er). The inset shows the crystal outline and the position of the analysis points (a-h) marked on the composition diagram. IB and Er adjacent to the composition points indicate whether the crystal is iron-boracite or ericaite respectively. (B) gives the variation in cation oxide in complete iron-boracite and ericaite crystals adjacent to the mixed crystal of (A) in the aggregate within iron-boracite nodule. The inset shows the analysis points in crystal B12. (C) shows the variation in these cation oxides in ericaites co-existing with iron-boracites in (D) in an aggregate in nodule 4. (D) shows the variation in composition of iron-boracites co-existing with ericaite crystals in (C). The majority of the iron-boracite and ericaite crystals show considerable variation in composition but they have similar ranges in compositions. B9 - crystal identification; C = analysis point in the centre of the crystal; M = analysis point between the centre and the edge; E = analysis point at the edge of the crystal.



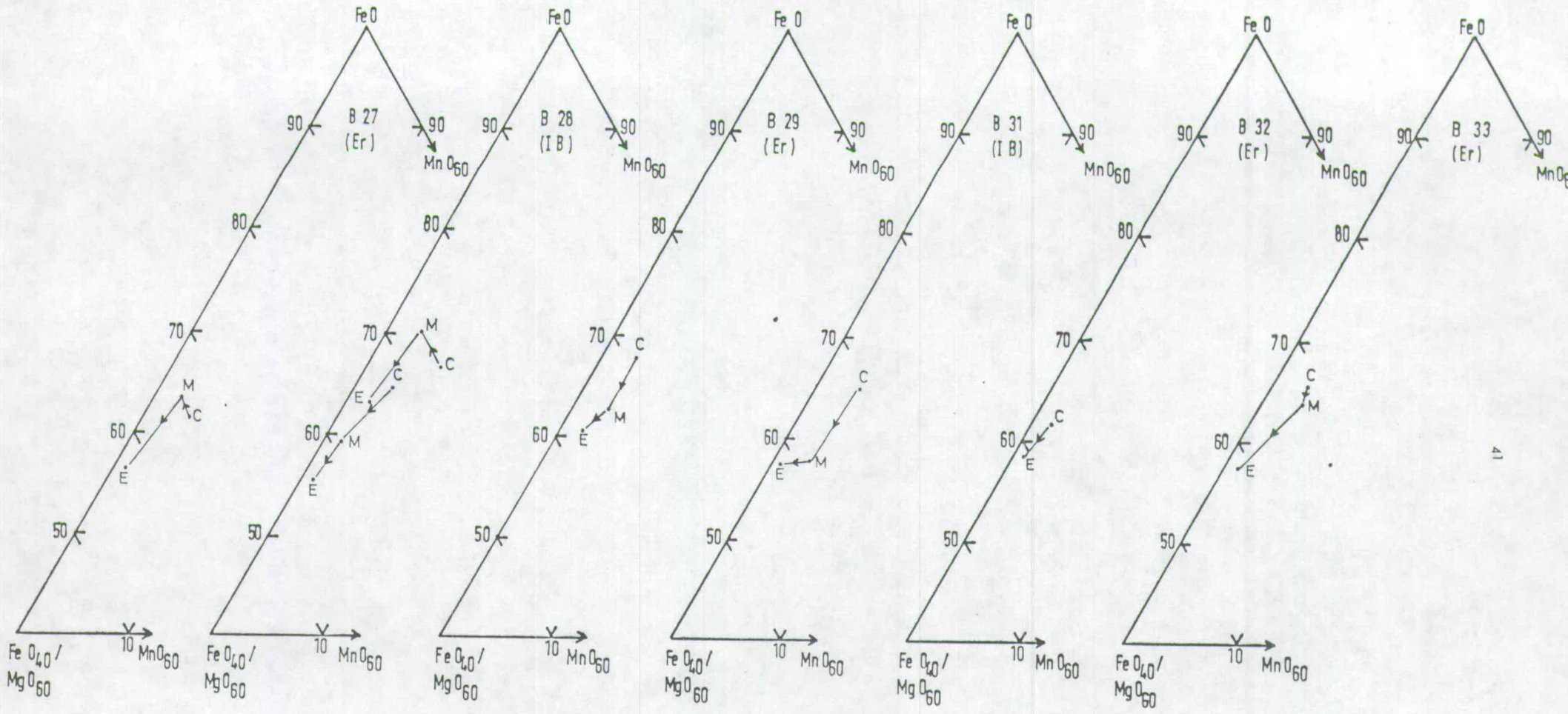


Figure 5.16

Parts of triangular diagrams showing the variations in apparent concentration of MgO, FeO and MnO (recalculated to 100% and determined using the electron microprobe), of points in 6 ericaite and iron-boracite crystals scattered in a parahilgardite nodule. B27 = crystal identification; Er = ericaite; I.B. = iron-boracite; C = analysis in the centre of the crystal; M = analysis between the centre and edge of the crystal; E = analysis at the edge of the crystal.

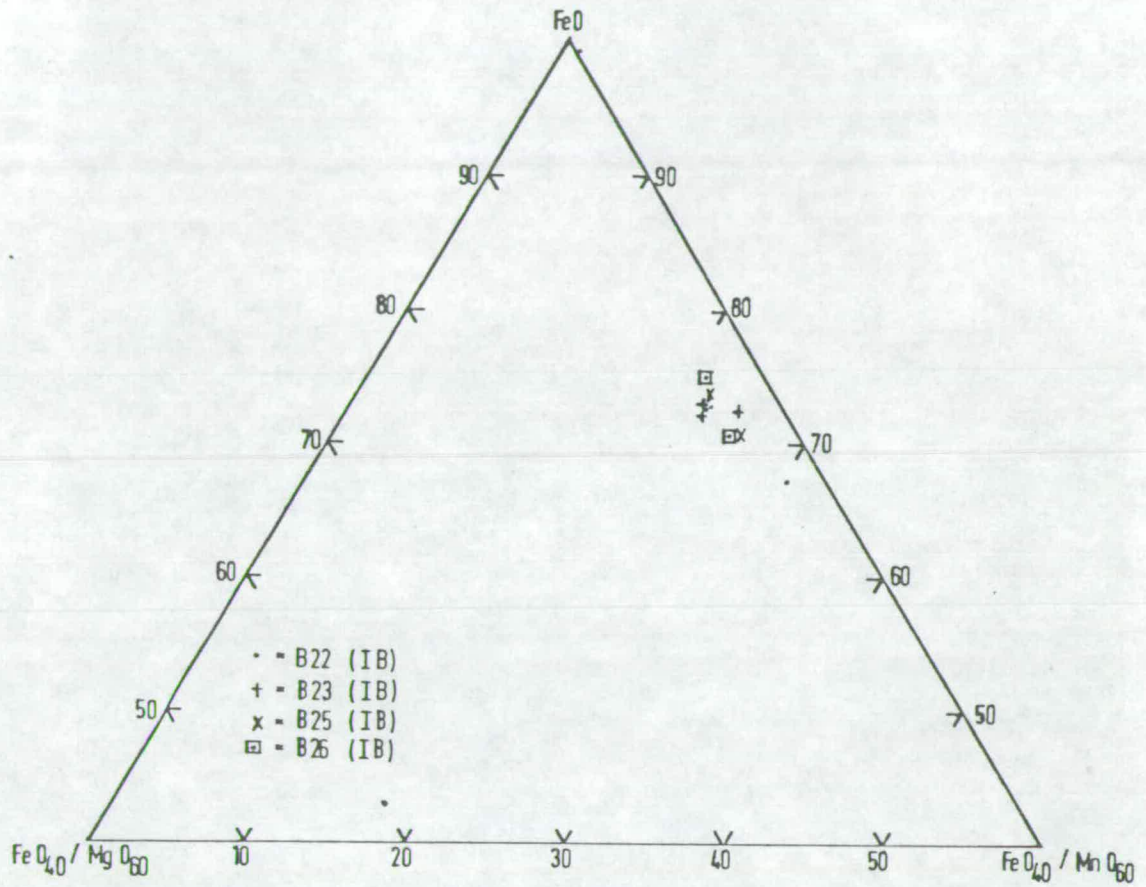


Figure 5.17

Part of an FeO-MgO-MnO triangular diagram showing the variation in apparent concentrations (analyses determined on the electron microprobe) of these cation oxides (recalculated to 100%) in remnant iron-boracite crystals from the S-20 borehole. The crystals show little variation in composition both internally and between crystals. I.B. = iron-boracite.

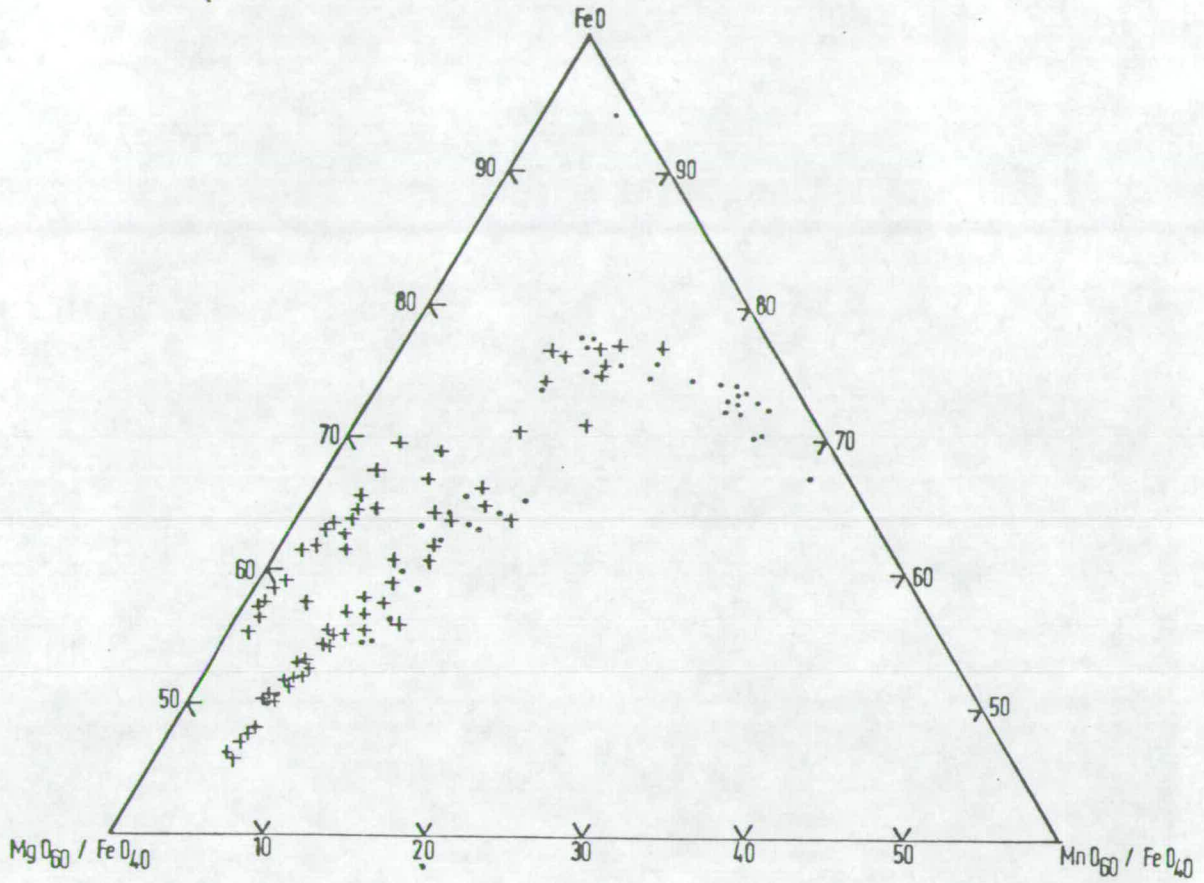


Figure 5.18

Plot of all the apparent concentrations of MgO, MnO and FeO (recalculated to 100%) in the iron-boracite and ericaite crystals analysed using the electron microprobe analyser.
 + = ericaite analyses; • = iron-boracite analyses.

Figure 5.19

Photomicrograph of the junction between a parahilgardite nodule and its host rock. Both the host rock and the nodule are composed of aggregated rosettes of parahilgardite although they are much smaller in the host rock. The black mineral around the outer edge of the nodule is halite. Scale x 7; crossed polars.

Figure 5.20

Photomicrograph of a part of a parahilgardite rosette in a nodule. The rosette outline is on the right of the picture. Note the 'V' shaped extinction bands in the dark central crystals and the lamellae in the adjacent crystals. Scale x 120; crossed polars.

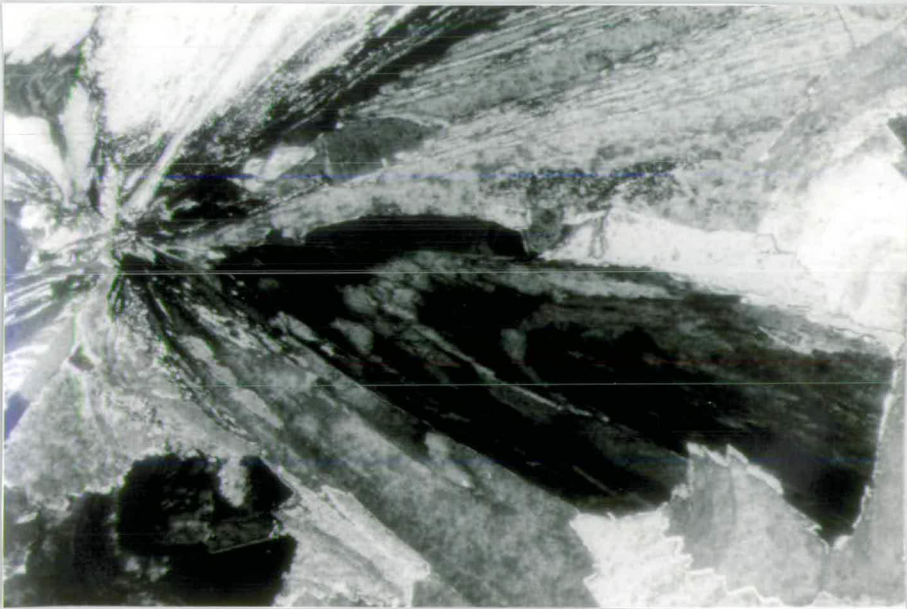
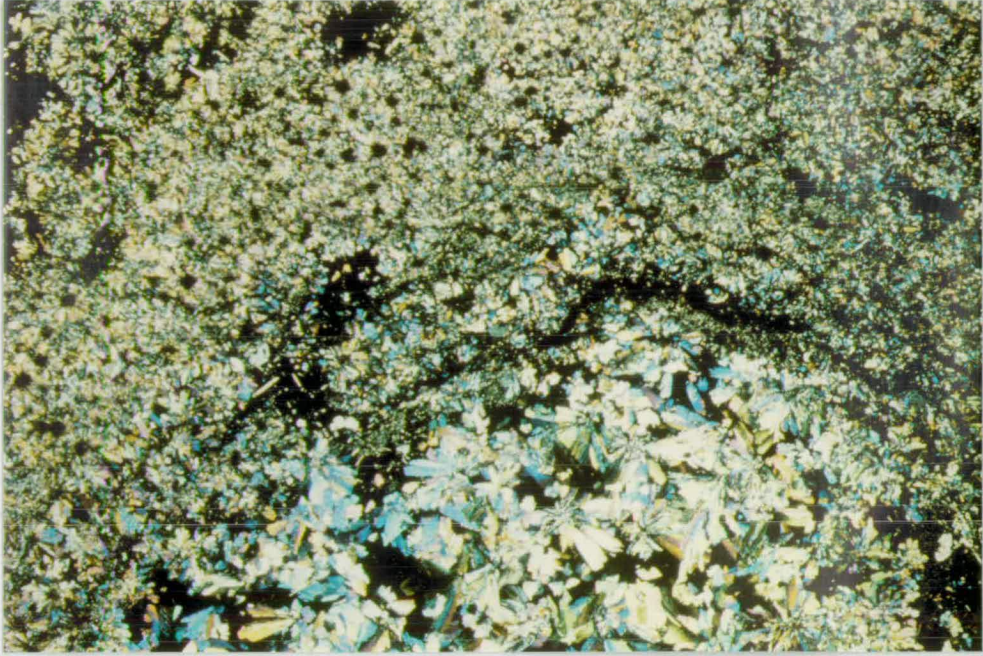
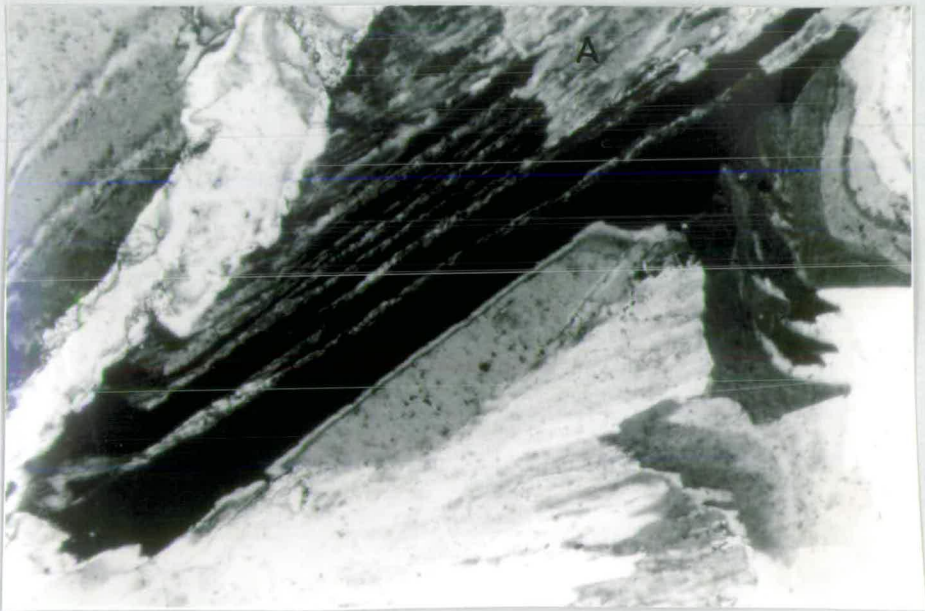


Figure 5.21

Photomicrograph of parahilgardite crystals in which the extinction bands resemble "ostrich plumes". The black background is sylvite. Scale x 75; cross-polars.

Figure 5.22

Photomicrograph of deformation lamellae in nodular parahilgardite. Some of the lamellae vary in thickness and pinch-out. In area A of the crystal many of these lamellae have coalesced to give the crystal a turbid appearance. Scale x 120; crossed polars.



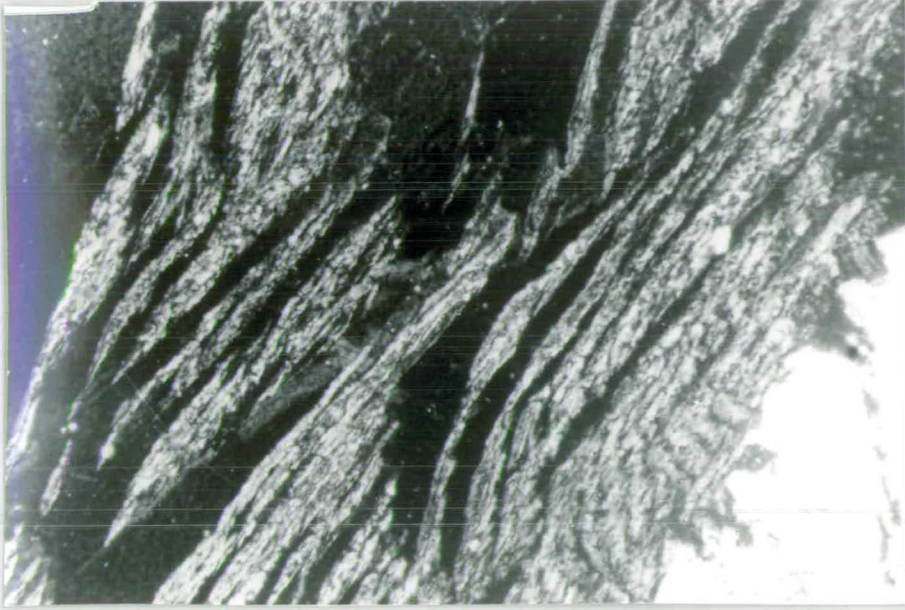


Figure 5.23

Photomicrograph of a parahilgardite crystal in which many of the deformation lamellae have coalesced. Some of the lamellae are curved whilst others are straight and their thickness is variable. Scale x 120; crossed polars.

Figure 5.24

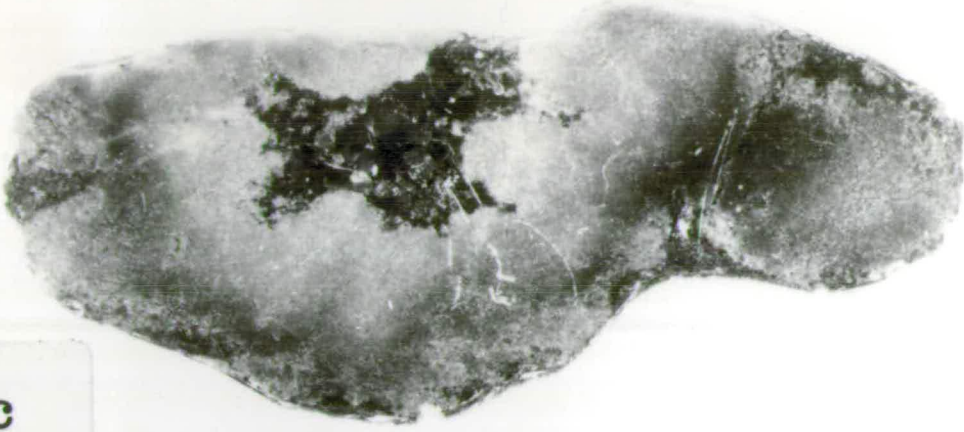
Three typical nodules from the area of iron-boracite nodules (Figure 5.9) in bed B.S.3.

- (C) An iron-boracite-sylvite nodule in which sylvite is enclosed in the centre of a large number of iron-boracite aggregates which have coalesced.

- (B) An iron-boracite-sylvite-magnesite nodule composed of aggregates of iron-boracite crystals (light coloured) set in a matrix of sylvite and magnesite.

- (A) A sylvite-magnesite nodule composed of randomly orientated sheaves of magnesite set in a matrix of red sylvite. (iron-boracite is only an accessory mineral in this nodule).

c

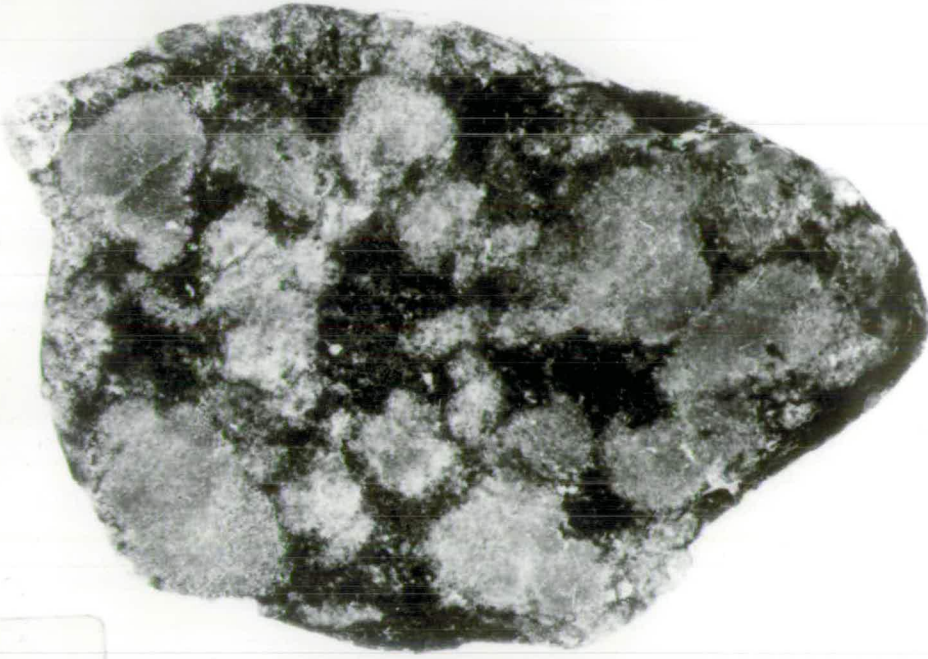


5cm

0



b



a



Figure 5.25

Photomicrograph of an almost pure iron-boracite nodule composed largely of granular crystals. Note the presence of small quantities of interstitial clay (black). The white around the edge of the picture is glass of the thin section. Scale x 5; plane polarized light.

Figure 5.26

Photomicrograph of 2 nodules from the iron-boracite nodule area of bed B.S.3. The nodule in the centre of the picture is composed of iron-boracite (grey cubes), sylvite (red), halite (white), magnesite (grey laths) and clays (black). Halite encloses similarly orientated sylvite grains indicating that the former is a replacement mineral. Magnesite plates, which project from the sylvite cleavage into adjacent halite crystals become discontinuous. The iron-boracite crystals have only been replaced on a small scale. Note the clay in the kernels of many of the iron-boracite crystals. Scale x 5; plane polarized light.

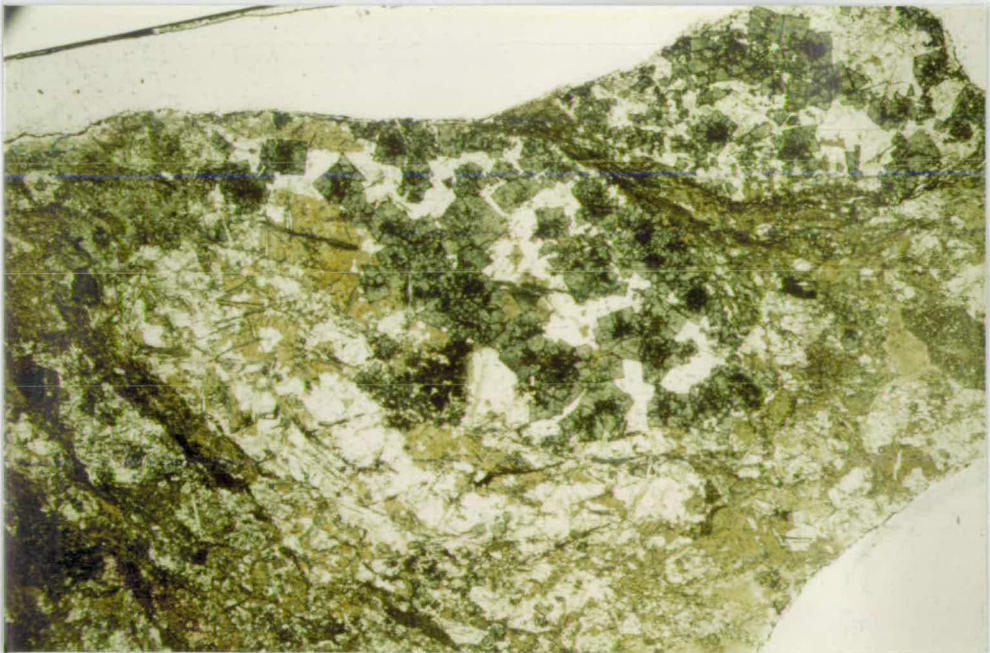
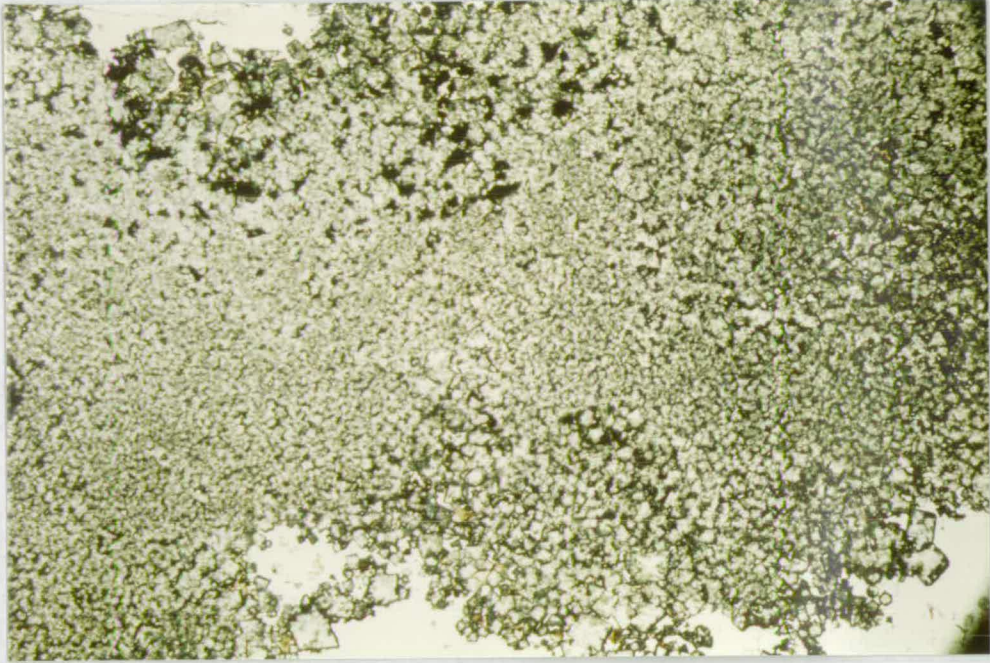


Figure 5.27

Photomicrograph of anhedral sylvite crystals with rims of hematite and occasional mud inclusions round their outside enclosed in aggregated iron-boracite crystals. Note the stringers of hematite crystals do not always follow the intergranular boundaries. Scale x30; plane polarized light.

Figure 5.28

Photomicrograph of a sylvite (black), magnesite (large laths (plates in cross-section)), talc (small laths (plates in cross-section)) rock, from an iron-boracite-sylvite-magnesite nodule. The talc and some of the magnesite crystals define the former cleavages of sylvite in a north-westerly to south-easterly, and north-easterly to south-westerly directions. The two largest magnesite plates (grey), orientated in a north-north-westerly to south-south-easterly direction define the present cleavage of the sylvite crystal. See Table 5.15 for explanation. Scale x 74; crossed polars.

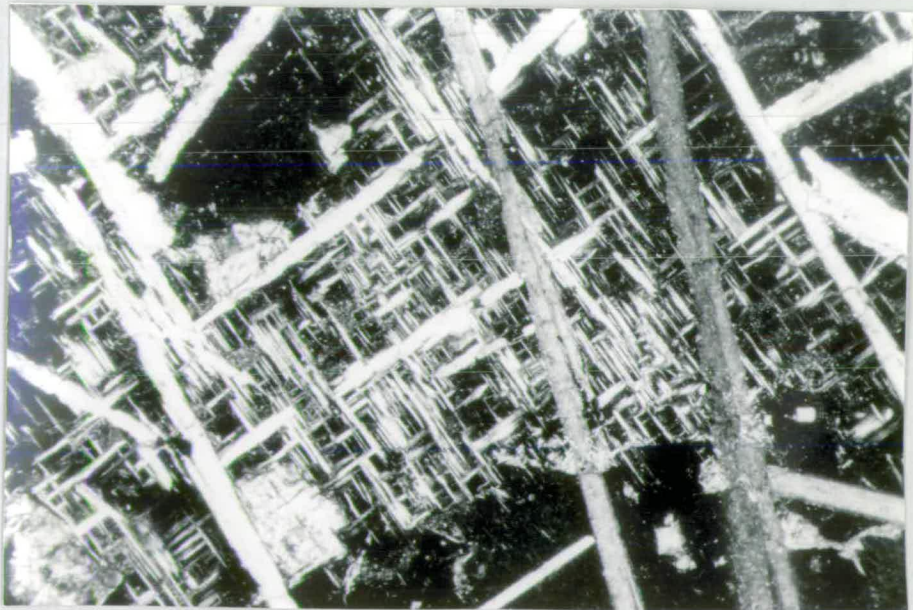
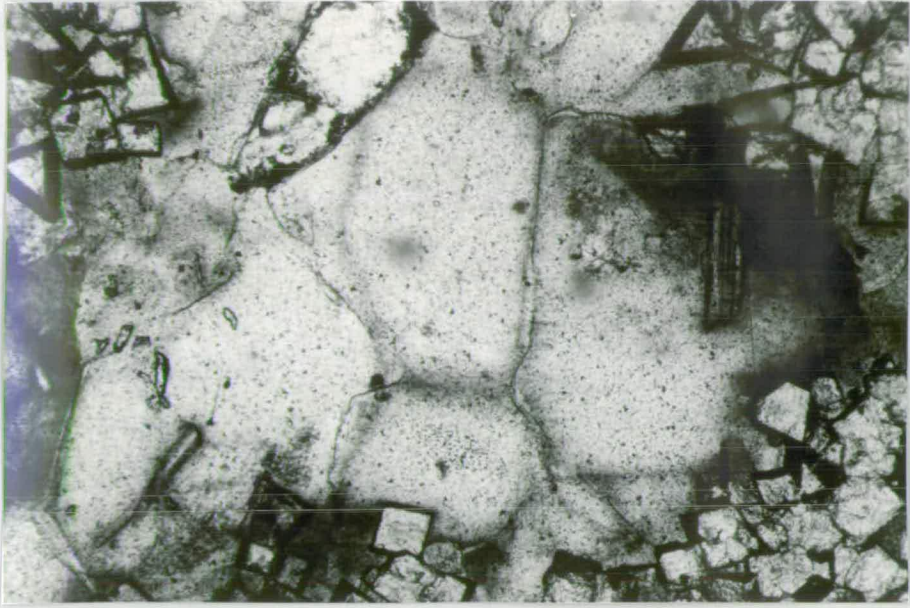


Figure 5.29

Photomicrograph of magnesite plates (white) which have been partially replaced by sylvite (black) in a sylvite-magnesite nodule. The very fine grained plates (laths in cross-section) cutting across the magnesite towards the bottom of the picture are talc. They may have replaced the magnesite, or, they may have grown in the cleavage of replacive sylvite. Scale x 60; crossed polars.

Figure 5.30

Photomicrograph of remnant iron-boracite cubes which have been almost completely replaced by sylvite (grey) in an iron-boracite-sylvite-magnesite nodule. Notice the sylvite has not replaced the magnesite plates (laths with high relief) which have grown in its cleavage. Scale x 30; plane polarized light.

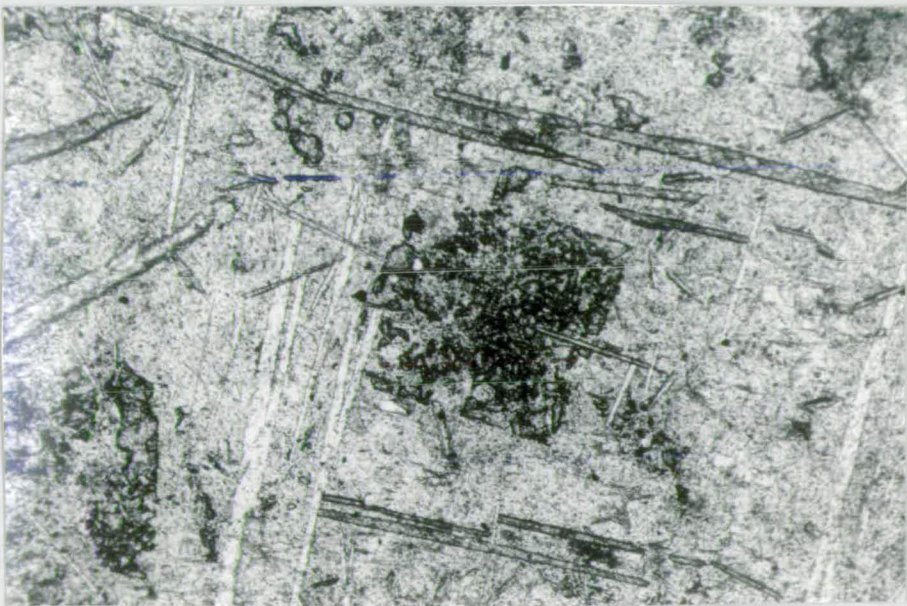
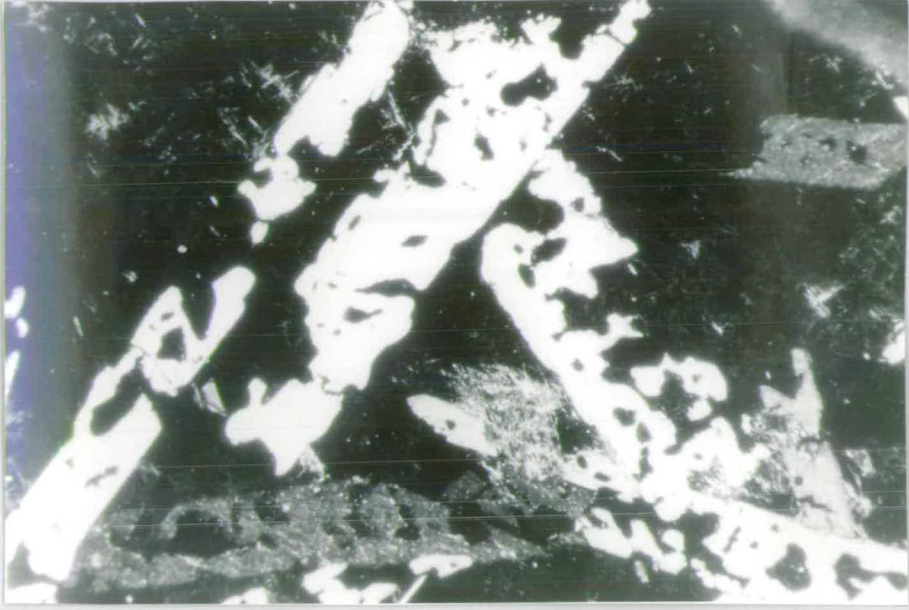


Figure 5.31

Diagram showing sylvite and sheaves of magnesite which have been partially replaced by colourless halite near the outer edge of a sylvite-magnesite-halite nodule. Stippled crystals = magnesite; crystals with the cubic cleavage and hatched edges = sylvite; unornamented crystals with the cubic cleavage = halite. Scale x 37.

Figure 5.32

Photomicrograph of small rosettes of parahilgardite (white, high relief) in the parahilgardite nodule host rock. Many of the rosettes have centres of clay (black) or sylvite (grey). The parahilgardite crystals appear to have grown by displacement. The bright white anhedral crystals at the top of the picture are halite. Scale x 30; plane polarized light.

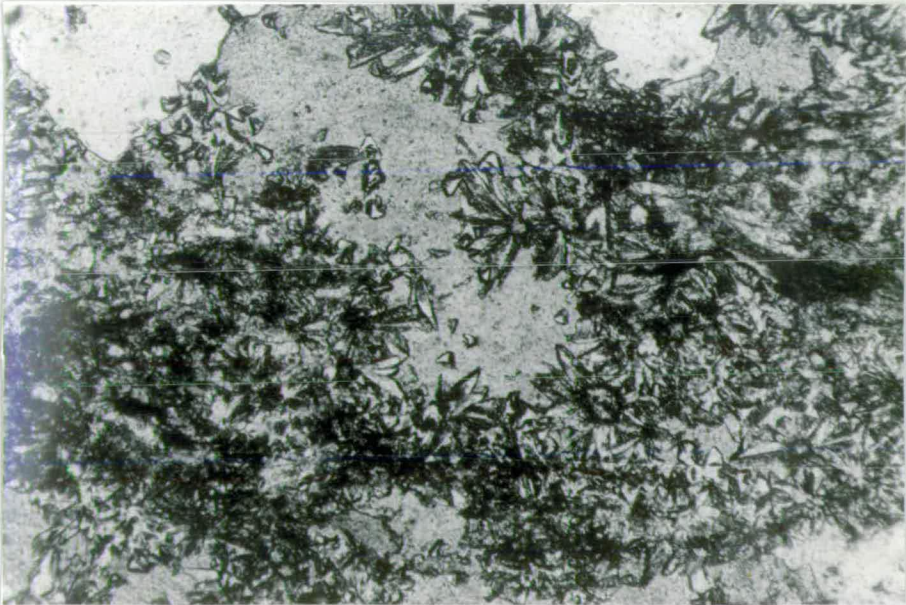
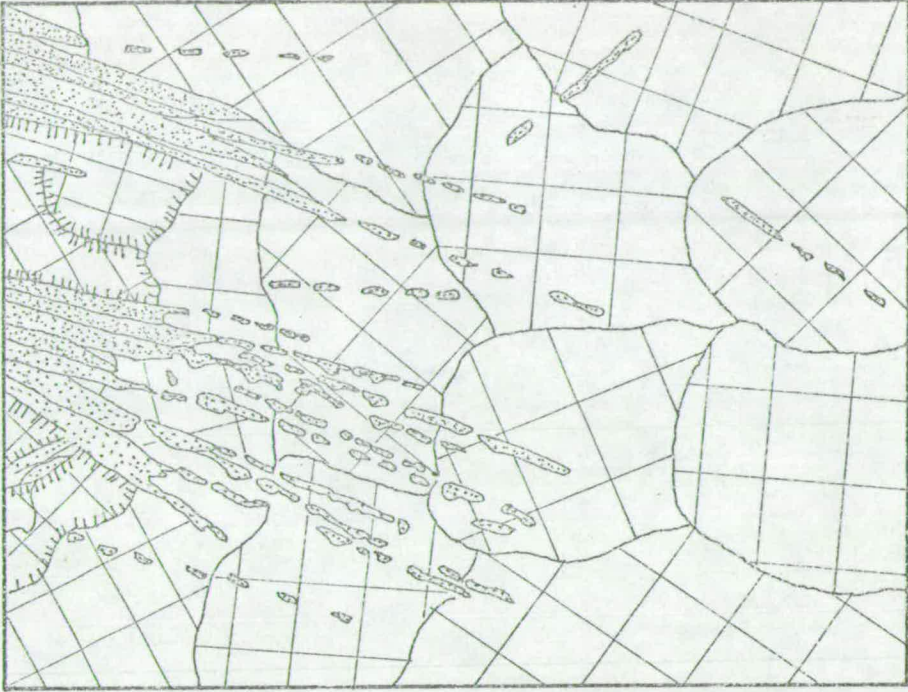


Figure 5.33

Photomicrograph of aggregated rosettes of parahilgardite in a parahilgardite nodule. The black interstitial mineral is sylvite. Scale x 10; crossed polars.

Figure 5.34

Photomicrograph of parahilgardite rosettes near the outsides of a nodule which have been replaced by colourless halite (black). Often the halite has replaced the lamellar parahilgardite. Scale x 15; crossed polars.

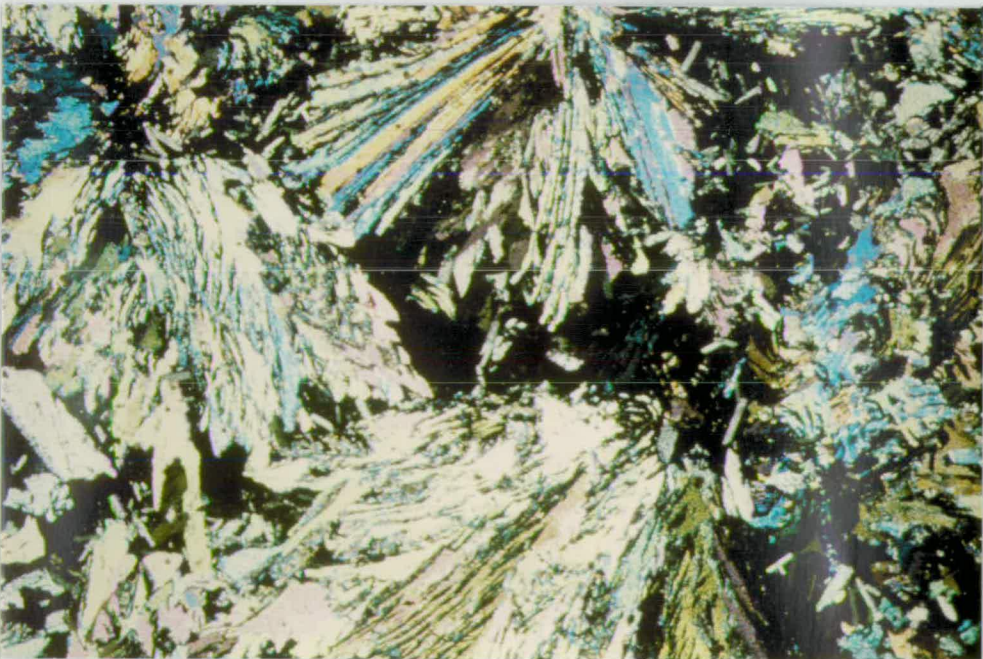


Figure 5.35

Chemical, Modal and Mineralogical data for the sequence examined in the S-20 borehole.

- (a) Variation in the principal chemical components of the S-20 borehole; calculated from chemical analyses of samples analysed at Newcastle University.
- (b) Volume percentages of the principal minerals of the S-20 borehole; determined by modal analysis of 45 thin sections over the given depth range.
- (c) Distribution of the major and minor minerals observed in 45 thin sections of these rocks.

KEY

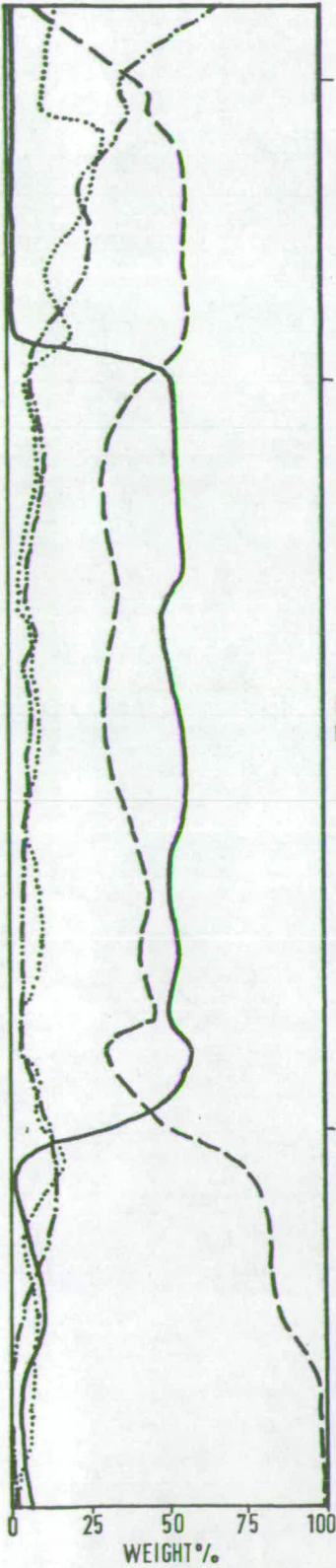
- WATER SOL. Ca SO₄
- WATER SOL. K Cl
- - - WATER SOL. NaCl
- · - · - INSOLUBLE RESIDUES

KEY

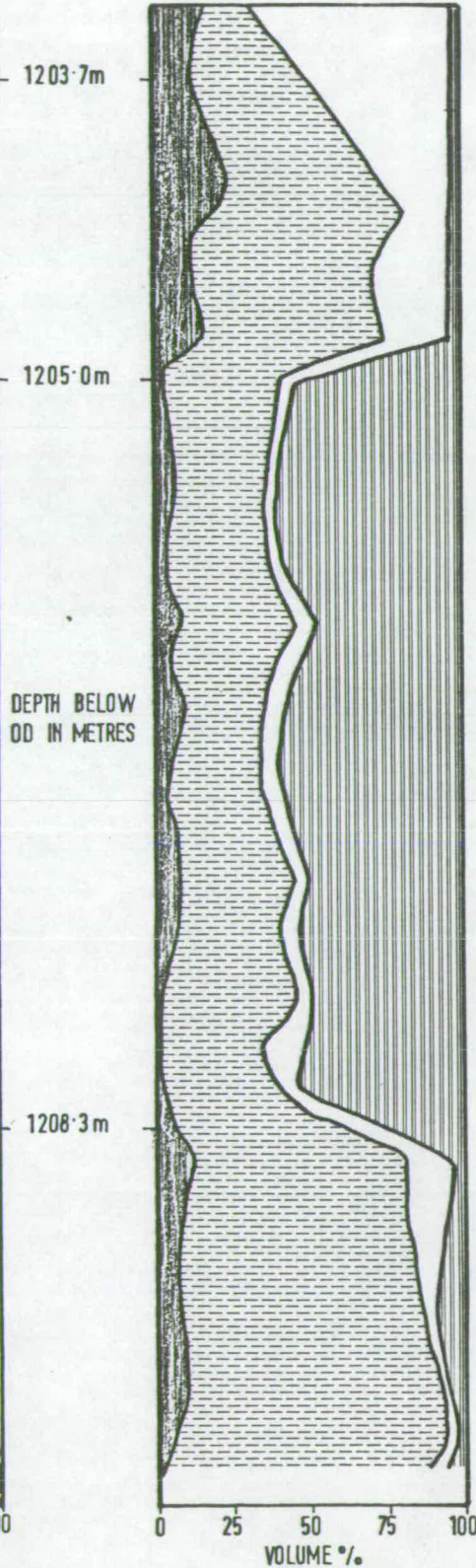
- VOLUME% ANHYDRITE
- " " NaCl
- " " CLAYS
- " " SYLVITE

KEY

- A - Anhydrite
- N - NaCl
- C - Clays
- SY - KCl
- MG - MgCO₃
- B - Iron boracite
- Q - Quartz

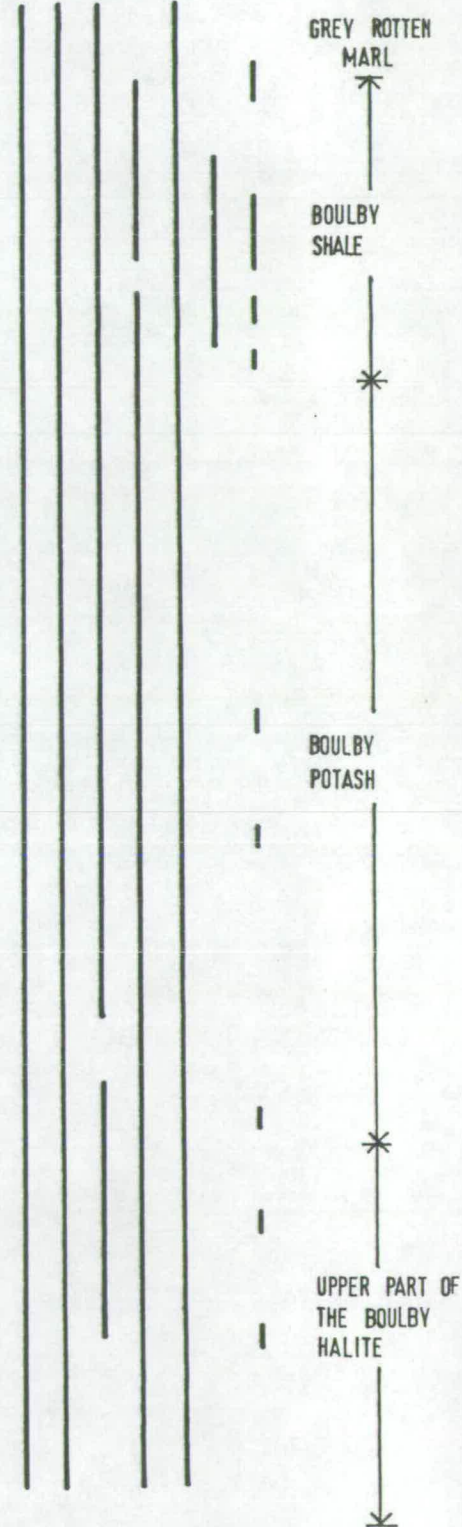


(a)



(b)

A N C SY MG B Q



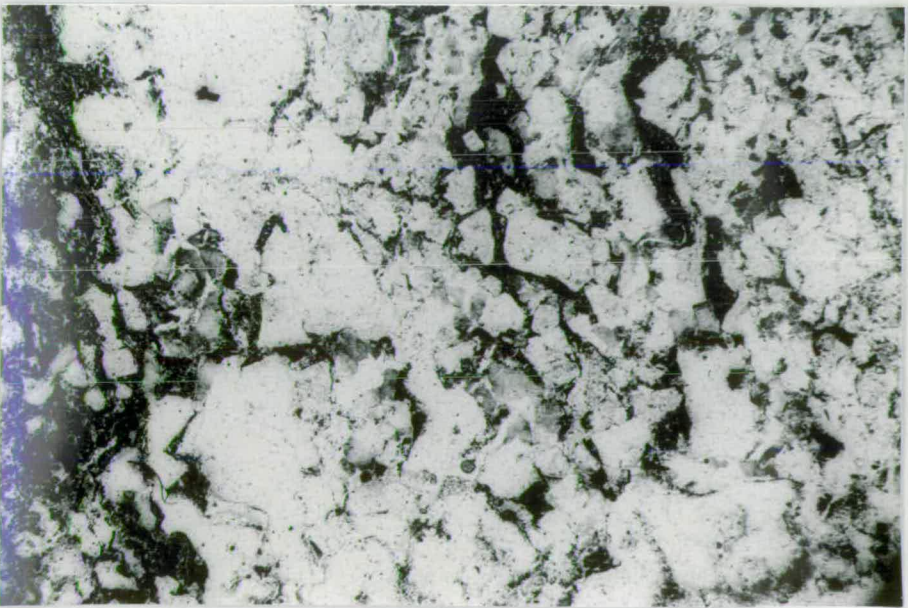
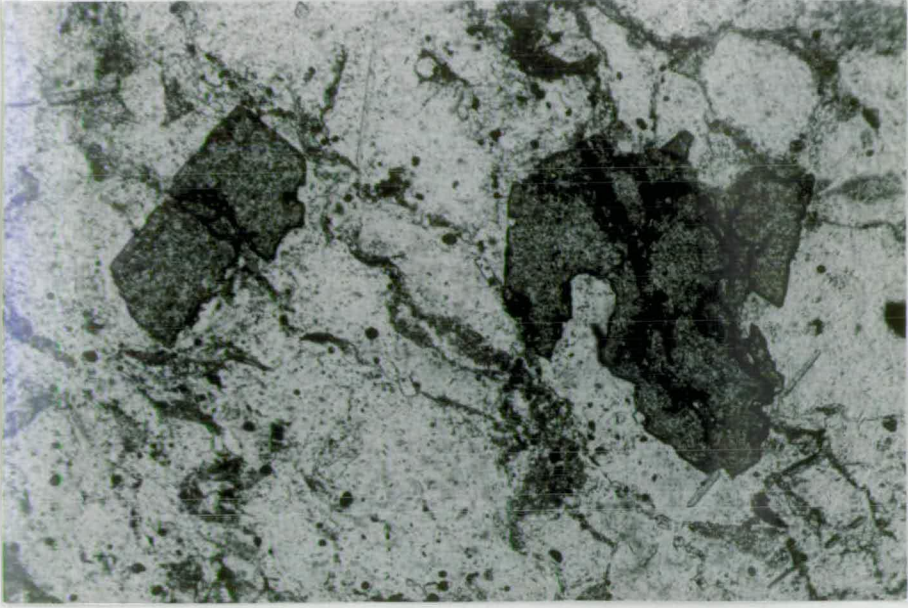
(c)

Figure 5.36

Photomicrograph of 2 typical remnant crystals of iron-boracite (grey and high relief) which are all that remain of the iron-boracite nodules in the area of the Mine enclosed by roadways 2E, 2S, 5W and 3N since their replacement by halite. Notice that many of the clay laminae (grey with low relief) are laterally discontinuous due to disruption by halite. The texture, less the iron-boracite crystals is also typical of bed B.S.4. in this area of the Mine. Scale x 15; plane polarized light.

Figure 5.37

Photomicrograph of a halite-clay rock from bed B.S.5. in the area of the Mine enclosed by roadways 2E, 2S, 5W and 3N. On the left hand side of the picture typical small halite porphyroblasts containing hematite (clouded appearance) are set in a matrix of clays. However in the centre secondary colourless halite encloses fragments of the clays and the clouded halite. It has partially replaced these minerals in this rock. Scale x 12; plane polarized light.



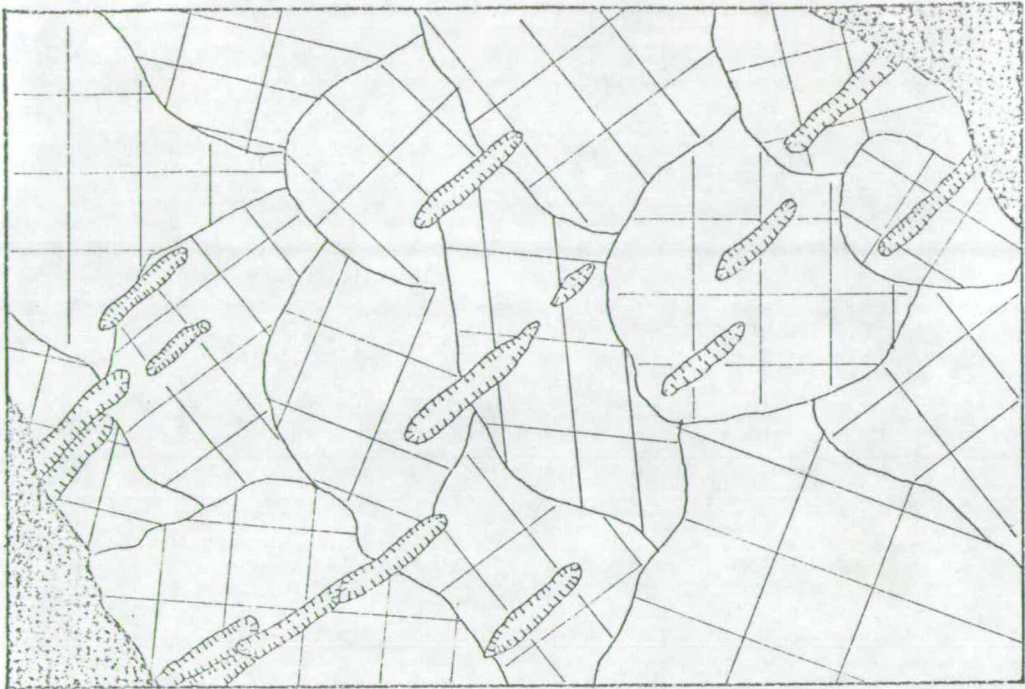


Figure 5.38

Diagram of part of a sylvinite vein from the East Spearhead. Parallel aligned elongate sylvite crystals, in similar optical orientation, are totally enclosed in granular halite which appears to have replaced sylvite. Sylvite = elongate crystals with hatched boundaries; halite = unornamented crystals with cubic cleavage; clay-shale sidewalls of the vein = heavy stipple. Scale x 5.

FIGURES FOR CHAPTER 6

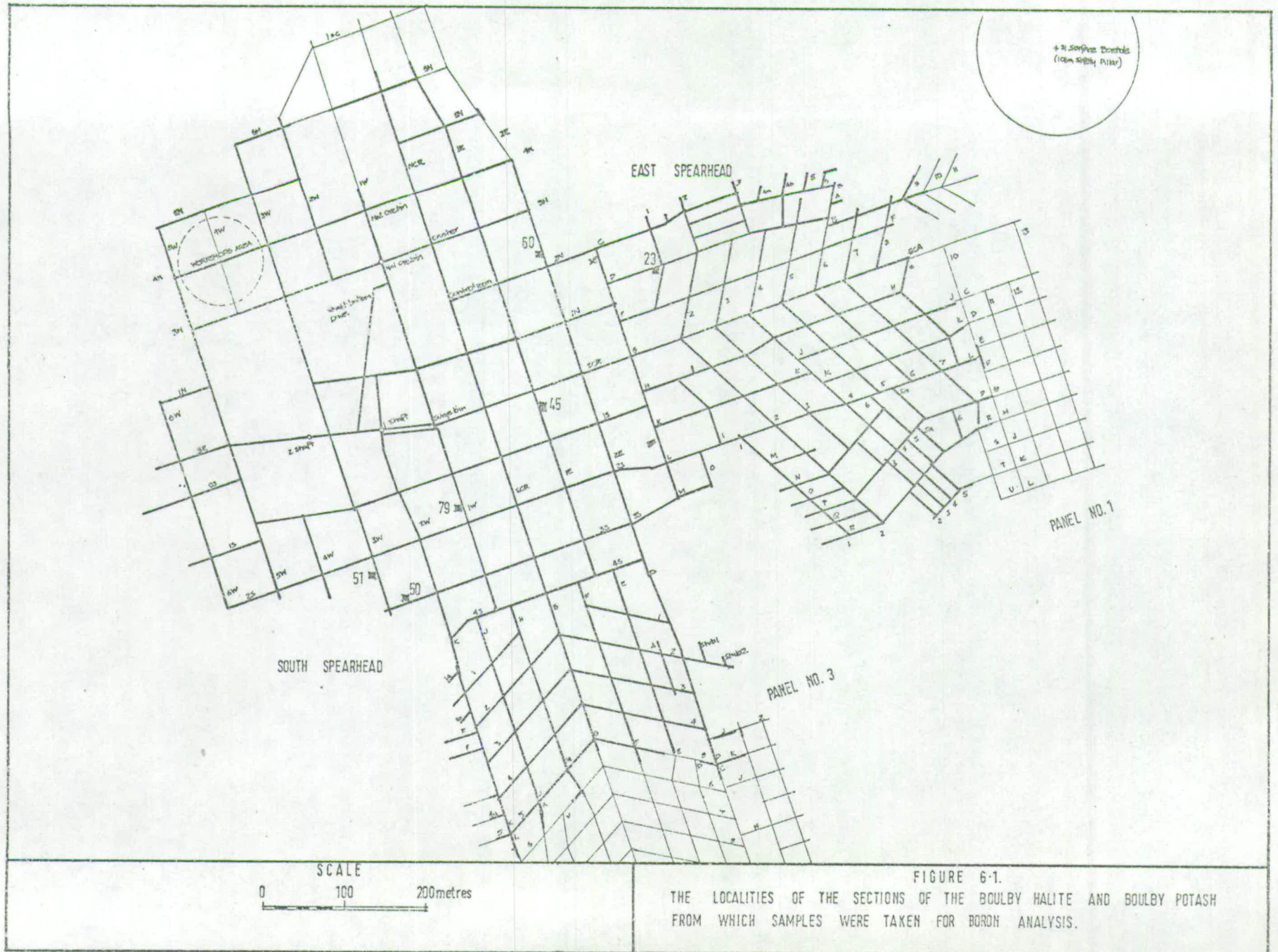
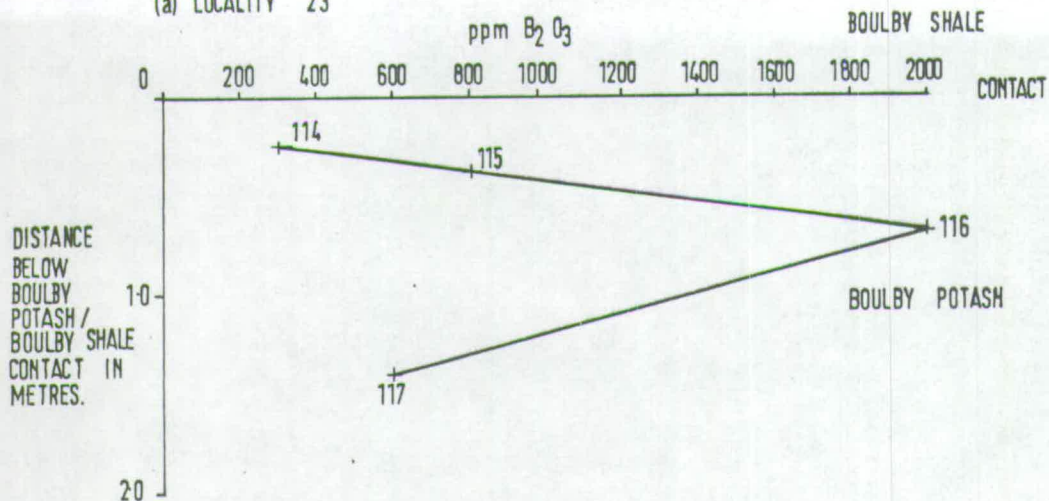


FIGURE 6-1.
THE LOCALITIES OF THE SECTIONS OF THE BOULBY HALITE AND BOULBY POTASH
FROM WHICH SAMPLES WERE TAKEN FOR BORON ANALYSIS.

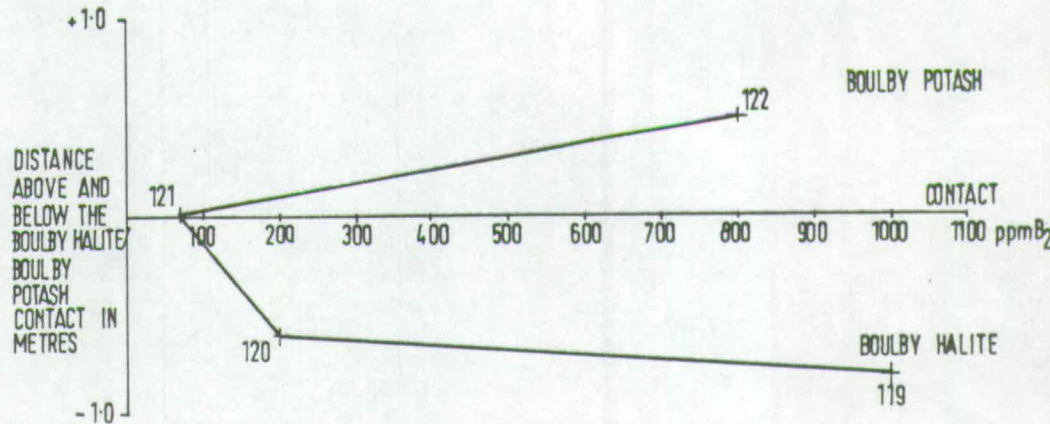
Figure 6.2

Profiles of the boron content of 6 sections through the Boulby Halite and Boulby Potash. The localities of the profiles are shown in Figure 6.1.

(a) LOCALITY 23

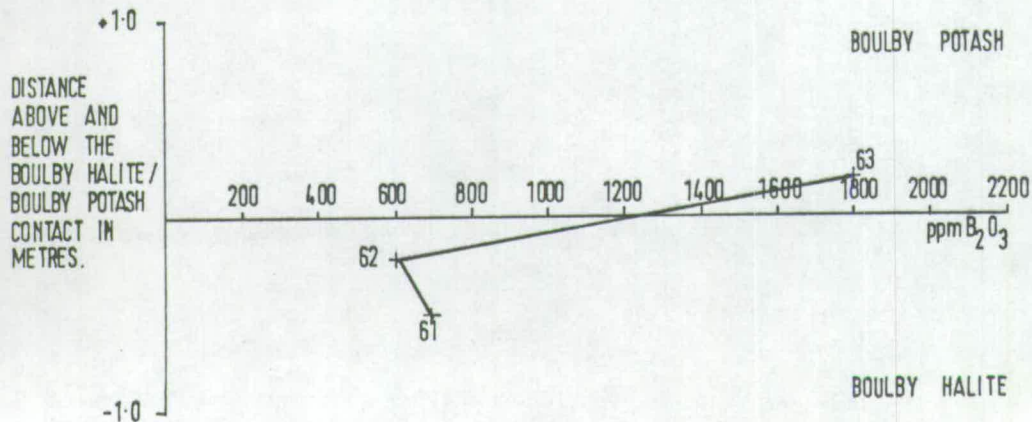


(b) LOCALITY 60

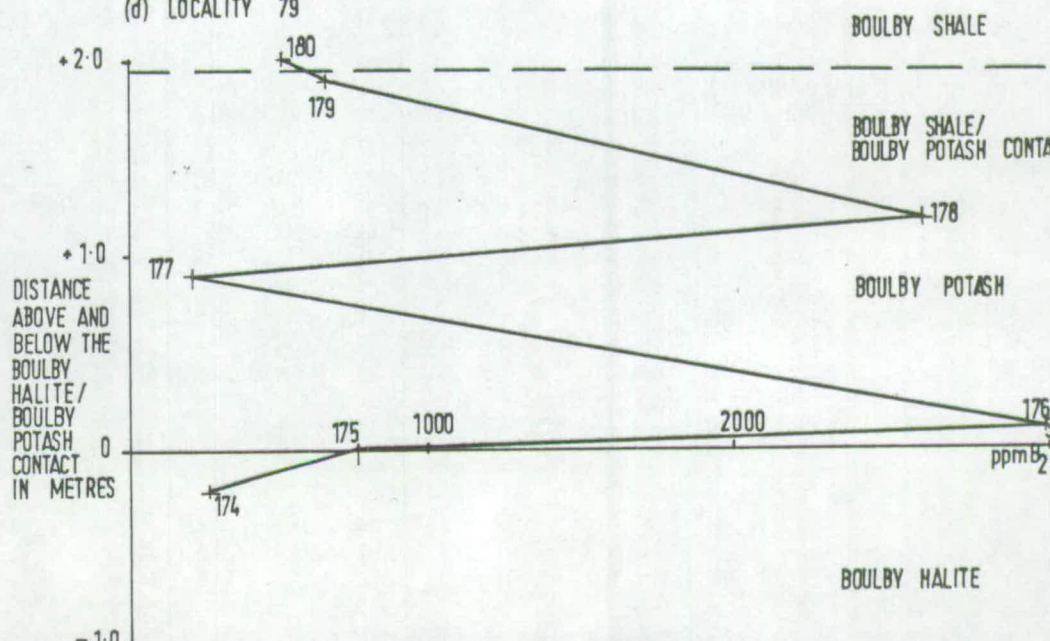


58

(c) LOCALITY 45

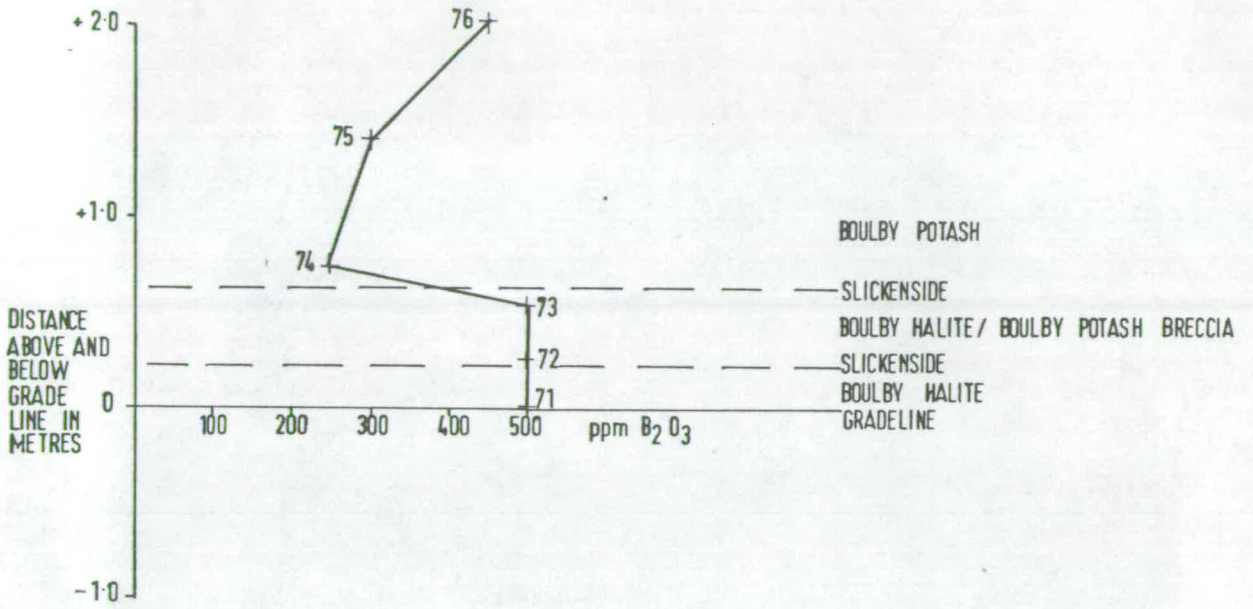


(d) LOCALITY 79



(e) LOCALITY 50.

59



(f) LOCALITY 51.

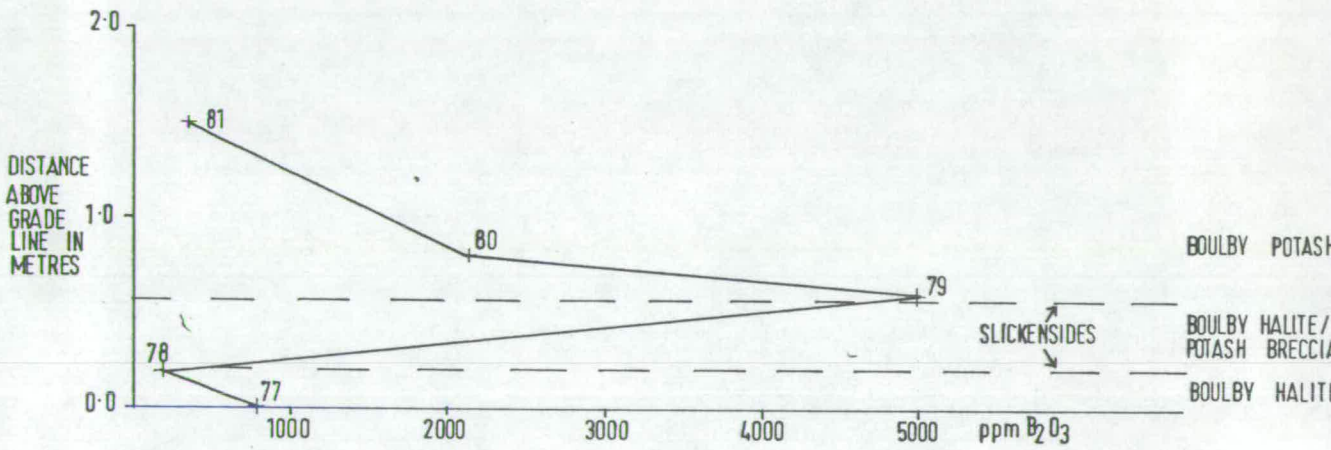


Figure 6.2 (cont)

FIGURES FOR CHAPTER 7

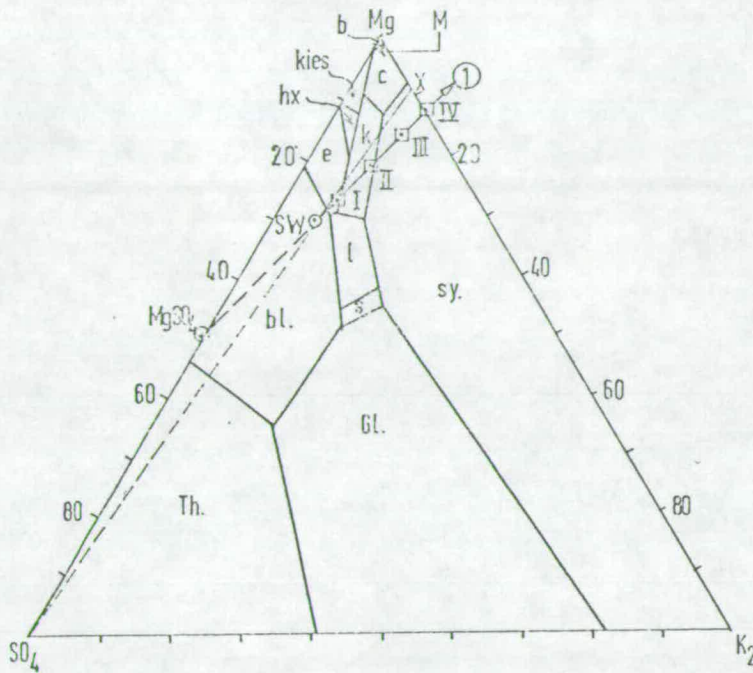


Figure 7.1

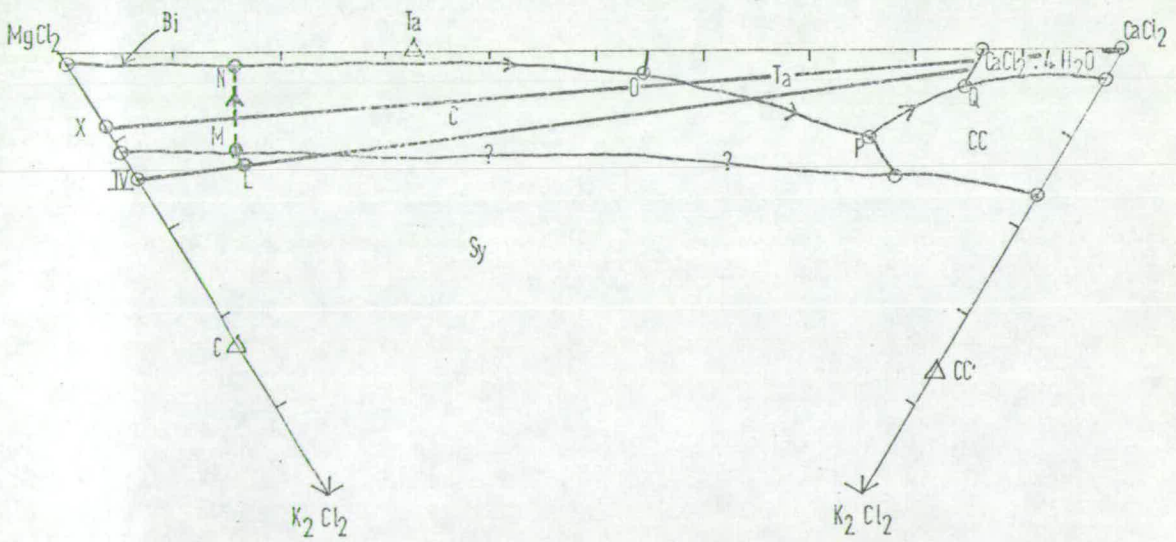
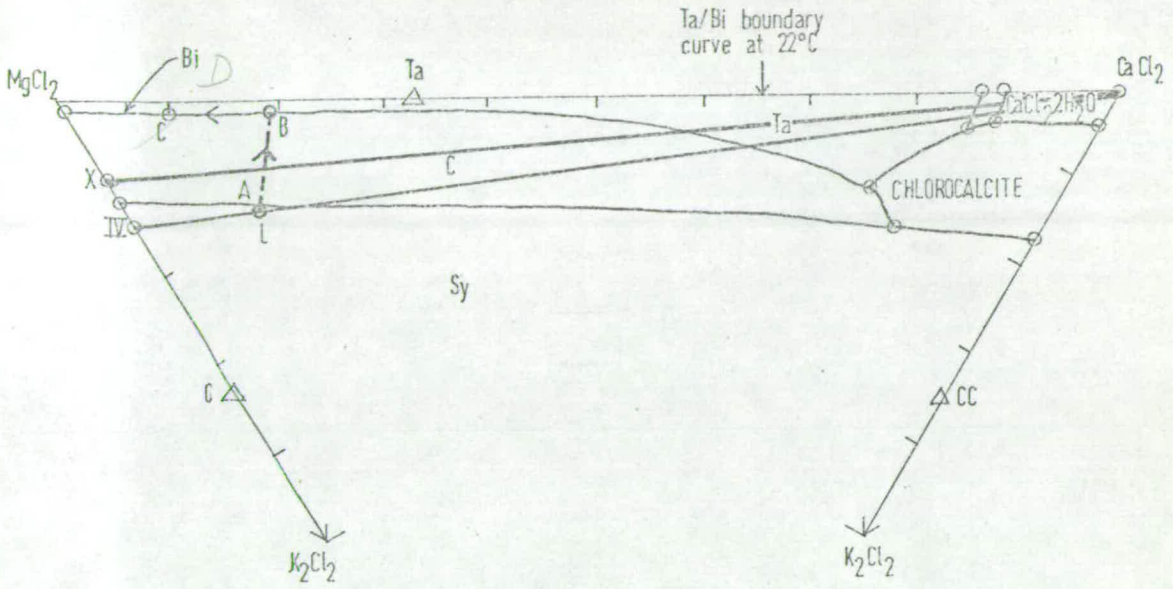
Jänecke ternary diagram for the normal seawater system $\text{MgCl}_2\text{-KCl-NaCl-Na}_2\text{SO}_4\text{-H}_2\text{O}$ at 25°C . The line SW-I-II-III-IV indicates the compositions of seawater resulting from depletion in MgSO_4 . The line S.W-X indicates the compositions of seawater resulting from depletion in (SO_4^{2-}) because of an influx of CaCl_2 solutions or bacterial reduction of (SO_4^{2-}) to H_2S . The system is saturated in NaCl and H_2O is being removed by evaporation. b = bischofite; c = carnallite; kies = kieserite; k = kainite; hx = hexahydrite; e = epsomite; sy = sylvite; l = leonite; s = schoenite; bl = bloedite; Th = thenardite; Gl = glaserite. Potassium chloride is always shown as a double molecule in these systems (Braitsch, 1972).

Figure 7.2

Ternary diagram for the system $\text{MgCl}_2\text{-CaCl}_2\text{-KCl-NaCl-H}_2\text{O}$ at 93°C (Molar %) Calculated by Braitsch (1972) after Assarsson (1957). The points x and IV are as for the system $\text{MgCl}_2\text{-KCl-NaCl-Na}_2\text{SO}_4\text{-H}_2\text{O}$. The system is saturated in NaCl and H_2O is removed by evaporation. Bi = bischofite; Ta = tachyhydrite; c = carnallite; cc = chlorocalcite.

Figure 7.3

Diagrammatic representation of the system $\text{MgCl}_2\text{-CaCl}_2\text{-KCl-NaCl-H}_2\text{O}$ at 35°C (Molar %). The exact position of the sylvite-carnallite boundary curve is uncertain although Braitsch (1972) has suggested it may lie closer to the KCl composition point; but he gave no reason for this suggestion. Symbols as for Figure 7.2.



FIGURES FOR CHAPTER 8

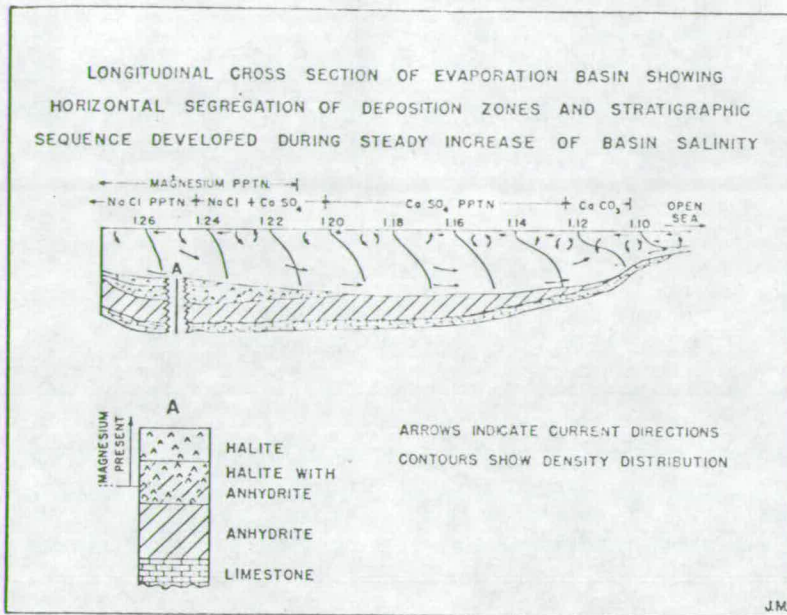


Figure 8.1

Diagrammatic representation of the possible configuration of the basin/lagoon in which the beds of the third Zechstein evaporite cycle may have been deposited. The basin/lagoon would probably have been much more elongate than shown above. Modified after Scruton (1953).

FIGURES FOR CHAPTER 11

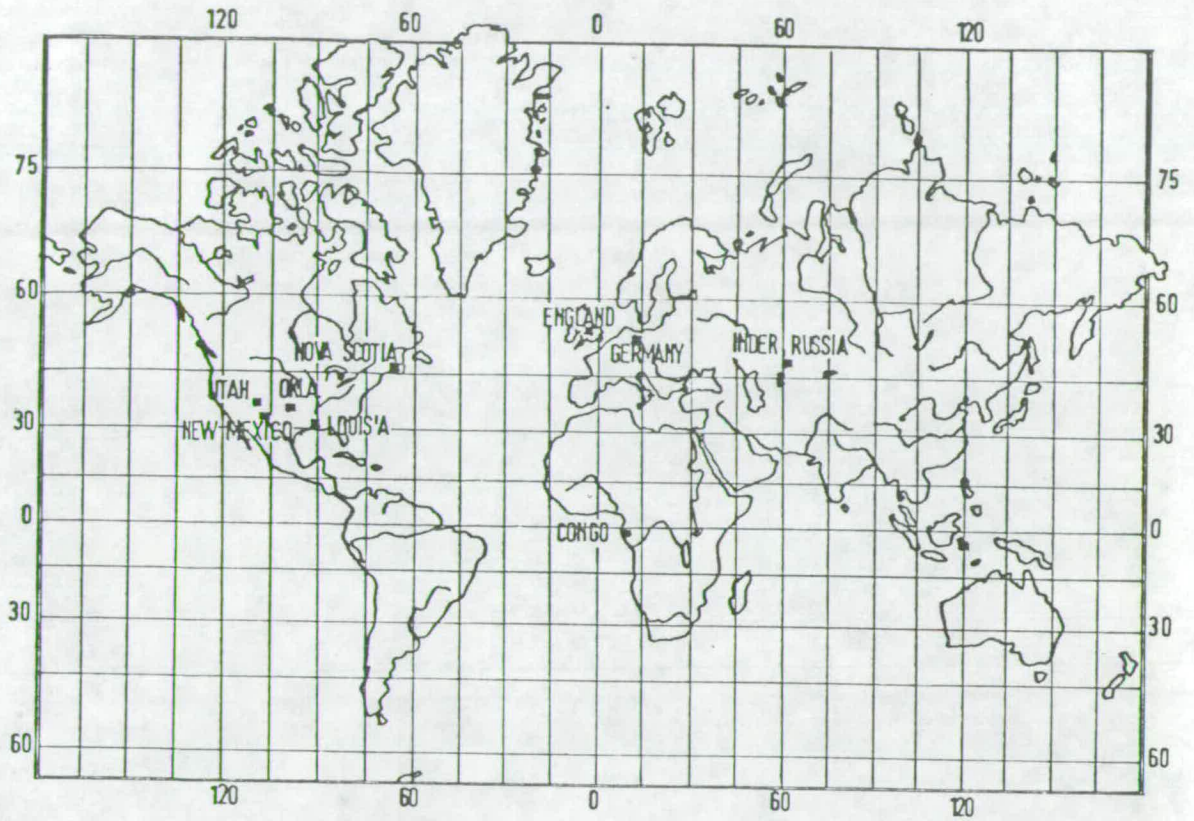


Figure 11.1

Map of the marine borate mineral localities of the world.

Figure 11.2

White stassfurtite nodules in a sylvite-halite rock of the Stassfurt seam in the Salzdettfurth Mine, south of Hanover, north Germany. The nodules are unevenly distributed in the rock and bear little resemblance to the iron-boracite or parahilgardite nodules at Boulby. The large white nodule in the centre of the picture is 15 cm. in width.

Figure 11.3

Photomicrograph of granular to elongate boracite crystals in a stassfurtite nodule. These crystals are unlike the iron-boracite in the nodules of Boulby. Scale x 20; plane polarized light.

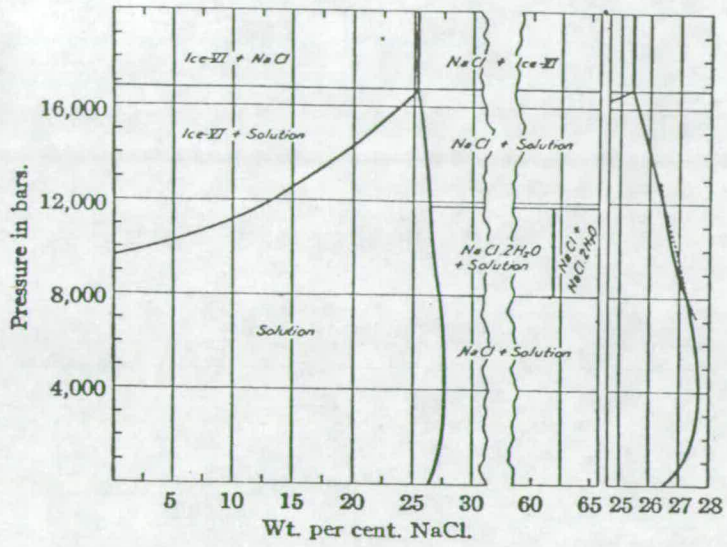


Figure 12.1

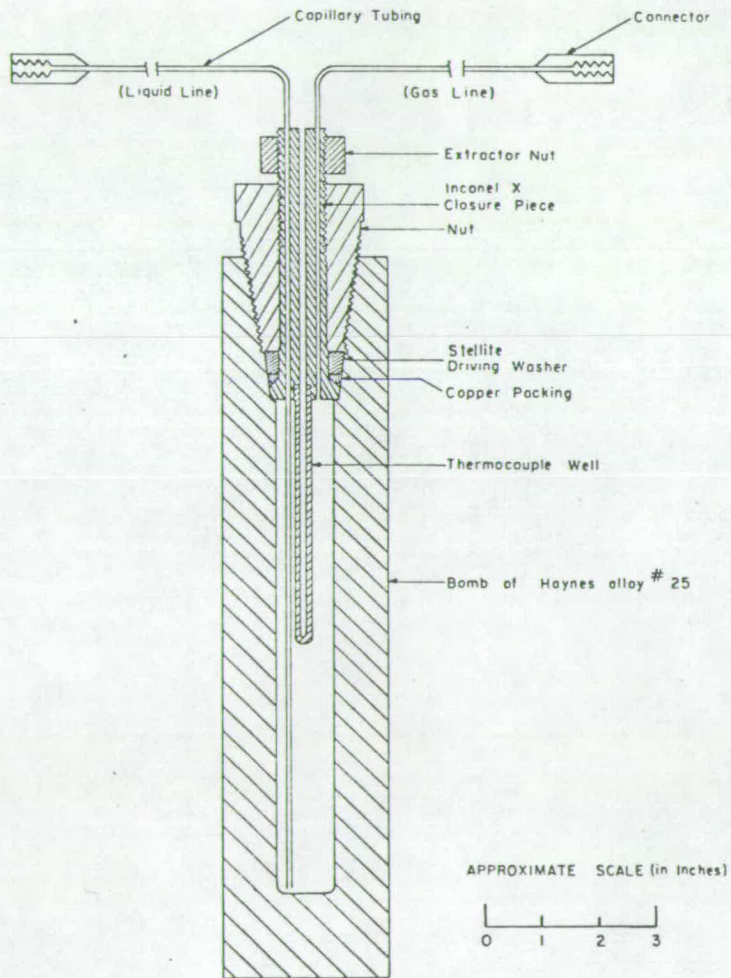
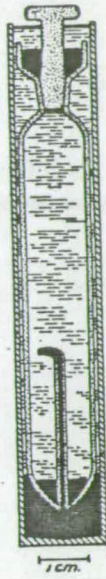
The equilibrium diagram for the system NaCl-H₂O at 25°C and up to 16 kilobars after Adams (1931). The freezing pressure curve and the solubility curve intersect at a pressure eutectic.

Figure 12.2

Piezometer of the type used by Adams (1931) to measure volume changes of solutions. It consists of a bulb of pyrex glass, with a ground glass stopper surrounded by a mercury seal and at the bottom a re-entrant capillary tube drawn down at its top. The bulb is contained in a thin-walled cylindrical capsule of stainless steel which holds up to 3 mls. of mercury.

Figure 12.3

Pressure vessel of the type used by Souririjan and Kennedy (1962).



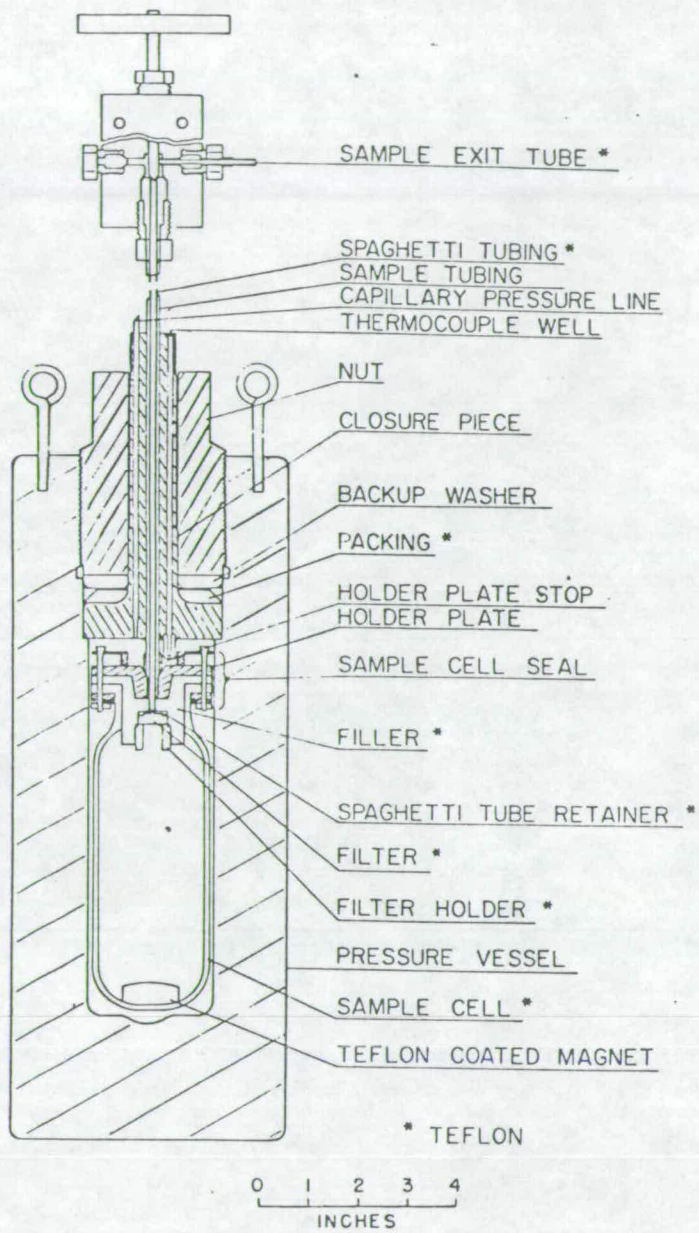


Figure 12.4

Hydrothermal Solution Equipment of the type used by Dickson et al (1963).

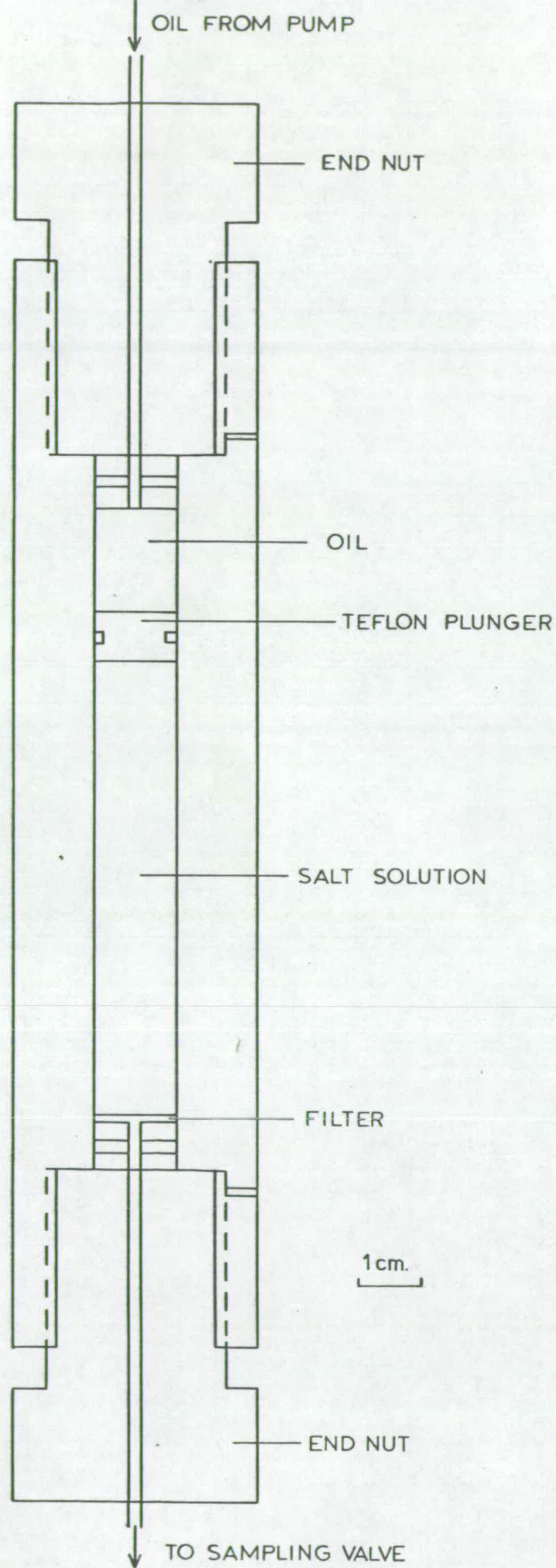


FIGURE 12-5 The pressure vessel used in these experiments .

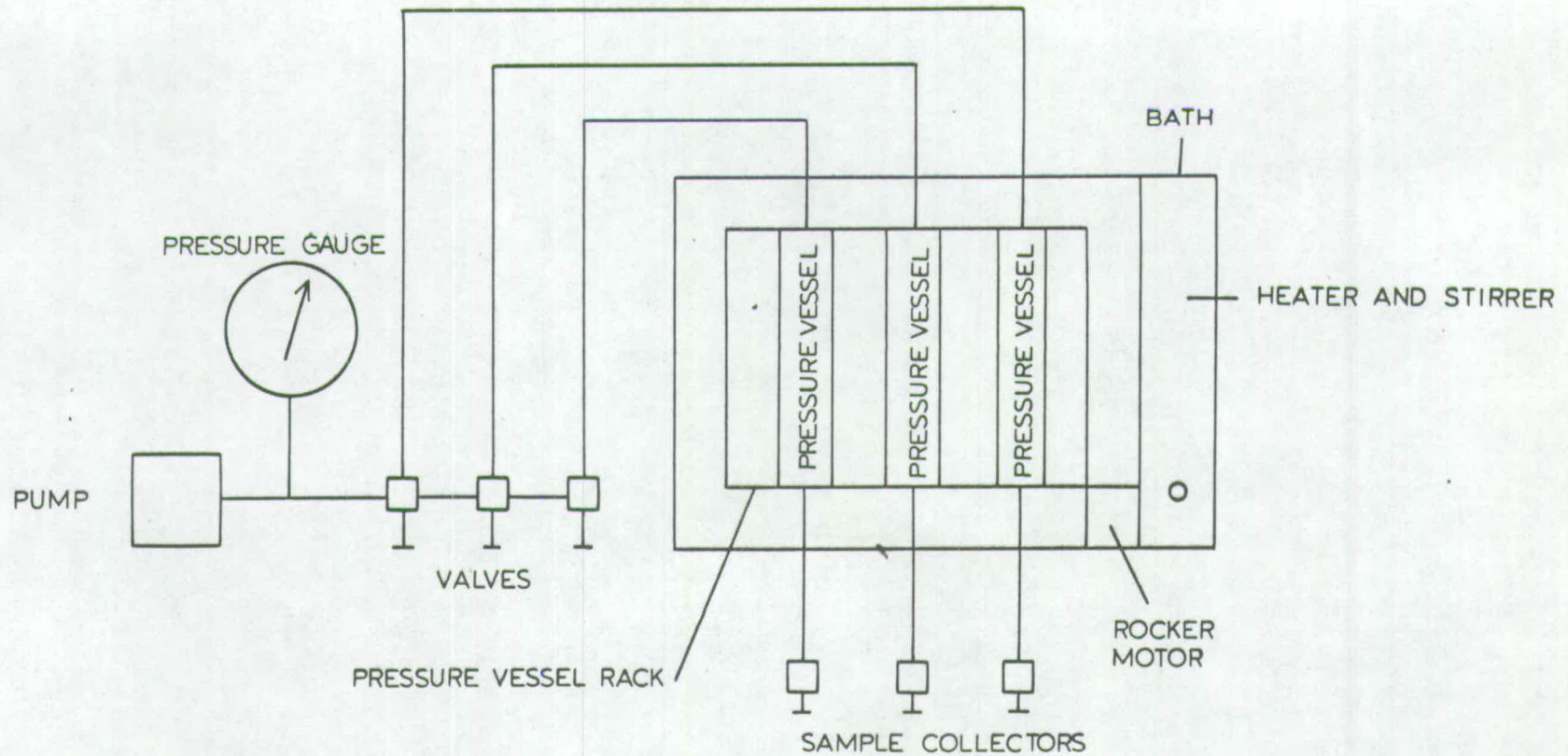
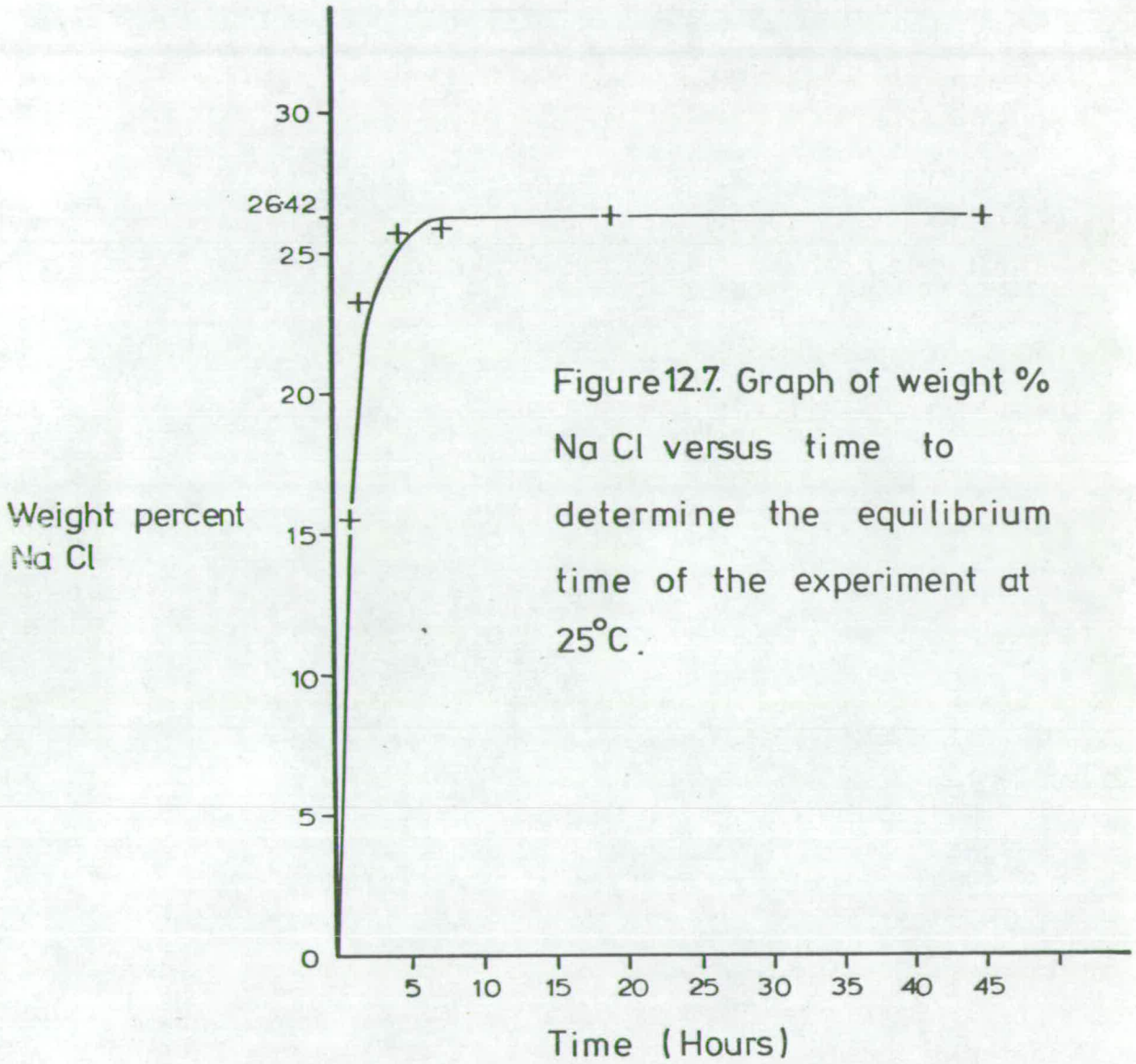


FIGURE 12.6. Plan of the Pressure Circuit employed in these experiments to study the system $\text{NaCl}-\text{H}_2\text{O}$.



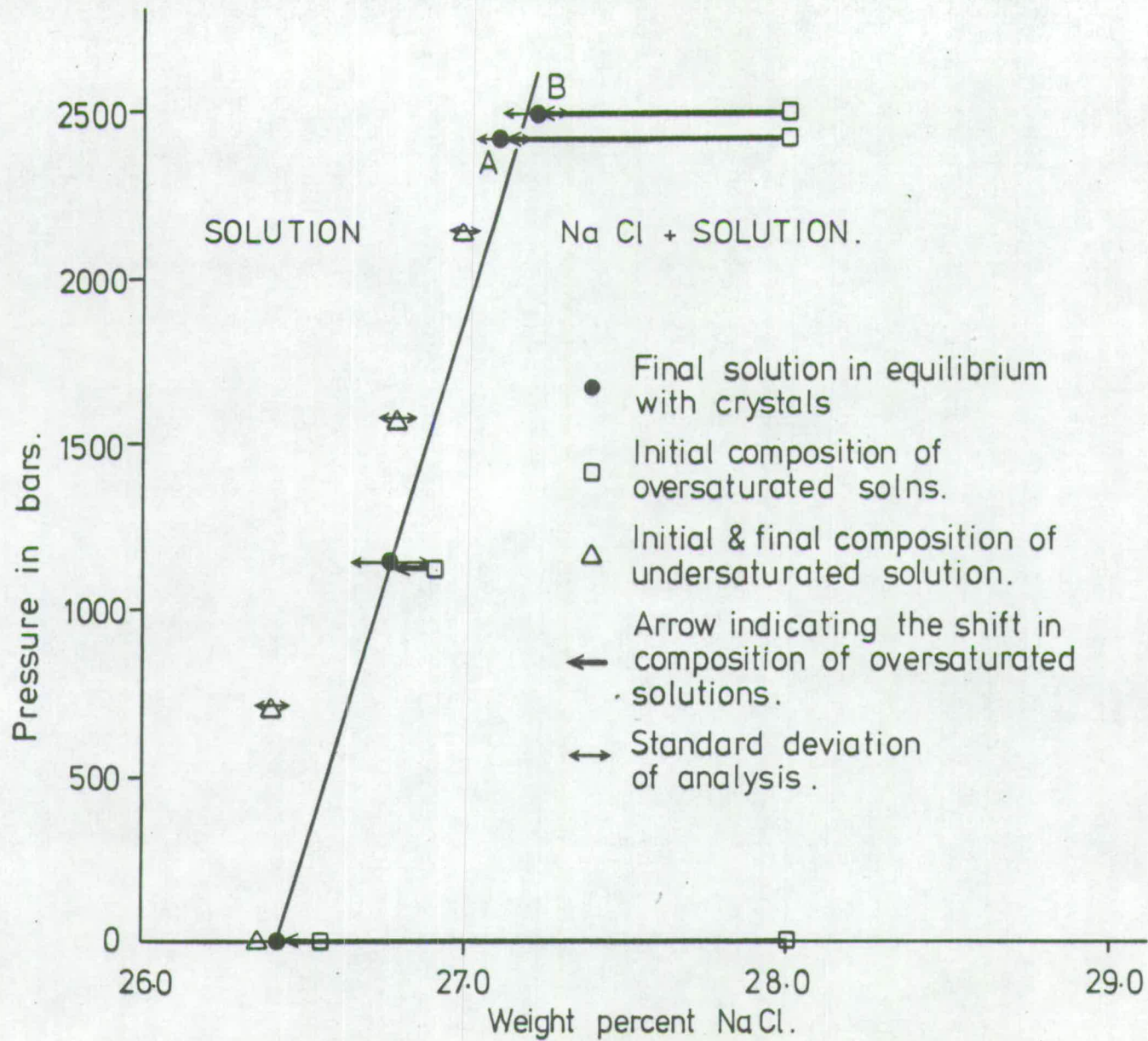


Figure 12.8:- The equilibrium solubility curve in the system NaCl-H₂O at 25°C and pressures from 0 - 2.5 kilobars .

FIGURES FOR APPENDIX 2

Figure A2.1

Diagrammatic representation of the possible structure depicted by the beds of boreholes A, B and F. The rectangle marks the section observed in the boreholes. Not to scale.

Figure A2.2

Diagrammatic representation of the possible structure depicted by the beds of boreholes C, L, M-D2 and possibly M. The rectangle marks the section observed in the boreholes. Not to scale.

Figure A2.3

Diagrammatic representation of the possible structure depicted in borehole U. The rectangle marks the section observed in the boreholes. Not to scale.

Figure A2.1

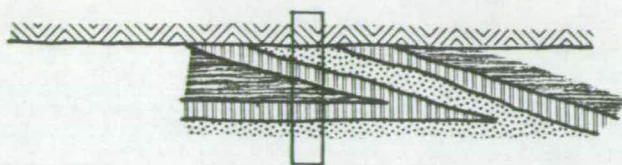


Figure A2.2

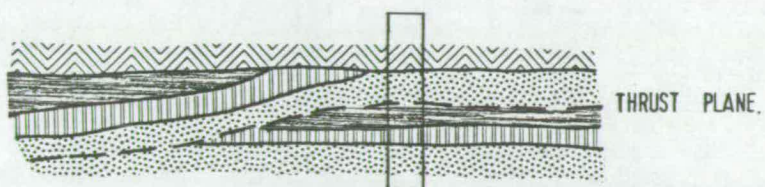
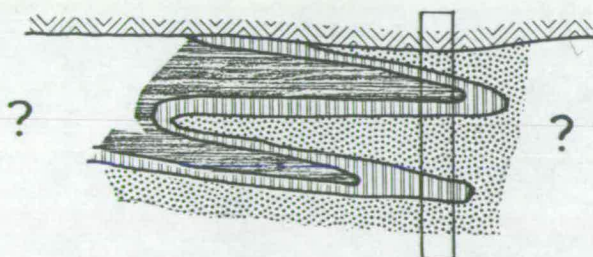


Figure A2.3

KEY

Rocks of the Rotten Marl

Rocks of the Boulby Shale

Rocks of the Boulby Potash

Rocks of the Boulby Halite

FIGURES FOR APPENDIX 5

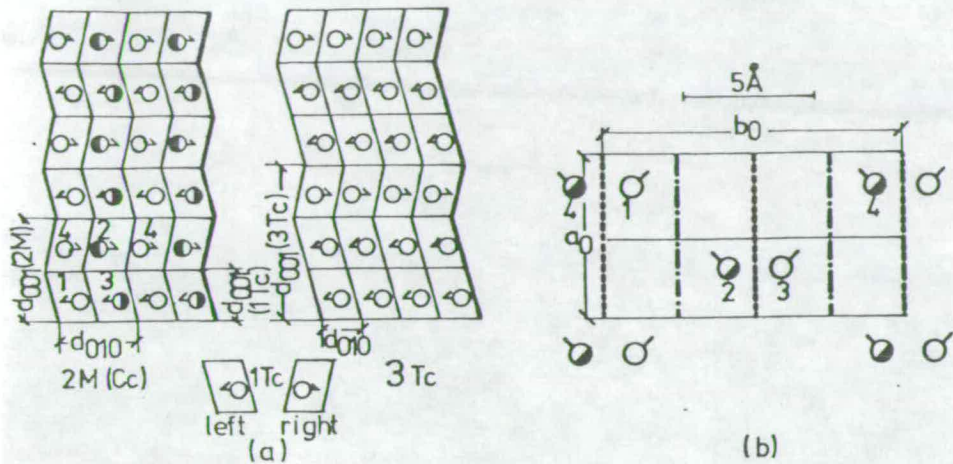


Figure A5.1

(a) Geometric interpretation of the polymorphic relations in the hilgardite group. Projection parallel to $[100]$; 1 Tc = triclinic, with left and right elementary cells (strontiohilgardite); 2M (Cc) = a stack of left and right handed component cells; open circle = points at height x ; half-filled circles = points at height $x + \frac{1}{2}$ above the marker plane. These symbols have the same meaning in (b). 3 Tc = scheme for parahilgardites (left-handed crystal).

(b) Symmetry elements and general point positions in the space group Cc. These correspond to the hilgardite cell.

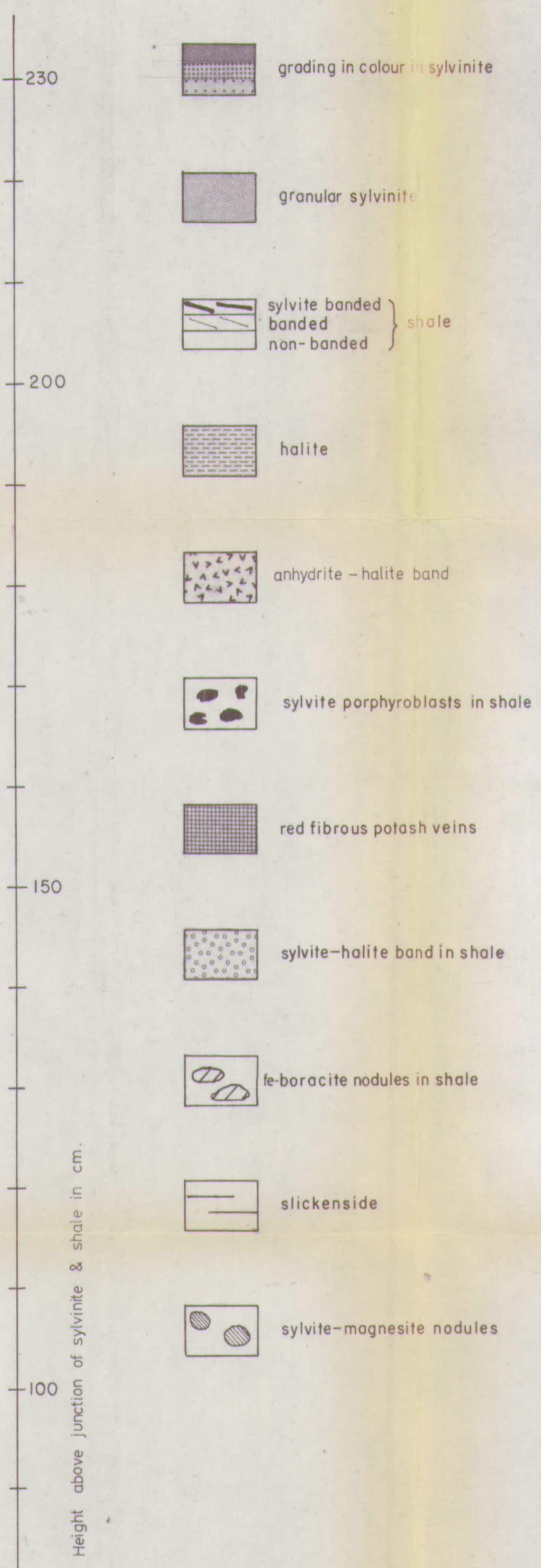
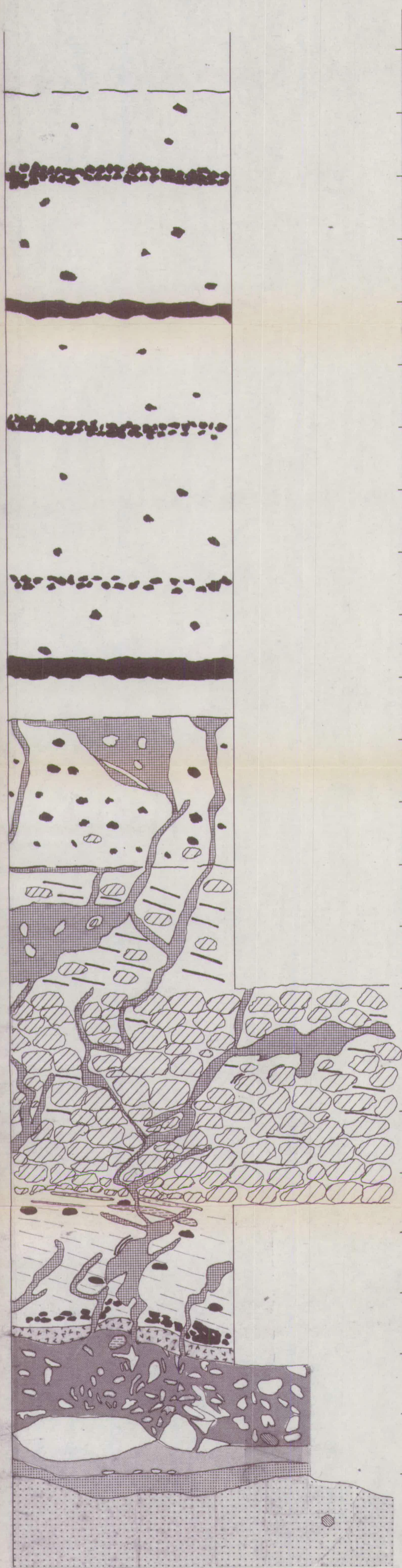
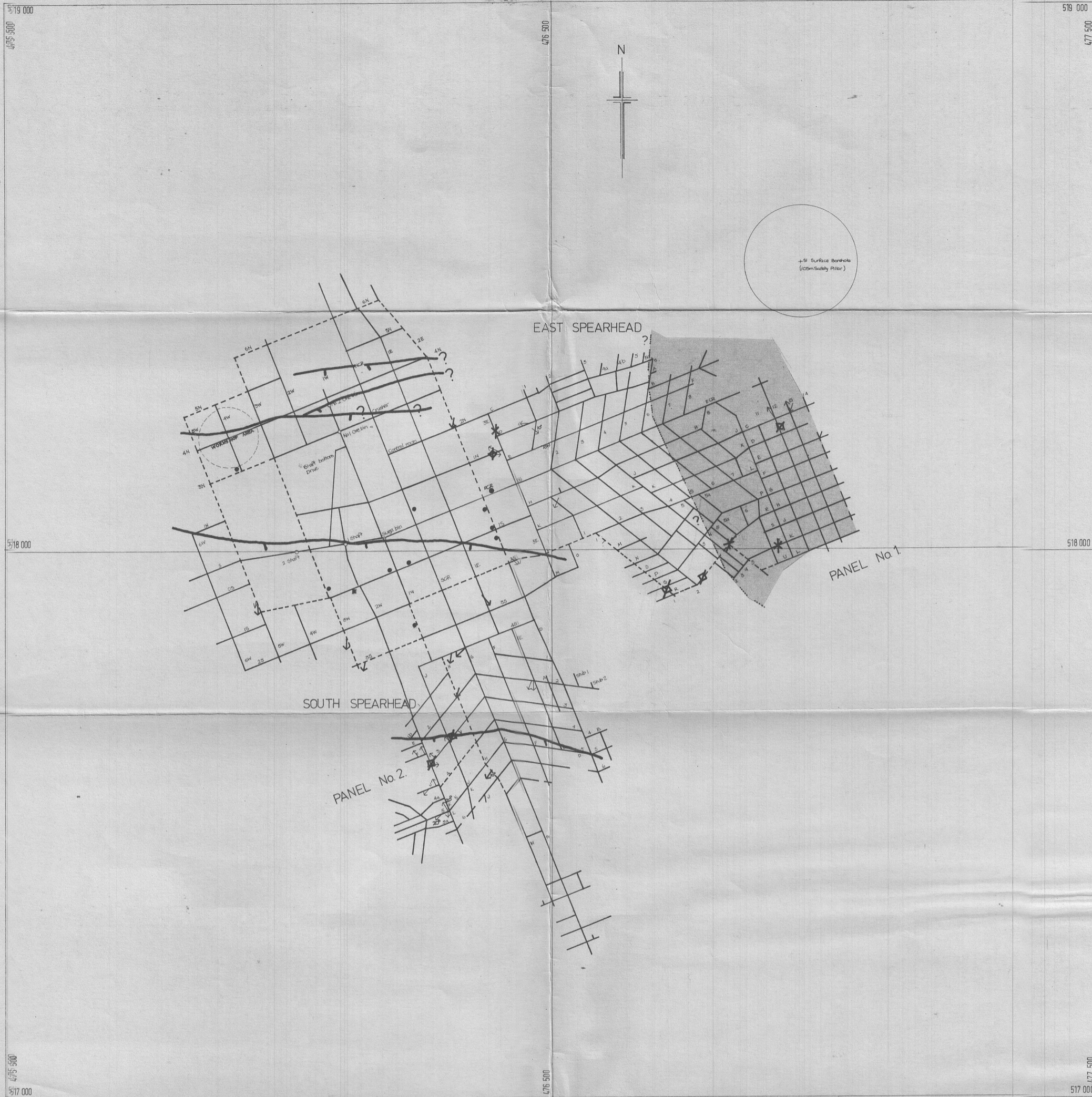
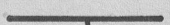


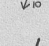




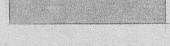
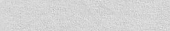
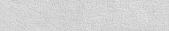


PLATE III
 Type Section
 of the Borate Nodule Bed in
 roadway D, 8 metres west of
 No. 1 cross cut south of D.
 (on south wall)



LEGEND

-  Base Boulby Potash Monoclines.
-  Monocline at the top of the Boulby Potash.
-  Anticline at the top of the Boulby Potash.
-  Direction of slickensiding in the Boulby Shale with angle of dip if known.
-  Direction of slickensiding in the upper part of the Boulby Halite and the Boulby Potash with angle of dip if known.
-  Inclusions of Boulby Shale in Boulby Potash in areas where only Boulby Potash is mined.
-  Inclusions of Rotten Marl in the Boulby Potash in areas where only Boulby Potash is mined.
-  Western margin of the zone of overfolding of the upper part of the Boulby Halite, the Boulby Potash and the Boulby Shale.
-  Area of overfolding of the upper part of the Boulby Halite, the Boulby Potash and the Boulby Shale.
-  Workings up until 10th January, 1977.
-  Main Travelling roads.

**STRUCTURAL MAP OF THE BOULBY MINE
UP UNTIL 10th JANUARY, 1977.**

PLATE II

SCALE 1:5000



PLATE I

The lithologies of the upper part of the Boulby Halite, the Boulby Potash and the Boulby Shale in boreholes from the C.P.L. concession area.

